ALMA MATER STUDIORUM
UNIVERSITÀ DEGLI STUDI DI BOLOGNA

Dottorato di Ricerca in Ingegneria Elettronica, Telecomunicazioni e Tecnologie dell'Informazione

Ciclo XXX

Settore concorsuale: 09/F2 - TELECOMUNICAZIONI

Settore scientifico disciplinare: ING-INF/03 - TELECOMUNICAZIONI

SPARSE SIGNAL PROCESSING AND STATISTICAL INFERENCE FOR INTERNET OF THINGS

Presentata da:
AHMED MOHAMED ALY ELZANATY

Coordinatore Dottorato:
Prof. Ing.
ALESSANDRO
VANELLI-CORALLI

Supervisore:
Chiar.mo Prof. Ing.
MARCO CHIANI

Co-supervisore:
Prof. Ing.
ANDREA GIORGETTI

ESAME FINALE 2018

ALMA MATER STUDIORUM
UNIVERSITY OF BOLOGNA

Ph.D. Programme in Electronics, Telecommunications, and Information Technologies Engineering

Cycle XXX

Sector: 09/F2 - TELECOMMUNICATIONS

Scientific disciplinary sector: ING-INF/03 - TELECOMMUNICATIONS

SPARSE SIGNAL PROCESSING AND STATISTICAL INFERENCE FOR INTERNET OF THINGS

Thesis by:
AHMED MOHAMED ALY ELZANATY

Ph.D. Programme Coordinator:
Prof. Ing.
ALESSANDRO
VANELLI-CORALLI

Supervisor:
Chiar.mo Prof. Ing.
MARCO CHIANI

Co-supervisor:
Prof. Ing.
ANDREA GIORGETTI

FINAL EXAM 2018

Typeset using LaTeX.

Abstract

Data originating from many devices and sensors within the Internet of Things (IoT) framework can be modeled as sparse signals. Efficient compression techniques of such data are essential to reduce the memory storage, bandwidth, and transmission power.

The idea of utilizing sparsity has been studied within several disciplines, e.g., signal processing, wireless communication, and statistical analysis. In this thesis, I develop some theory and propose practical schemes for IoT applications to exploit the signal sparsity for efficient data acquisition and compression under the frameworks of compressed sensing (CS) and transform coding.

Firstly, the design of finite measurement matrices in the context of CS is considered. The proposed probabilistic analysis determines, based on random matrix theory, how aggressively the signal can be sub-sampled and recovered from a small number of linear measurements. The reconstruction is guaranteed for all sparse signals with a predefined probability, via various recovery algorithms. More precisely, the proposed method relies on the exact distributions of the extreme eigenvalues of Wishart matrices to bound the restricted isometry constant of finite dimensional Gaussian measurement matrices. We investigated also the stable and robust reconstruction of not exactly sparse (compressible) signals from noisy measurements.

Secondly, the measurement matrix design for simultaneously acquiring multiple signals is considered. This problem is particularly important for IoT networks, where a huge number of nodes are involved. In this scenario, our analytical methods provide limits on the compression of joint sparse sources by analyzing the weak restricted isometry constant of Gaussian measurement matrices.

Thirdly, designing efficient encoders for noisy sparse sources, which is essential for transform coding, is addressed. Two practical approaches for signal denoising and compression, based on statistical inference and channel coding theories, are proposed. Also, considering that sparse signals can be modeled as Bernoulli-Gaussian and Bernoulli-uniform distributions, the

performance of the encoders are derived in terms of the operational rate-distortion and energy-distortion, in the presence of noise. Furthermore, a case study for the compression of real signals from a wireless sensor network using the proposed encoders is considered. These techniques can reduce the power consumption and increase the lifetime of IoT networks.

Finally, while working on wireless communication with IoT devices, the need for synchronization techniques has been essential to ensure reliable radio links. In particular, optimal and suboptimal metrics for noncoherent frame synchronization are derived, based on statistical inference theory. The proposed tests outperform the commonly used correlation detector in terms of synchronization error probability, leading to accurate data extraction and reduced power consumption.

Contents

List of Acronyms

AC address coding

ADC analog-to-digital converter

ARIC asymmetric restricted isometry constant

AWGN additive white Gaussian noise

AWRICs asymmetric weak restricted isometry constants

BCH Bose, Chaudhuri, and Hocquenghem

BCHSC BCH based source coding

BG Bernoulli-Gaussian

BPSK binary phase shift keying

BSC binary symmetric channels

BU Bernoulli-uniform

CDF cumulative distribution function

CCDF complementary cumulative distribution function

CDMA code division multiple access

CoSaMP compressive sampling matching pursuit

CS compressed sensing

DCT discrete cosine transform

DR distortion-rate

EED exact eigenvalues distribution

FS frame synchronization

GIC generalized information criterion

IDR information distortion-rate

IHT iterative hard thresholding

i.i.d. independent, identically distributed

IoT Internet of Things

LRIC lower restricted isometry constant

LRICt lower restricted isometry constant threshold

LF likelihood function

LLF log-likelihood function

LLRT log-likelihood ratio test

LRT likelihood ratio test

LWRIC lower weak restricted isometry constant

LWRICt LWRIC threshold

MDS mixed distributed source

MF matched filter

ML maximum likelihood

MMV multiple measurement vectors

M**-PSK** M-ary phase shift keying

M**-QAM** M-ary quadrature amplitude modulation

MSO maximum sparsity order

NLA nonlinear sparse approximation

ODE operational distortion-energy

ODR operational distortion-rate

OMP orthogonal matching pursuit

OSMP orthogonal subspace matching pursuit

PDF probability density function

PMF probability mass function

PSEP pairwise synchronization error probability

PSK phase shift keying

8**-PSK** 8-phase shift keying

QPSK quadrature phase shift keying

RIC restricted isometry constant

RICt restricted isometry constant threshold

RIP restricted isometry property

RS Reed-Solomon

RSSC RS based source coding

r.v. random variable

SA-Music subspace-augmented MUSIC with OSMP

SMV single measurement vector

SNR signal-to-noise ratio

SP subspace pursuit

SW sync word

TW Tracy-Widom

URIC upper restricted isometry constant

URICt upper restricted isometry constant threshold

UWRIC upper weak restricted isometry constant

UWRICt UWRIC threshold

WM Wishart matrix

WRIC weak restricted isometry constant

WRICt weak restricted isometry constant thresholds

WSN wireless sensor network

List of Figures

Chapter 1

Introduction

1.1 Motivation

The Internet of Things (IoT) is a dynamic global network of devices, e.g., sensors, actuators, surveillance cameras, vehicles, wearable devices, and home appliances. These interconnected objects are uniquely identifiable and they can autonomously transmit and receive useful data over the network. The collected data can be exploited into sophisticated applications which permits for significant improvements of human life. The IoT technology when combined with sensors and actuators evolves into the more general class of cyber-physical systems including several applications such as smart homes and cities, intelligent transportation, and precision agriculture.

The tremendous increase of data generated within the frameworks of IoT and cyber-physical systems necessitates designing efficient acquisition, compression, and noise reduction schemes. For example, the number of devices connected to the Internet is predicted to exceed 20 billion in 2020, as shown in Fig. 1.1, leading to a huge amount of data estimated as 50 zettabytes. The data generated annually is expected to reach 160 zettabytes by 2050, and almost half of this amount is originated from endpoints, e.g., mobile phones, IoT devices, cameras, and connected vehicles, as shown in Fig. 1.2 [1]. Thus, overwhelming resources, such as storage, power, and bandwidth, are required to handle this data.

However, the intrinsic information contained in such data is much smaller than their actual size. Hence, the required resources can be significantly decreased by exploiting some of the data structures. One of these properties is the sparsity/compressibility, i.e., the ability to describe/approximate signals with a fewer number of coefficients compared to their dimension in appropriate domains, e.g., time, frequency, discrete cosine transform (DCT), and

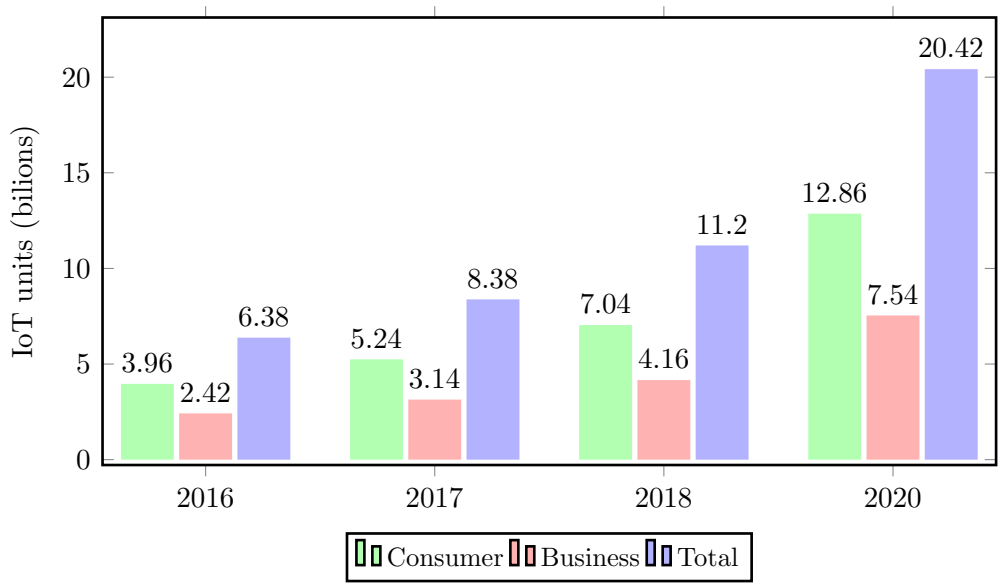

Figure 1.1: The number of installed IoT devices by consumers and business as predicted by Gartner Inc. (January 2017).

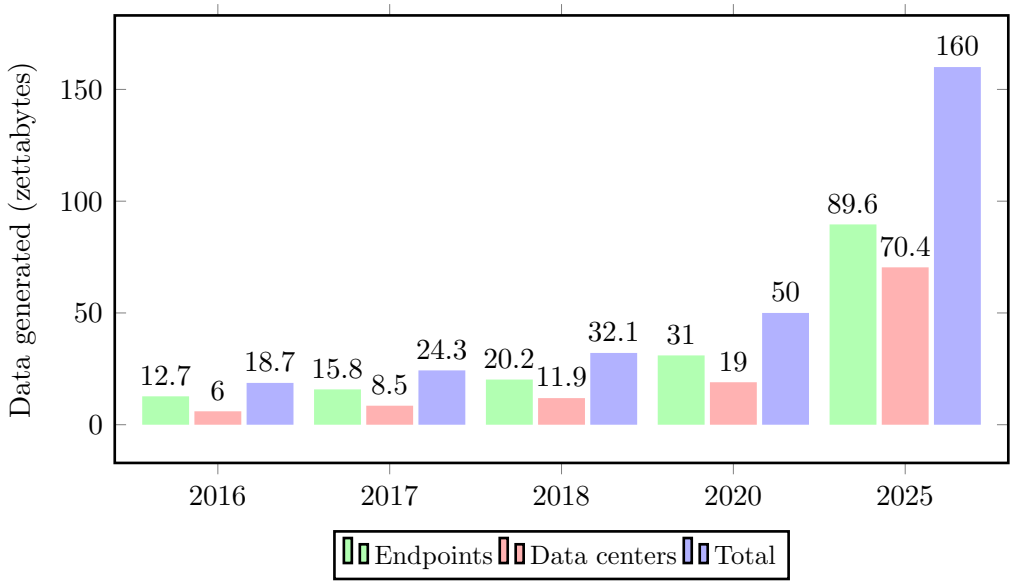

Figure 1.2: The amount of generated data by endpoints and data centers as predicted by IDC Inc. (April 2017).

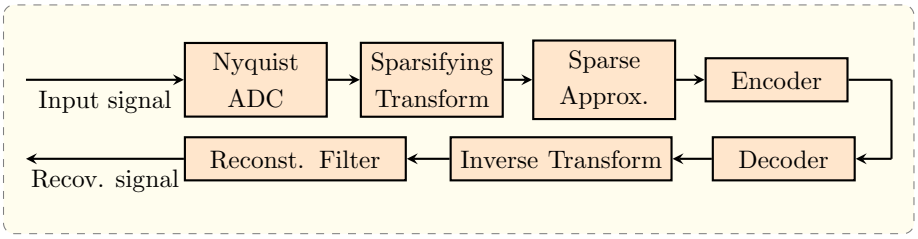

(a) Block diagram of transform coding.

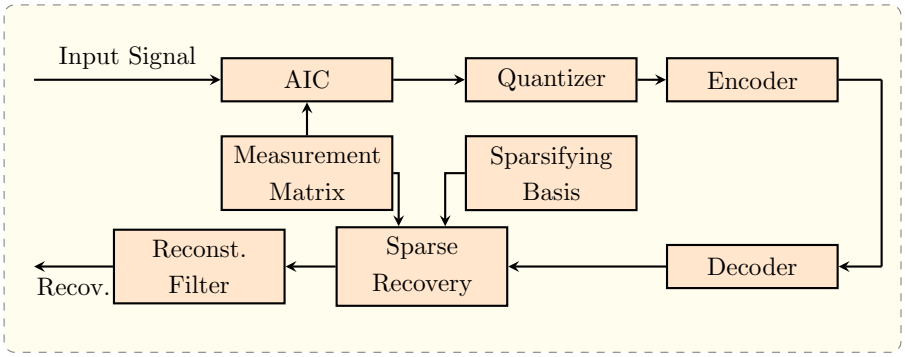

(b) Block diagram of CS based source compression.

Figure 1.3: Source coding schemes for compressible signals.

wavelet. In fact, many signals of interest such as image, audio, video, and IoT data are compressible [2, 3]. Therefore, the growing challenge is to efficiently acquire, represent, and reconstruct these signals with the minimum possible rate and energy consumption.

1.2 Sparse Signal Processing Paradigms

The idea of exploiting sparsity has been studied within several disciplines including signal processing and information theory communities, e.g., source compression, transform coding, CS, and approximation theory [2–6].

Regarding transform coding, the signal is represented in a suitable basis and only few coefficients are encoded, as shown in Fig. 1.3a. At first, band-limited signals must be captured using analog-to-digital converter (ADC) with sampling rate higher than the Nyquist rate. In order to reduce the data size, it is required to represent the signal into an appropriate domain that compacts its energy into few coefficients. Then, nonlinear sparse approximation (NLA) is performed by selecting the largest coefficients in amplitude

Table 1.1: Comparison between transform coding and CS for the compression of sparse signals.

	Transform Coding	CS
Sampling Rate	Nyquist	Sub-Nyquist
Encoder Complexity	Moderate	Low
Decoder Complexity	Moderate	High
Basis knowledge	Encoder and Decoder	Decoder
Rate-Distortion behavior	Good	Poor

and discarding the non-significant ones. Finally, the resulting sparse signal is encoded. With the proper design of the basis, the sparse approximation method, and the encoder, the transform coder can achieve a high compression ratio with limited distortion. However, the basis at which the signal is sparse should be known at both the encoder and decoder. Also, for sampling wideband signals, the Nyquist rate could be very high, leading to costly and power-hungry technologies.

On the other hand, CS is a signal processing paradigm for recovering sparse and compressible signals from a small set of measurements acquired through a linear operator (measurement matrix). CS based techniques have been exploited to provide efficient solutions for several problems in signal processing and communication, e.g., source and channel coding, cryptography, random access, radar, spectrum sensing, channel estimation and network tomography [5, 7–27]. For example, CS as source coder is illustrated in Fig. 1.3b. In this scheme the compressible signal is acquired by an Analog-to-Information Converter (AIC) allowing to sample at the information-rate of the data, which is much slower than the Nyquist rate [8, 22, 28–30]. A possible implementation for AICs is by correlating the input signal with a bank of random bipolar pulse trains, then sampling at the end of the integration interval, where the acquisition can be viewed as a multiplication of the discretized signal by a measurement matrix with independent, identically distributed (i.i.d.) entries drawn from Rademacher distribution. Then, the measurements are quantized using uniform scalar quantizer and finally entropy encoded. After decoding at the receiver side, the signal is approximately reconstructed through sparse recovery algorithms, e.g., optimization

and greedy based methods, from the quantized measurements. The key advantages of CS over transform coding are as following.

1. The sparsifying basis is needed only for signal reconstruction at the decoder, leading to simpler encoders which require lower computational capabilities.

2. Sparse wideband signals can be acquired efficiently through random sampling with relaxed conditions on the sampling rate [31, 32], compared to the Nyquist sampling that does not exploit the additional signal structure [33–38].

Nevertheless, the resulting distortion for the CS source coder is higher than that based on transform coding [39].

The differences between transform coding and CS as source coder are summarized in Table 1.1. Clearly, opting for either transform coding or CS depends heavily on the targeted application, i.e., the signal properties, the availability of computational power at either encoder or decoder, and the prior knowledge of the sparsity basis.

1.3 Thesis Contributions

The main contributions of this thesis can be summarized as follows:

1. Designing the measurement matrix in the context of CS with single measurement vector (SMV):

   - accurate symmetric and asymmetric restricted isometry constant (RIC) analysis for finite dimensional problems, accounting for the exact distribution of the singular values of finite Gaussian matrices;
   - tight bounds on the maximum achievable sparsity order which guarantees an arbitrary target recovery probability, for a given number of measurements and signal dimension (instead of the common overwhelming probability approach);
   - study for stable and robust recovery of compressible signals with bounds on the reconstruction error;
   - simple approximations for the RICs based on the Tracy-Widom's laws.

2. Investigating joint sparse recovery within the framework of CS with multiple measurement vectors (MMV):

- probabilistic analysis of the weak restricted isometry constants (WRICs) for finite Gaussian matrices;
- lower bounds on the probability of satisfying an arbitrary recovery condition, tighter than those based on the concentration inequalities;
- unified average case framework to quantify the recovery limits of joint sparse reconstruction algorithms, for both noiseless and noisy measurements;
- estimating the maximum joint support cardinality of row sparse matrices such that a target probability of recovery is assured;
- deriving sufficient reconstruction conditions, in terms of the asymmetric WRICs, which permit the recovery of signals with higher sparsity orders, compared to those obtained through the symmetric WRIC.

3. Proposing two novel source encoders for noisy sparse sources:

   - deriving a blind estimator for the sparsity order based on a model order selection rule;
   - designing an excision filter to differentiate signal entries from noise;
   - proposing efficient source encoders for sparse signals by exploiting the syndromes associated with channel block codes;
   - obtaining the distribution of the error due to quantization and input noise, for mixed distributed sources encompassing Bernoulli and an arbitrary continuous distribution;
   - accurate performance measure of the proposed encoders in terms of the operational distortion-rate, for noisy Bernoulli-uniform and Bernoulli-Gaussian sources;
   - analyzing the operational distortion-energy, particularly important to design power efficient networks in IoT scenarios;
   - utilizing the proposed encoders for the compression of real signals gathered from a wireless sensor network deployed in Torgiovannetto (Assisi, Italy).

4. Designing efficient frame synchronization (FS) mechanism for IoT devices:

   - deriving an optimal metric for noncoherent FS of M-PSK modulations with $M \geq 4$;

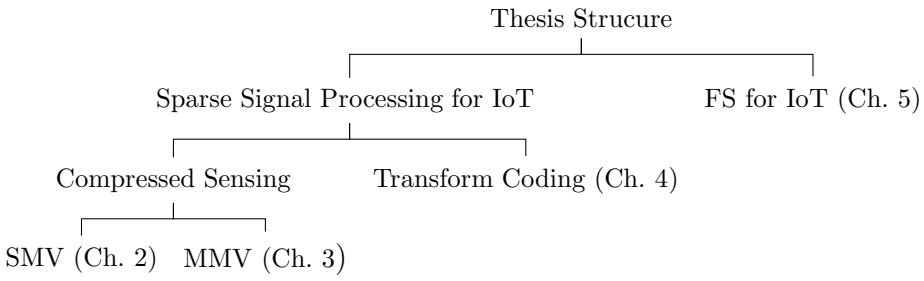

Figure 1.4: The thesis structure.

- obtaining low-complexity metrics for QPSK and 8-PSK;
- analyzing for M-PSK a simple metric consisting in the noncoherent correlator modified by removing a correction term;
- investigating the performance improvement of the new test when applied to M-QAM systems.

1.4 Thesis Structure

The rest of the thesis is outlined in four chapters (Fig. 1.4) as follows.

Chapter 2 provides a new approach for the analysis of the RIC of finite dimensional Gaussian measurement matrices, in the context of CS. The proposed method relies on the exact distributions of the extreme eigenvalues of Wishart matrices. The presented framework provides, for finite size problems, a tight lower bound on the maximum sparsity order allowing signal recovery from a given number of measurements with a predefined target probability.

Chapter 3 presents tight upper bounds on the weak restricted isometry constant of finite Gaussian measurement matrices under the framework of CS for MMV. The limits are used to develop a unified framework for the guaranteed recovery assessment of jointly sparse matrices.

Chapter 4 proposes two practical approaches for source compression of noisy sparse sources. The proposed schemes are based on channel coding theory to construct efficient source encoders by exploiting the signal sparsity. Also, accurate analysis of the system performance is provided in terms of the operational distortion-rate and operational distortion-energy functions.

Finally, **Chapter 5** investigates FS for M-PSK signals in the presence of additive white Gaussian noise and phase offset due to imperfect carrier phase estimation. In particular, optimal and simple suboptimal metrics for noncoherent FS of M-PSK modulation are derived. The proposed technique is analyzed for M-QAM systems, as well as in the presence of small frequency offsets.

Chapter 2

Compressed Sensing Design for Finite Gaussian Matrices

2.1 Introduction

Compressed sensing (CS) is a signal processing paradigm for efficiently recovering a signal from a small set of linear measurements, provided that the sensed data is sparse, i.e., the number of its non-zero elements, s, is much less than its dimension n. If properly chosen, the number of measurements, m, can be much smaller than the signal dimension [4, 5, 28, 40–42]. In fact, CS provides efficient solutions for several problems in signal processing and communication, e.g., source and channel coding, cryptography, random access, radar, sub-Nyquist data acquisition, spectrum sensing, channel estimation, and network tomography [5, 7, 9–27]. The usability of these applications depends on the maximum sparsity order s such that recovery is guaranteed with high probability for given m and n. For example, such s determines the maximum allowable number of:

- corrupted samples which can be detected and corrected using error control schemes for impulsive noise [5, 43];
- non-zero elements that can be recovered using compressive source coding [9];
- RFID tags which can be simultaneously active for tag acquisition via CS [19];
- users that can feed back their channel state information in MIMO broadcast channel [25].

The three main possible approaches to find the maximum sparsity order s guaranteeing recovery of all sparse vectors are based on the restricted isometry property (RIP) analysis, geometric methods, and coherence analysis. The RIP tells how well a linear transformation preserves distances between sparse vectors, and is quantified by the so-called restricted isometry constant (RIC) [5]. In general, the smaller the RIC, the closer the transformation to an isometry (a precise definition of the RIC is given later). Geometric based methods are useful for the recovery analysis of exactly sparse signals via ℓ_1-minimization in the noiseless case [44–47]. Sparse reconstruction can also be studied looking at the coherence of the measurement matrix. However, the resulting bounds are too pessimistic compared to RIP-based bounds [6, eq. (6.9) and eq. (6.14)]. This significant gap justifies preferring the RIP based analysis, whenever bounding the RIC is feasible. Furthermore, non-uniform recovery guarantees, like those based on Gaussian widths, provide tight bounds for the reconstruction of a fixed sparse vector, in contrast to the RIP method, which considers the recovery of all sparse vectors (uniform recovery) [6], [48].

Moreover, the RIP theory is more general compared to the geometric approach, as it also considers the stability for not exactly sparse (compressible) signals and the robustness to noise, under different measurement matrices, for a wider range of sparse recovery algorithms. In fact, sufficient conditions for exact recovery have been obtained in terms of the RIC for several algorithms (see, e.g., [5, 49–54] for ℓ_1-minimization, [55, 56] for iterative hard thresholding (IHT), and [57–60] for greedy algorithms).

It has been shown, by using information-theoretic methods, that Gaussian random matrices with independent, identically distributed (i.i.d.) entries are optimal in terms of minimizing the number of measurements required for recovery [61]. Hence, precisely analyzing the RIP of such matrices is important. In fact, Gaussian matrices have been proved to satisfy the RIP with overwhelming probability [5, 40]. The two main tools adopted for the proof are the concentration of measure inequality for the distribution of the extreme eigenvalues of a Wishart matrix, and the union bound which accounts for all possible signal supports. However, if the aim is to quantify the maximal allowable sparsity order s for a given number of measurements, the use of the concentration inequalities leads to overly pessimistic results. In this regard, in [62–64] an improved analysis was presented, by bounding the asymptotic behavior of the distributions given in [65] for the extreme eigenvalues of a Wishart matrix instead of the concentration inequalities. Explicit bounds for the RIC have been obtained in some specific asymptotic regions [64], but no bounds are known in the general non-asymptotic setting. In fact, for finite measurement matrices the asymptotic analysis of the eigenvalues in [62–64]

gives approximations of the true distributions; therefore, they cannot provide guaranteed bounds for a particular problem dimension (s, m, n).

This chapter provides an accurate statistical analysis of the RIC for finite dimensional Gaussian measurement matrices, supporting the design of real CS applications (involving always finite size problems), with guaranteed recovery probability. In particular, we calculate the tightest, to our knowledge, lower bound on the probability of satisfying the RIP for an arbitrary condition on the RIC. For a specified number of measurements, the maximal sparsity order can then be found such that perfect recovery is feasible for all s-sparse vectors, i.e., the matrix satisfies the RIP, considering, on a random draw of the measurement matrix, a target probability $1 - \epsilon$ of successful recovery. Differently, the usually adopted asymptotic setting considers that this probability tends to 1 (overwhelming probability).

To get better estimates on the maximal sparsity order, tight lower bounds on the cumulative distribution functions (CDFs) of the asymmetric restricted isometry constants (ARICs) are derived, based on the exact probability that the extreme singular values of a Gaussian submatrix are within a range. Hence, starting from the derived CDFs, we can find thresholds, below which the ARICs lie with a predefined probability. These percentiles allow to calculate a lower bound on the maximal recoverable signal sparsity order, using several reconstruction methods, such as ℓ_1-minimization, greedy, and IHT algorithms. The new analysis is used in conjunction with the recovery conditions relaxed to asymmetric boundaries, as suggested in [62], to prove exact recovery for signals with larger sparsity orders. In this regard, we relax the symmetric RIC based condition in [54] to a weaker asymmetric one. Additionally, we provide approximations for the RIC CDFs based on the Tracy-Widom (TW) distribution, along with a convergence investigation. In comparison with previous literature, the proposed analysis gives, for finite dimensional problems, a better estimation of the signal sparsity allowing guaranteed recovery.

The contributions of this chapter can be summarized as follows:

- accurate symmetric and asymmetric RIC analysis for finite dimensional problems, accounting for the exact distribution of eigenvalues of finite Wishart matrices (differently from previous methods based on asymptotic behavior of the distributions or loose concentration of measure bounds);

- limits on compressive data acquisition in terms of the maximum achievable sparsity order guaranteeing arbitrary target reconstruction probability (instead of the common overwhelming probability approach) via various recovery algorithms;

- accurate study for stable and robust recovery of compressible signals with tight bounds on the reconstruction error;
- simple approximations for the RICs based on the TW's laws.

Throughout this chapter, we indicate with $\det(\cdot)$ the determinant of a matrix, with $\text{card}(\cdot)$ the cardinality of a set, with $\|\cdot\|_q = (\sum_{i=1}^{n} |x_i|^q)^{\frac{1}{q}}$ the ℓ_q norm of an n-dimensional vector, with $\|\cdot\|$ the ℓ_2 norm, with $\Gamma(\cdot)$ the gamma function, with $\gamma(a;x,y) = \int_x^y t^{a-1}e^{-t}dt$ the generalized incomplete gamma function, with $P(a,x) = \frac{1}{\Gamma(a)}\gamma(a;0,x)$ the regularized lower incomplete gamma function, with $P(a;x,y) = \frac{1}{\Gamma(a)}\int_x^y t^{a-1}e^{-t}dt = P(a,y) - P(a,x)$ the generalized regularized incomplete gamma function, with $\mathcal{N}(\mu,\sigma^2)$ the Gaussian distribution with mean μ and variance σ^2.

2.2 Problem Formulation

Consider that we have a single measurement vector (SMV)

$$\mathbf{y} = \mathbf{A}\mathbf{x} \tag{2.1}$$

where $\mathbf{y} \in \mathbb{R}^m$ and $\mathbf{A} \in \mathbb{R}^{m\times n}$ are known, the number of equations is $m < n$, and $\mathbf{x} \in \mathbb{R}^n$ is the unknown. Since $m < n$, we can think of $\mathbf{y}$ as a compressed version of $\mathbf{x}$. Without other constraints, the system is underdetermined, and there are infinitely many distinct solutions of (2.1). If we assume that at most $s < m$ elements of $\mathbf{x}$ are non-zero (i.e., the vector is s-sparse), then there is a unique solution (the right one) to (2.1), provided that all possible submatrices consisting of $2s$ columns of $\mathbf{A}$ are maximum rank. The solution can be found by solving the following ℓ_0-minimization [5]

$$\hat{\mathbf{x}} = \arg\min \|\mathbf{x}\|_0 \text{ subject to } \mathbf{y} = \mathbf{A}\mathbf{x} \tag{2.2}$$

where $\|\mathbf{x}\|_0$ is the number of the non-zero elements of $\mathbf{x}$. However, even when the maximum rank condition is satisfied, the solution of (2.2) is computationally prohibitive for dimensions of practical interest. A much easier problem is to find the ℓ_1-minimization solution. It is proved in [5], under some conditions on $\mathbf{A}$, that the solution provided by the ℓ_1-minimization

$$\hat{\mathbf{x}} = \arg\min \|\mathbf{x}\|_1 \text{ subject to } \mathbf{y} = \mathbf{A}\mathbf{x} \tag{2.3}$$

is the same as that of (2.2). The conditions on $\mathbf{A}$ are given in term of the RIC.

Definition 1 (The RIC [5])**.** The RIC of order s of $\mathbf{A}$, $\delta_s(\mathbf{A})$, is the smallest constant, larger than zero, such that the inequalities

$$1-\delta_s(\mathbf{A}) \leq \frac{\|\mathbf{A}_S\,\mathbf{c}\|^2}{\|\mathbf{c}\|^2} \leq 1+\delta_s(\mathbf{A}) \tag{2.4}$$

are simultaneously satisfied for every $\mathbf{c} \in \mathbb{R}^s$ and every $m \times s$ submatrix $\mathbf{A}_S$ of $\mathbf{A}$ with columns indexed by $S \subset \Omega \triangleq \{1, 2, ..., n\}$ with $\text{card}(S) = s$. Under this condition, the matrix $\mathbf{A}$ is said to satisfy the RIP of order s with constant $\delta_s(\mathbf{A})$.

Specifically, the importance of the RIP in CS comes from the possibility to use the computationally feasible ℓ_1-minimization instead of the impractical ℓ_0 one, under some constraints on the RIC. For example, it was shown that the ℓ_1 and the ℓ_0 solutions are coincident for every s-sparse vectors $\mathbf{x}$ if $\delta_s(\mathbf{A}) < \delta$ with $\delta = 1/3$ [54].

The next question is how to design a matrix $\mathbf{A}$ with a prescribed RIC. One possible way to design $\mathbf{A}$ consists simply in randomly generating its entries according to some statistical distribution. In this case, for a given n, s and δ, the target is to find a way to generate $\mathbf{A}$ such that the probability $\mathbb{P}\{\delta_s(\mathbf{A}) < \delta\}$ is close to one. An optimal choice is to build the measurement matrix $\mathbf{A}$ with i.i.d. entries $a_{i,j} \sim \mathcal{N}(0, 1/m)$ [5,61]. Then, in order to find the number of measurements m needed, we start by using the Rayleigh quotient inequality for a fixed S

$$\lambda_{\min}(\mathbf{W}) \leq \frac{\|\mathbf{A}_S\,\mathbf{c}\|^2}{\|\mathbf{c}\|^2} \leq \lambda_{\max}(\mathbf{W}) \tag{2.5}$$

where $\mathbf{W} = \mathbf{A}_S^T\mathbf{A}_S$, and $\lambda_{\min}(\mathbf{W})$ and $\lambda_{\max}(\mathbf{W})$ are its minimum and maximum eigenvalues, respectively. Considering that the inequalities in (2.4) should be satisfied for all the s-column submatrices of $\mathbf{A}$, the RIC constant can be written as

$$\delta_s(\mathbf{A}) = \max\left\{1-\min_{\substack{S\subset\Omega\\ \text{card}(S)=s}} \lambda_{\min}(\mathbf{W}),\ \max_{\substack{S\subset\Omega\\ \text{card}(S)=s}} \lambda_{\max}(\mathbf{W})-1\right\}. \tag{2.6}$$

Hence, the probability that the measurement matrix satisfies the RIP with a RIC at most δ, denoted as $\beta(\delta) \triangleq \mathbb{P}\{\delta_s(\mathbf{A}) \leq \delta\}$, is represented by

$$\beta(\delta) = \mathbb{P}\left\{\min_{\substack{S\subset\Omega\\ \text{card}(S)=s}} \lambda_{\min}(\mathbf{W}) \geq 1-\delta, \max_{\substack{S\subset\Omega\\ \text{card}(S)=s}} \lambda_{\max}(\mathbf{W}) \leq 1+\delta\right\}. \tag{2.7}$$

The union bound gives a lower bound for the probability of satisfying the RIP as

$$\beta(\delta) \geq 1 - \binom{n}{s} \left(1 - P_{sw}(\delta)\right) \tag{2.8}$$

where $\binom{n}{s}$ is the binomial coefficient and $P_{sw}(\delta)$ is the probability that $\mathbf{A}_S$ is well conditioned defined as:

$$P_{sw}(\delta) \triangleq \mathbb{P}\left\{1 - \delta \leq \lambda_{\min}(\mathbf{W}), \lambda_{\max}(\mathbf{W}) \leq 1 + \delta\right\}. \tag{2.9}$$

The probability $P_{sw}(\delta)$ is of fundamental importance, since it determines the performance of CS. In the next section, an approach for exactly calculating (2.9) for Gaussian matrices is proposed.

2.3 Eigenvalues Statistics

In this section, we start by recalling the known concentration inequality based bound on $1 - P_{sw}(\delta)$, which is the approach used in [4, 5]. Then, an alternative method to find $P_{sw}(\delta)$ for Gaussian measurement matrices are provided. The proposed technique relies on the exact probability that the eigenvalues of $\mathbf{W}$ are within a predefined interval.

2.3.1 Eigenvalues Statistics Based on the Concentration Inequality

Deviation bounds for the largest and the smallest eigenvalues of the Wishart matrix $\mathbf{W}$ are obtained using the concentration of measure inequality [4, 5], as

$$\mathbb{P}\left\{\sqrt{\lambda_{\max}(\mathbf{W})} \geq 1 + \sqrt{s/m} + o(1) + t\right\} \leq e^{-mt^2/2} \tag{2.10}$$

and

$$\mathbb{P}\left\{\sqrt{\lambda_{\min}(\mathbf{W})} \leq 1 - \sqrt{s/m} + o(1) - t\right\} \leq e^{-mt^2/2} \tag{2.11}$$

where $t > 0$ and $o(1)$ is a small term tending to zero as m increases, which will be neglected in the following. Using the inequality $\mathbb{P}\left\{A^c B^c\right\} \geq 1 - \mathbb{P}\left\{A\right\} - \mathbb{P}\left\{B\right\}$ where A, B are arbitrary events, and A^c, B^c are their complements, i.e., the union bound, we get

$$P_{sw}(\delta) \geq 1 - e^{-\frac{1}{2}m\left[\left(-1-\sqrt{s/m}+\sqrt{1+\delta}\right)^+\right]^2} - e^{-\frac{1}{2}m\left[\left(1-\sqrt{s/m}-\sqrt{1-\delta}\right)^+\right]^2} \tag{2.12}$$

where $(x)^+ = \max\{0, x\}$. We will see later that this bound, which we use as a benchmark, is far from the exact probability.

2.3.2 Exact Eigenvalues Statistics

We propose a method to compute exactly the probability that a Wishart matrix is well conditioned, i.e, its eigenvalues are within a predefined limit. The method is based on the following recent result [66].

Theorem 1. *The probability that all non-zero eigenvalues of the real Wishart matrix* $\mathbf{M} = \mathbf{G}_S^T \mathbf{G}_S$*, where* $\mathbf{G}_S$ *is* $m \times s$ *matrix with entries* $g_{i,j} \sim \mathcal{N}(0,1)$*, are within the interval* $[a,b] \subset [0,\infty)$ *is*

$$\begin{aligned} \psi_{ms}(a,b) &= \mathbb{P}\left\{a \le \lambda_{\min}(\mathbf{M}), \lambda_{\max}(\mathbf{M}) \le b\right\} \\ &= K' \sqrt{\det\left(\mathbf{Q}(a,b)\right)} \end{aligned} \tag{2.13}$$

with the constant

$$K' = \frac{\pi^{s^2}/2}{2^{s\,m/2}\Gamma_s(m/2)\Gamma_s(s/2)}\, 2^{\alpha s + s(s+1)/2} \prod_{\ell=1}^{s} \Gamma\left(\alpha + \ell\right)$$

where $\Gamma_s(a) \triangleq \pi^{s(s-1)/4} \prod_{i=1}^{s} \Gamma(a - (i-1)/2)$*, and* $\alpha = \frac{m-s-1}{2}$*. In* (2.13)*, when* s *is even the elements of the* $s \times s$ *skew-symmetric matrix* $\mathbf{Q}(a,b)$ *are*

$$\begin{aligned} q_{i,j} = \left[P\left(\alpha_j, \frac{b}{2}\right) + P\left(\alpha_j, \frac{a}{2}\right)\right] P\left(\alpha_i; \frac{a}{2}, \frac{b}{2}\right) \\ - \frac{2}{\Gamma(\alpha_i)} \int_{a/2}^{b/2} x^{\alpha+i-1} e^{-x} P(\alpha_j, x)\, dx \end{aligned} \tag{2.14}$$

for $i,j = 1,\ldots,s$*, where* $\alpha_\ell = \alpha + \ell$*. When* s *is odd, the elements of the* $(s+1) \times (s+1)$ *skew-symmetric matrix* $\mathbf{Q}(a,b)$ *are as in* (2.14)*, with the additional elements*

$$\begin{aligned} q_{i,s+1} &= P\left(\alpha_i; \frac{a}{2}, \frac{b}{2}\right) && i = 1,\ldots,s \\ q_{s+1,j} &= -q_{j,s+1} && j = 1,\ldots,s \\ q_{s+1,s+1} &= 0\,. \end{aligned} \tag{2.15}$$

Moreover, the elements $q_{i,j}$ *can be computed iteratively, without numerical integration or series expansion, by Algorithm 1.*

Since the entries of $\mathbf{A}_S$ are distributed as $\mathcal{N}(0, 1/m)$, the exact probability that $\mathbf{A}_S$ is well conditioned is calculated from Theorem 1 as

$$\begin{aligned} P_{sw}(\delta) &= \mathbb{P}\left\{\lambda_{\min}(\mathbf{W}) \ge 1-\delta, \lambda_{\max}(\mathbf{W}) \le 1+\delta\right\} \\ &= \psi_{ms}(m(1-\delta), m(1+\delta)) \end{aligned} \tag{2.16}$$

where $\psi_{ms}(a,b)$ can now be computed exactly from Algorithm 1. The exact expression (2.16) is computationally easy for moderate matrix dimensions (we used it up to $m = 1 \cdot 10^5$ and $s = 150$).

Algorithm 1 $\psi_{ms}(a,b)$ for real Wishart matrices

Input: s, m, a, b
Output: $\psi_{ms}(a,b) = \mathbb{P}\left\{a \leq \lambda_{\min}(\mathbf{M}), \lambda_{\max}(\mathbf{M}) \leq b\right\}$
  $\mathbf{Q} = \mathbf{0}$
  $\alpha_\ell = (m-s-1)/2 + \ell$
  $g(\alpha_\ell, x) = x^{\alpha_\ell} e^{-x}$
  for $i = 1 \to s-1$ **do**
    for $j = i \to s-1$ **do**
      $q_{i,j+1} = q_{i,j} + \frac{\Gamma(\alpha_i+\alpha_j)\, 2^{1-\alpha_i-\alpha_j}}{\Gamma(\alpha_j+1)\Gamma(\alpha_i)} P(\alpha_i + \alpha_j; a, b) - \frac{g(\alpha_j, a/2)+g(\alpha_j, b/2)}{\Gamma(\alpha_j+1)} P\left(\alpha_i; \frac{a}{2}, \frac{b}{2}\right)$
    end for
  end for
  if s is odd **then**
    append to $\mathbf{Q}$ one column according to (2.15) and a zero row
  end if
  $\mathbf{Q} = \mathbf{Q} - \mathbf{Q}^T$
  return $K' \sqrt{\det(\mathbf{Q})}$

2.3.3 Asymmetric Nature of the Extreme Eigenvalues

Clearly, the RIC in (2.6) depends on the deviation of the extreme eigenvalues from unity. It has been shown that the smallest and the largest eigenvalues of Wishart matrices asymptotically deviate from 1 [62]. Hence, the symmetric RIC can not efficiently describe the RIP of Gaussian matrices. Now, it is essential to illustrate whether such asymmetric behavior is still valid for finite measurement matrices. In this regard, we proposed to find the two percentiles $\lambda^*_{\min}(m,s,\eta)$ and $\lambda^*_{\max}(m,s,\eta)$ for the extreme eigenvalues of $\mathbf{W}$, such that

$$\mathbb{P}\left\{\lambda_{\min}(\mathbf{W}) \leq \lambda^*_{\min}(m,s,\eta)\right\} = \mathbb{P}\left\{\lambda_{\max}(\mathbf{W}) \geq \lambda^*_{\max}(m,s,\eta)\right\} = \eta\,.$$

In fact, such percentiles can be calculated form the exact eigenvalues distribution in Theorem 1 as

$$\lambda^*_{\min}(m,s,\eta) = \psi^{-1}_{\min}(\eta), \;\; \lambda^*_{\max}(m,s,\eta) = \psi^{-1}_{\max}(\eta) \tag{2.17}$$

where $\psi^{-1}_{\min}(\eta)$ and $\psi^{-1}_{\max}(\eta)$ are the inverse of $\psi_{ms}(0, m\,x)$ and $\psi_{ms}(m\,x, \infty)$, respectively.

In Fig. 2.1 we report the thresholds $\lambda^*_{\min}(m,s,\eta)$ and $\lambda^*_{\max}(m,s,\eta)$ as a function of s/m, for some finite values of m and a fixed exceeding probability $\eta = 10^{-10}$. We can see that they asymmetrically deviate from unity, as already observed for asymptotic large matrices in [62]. Additionally, since

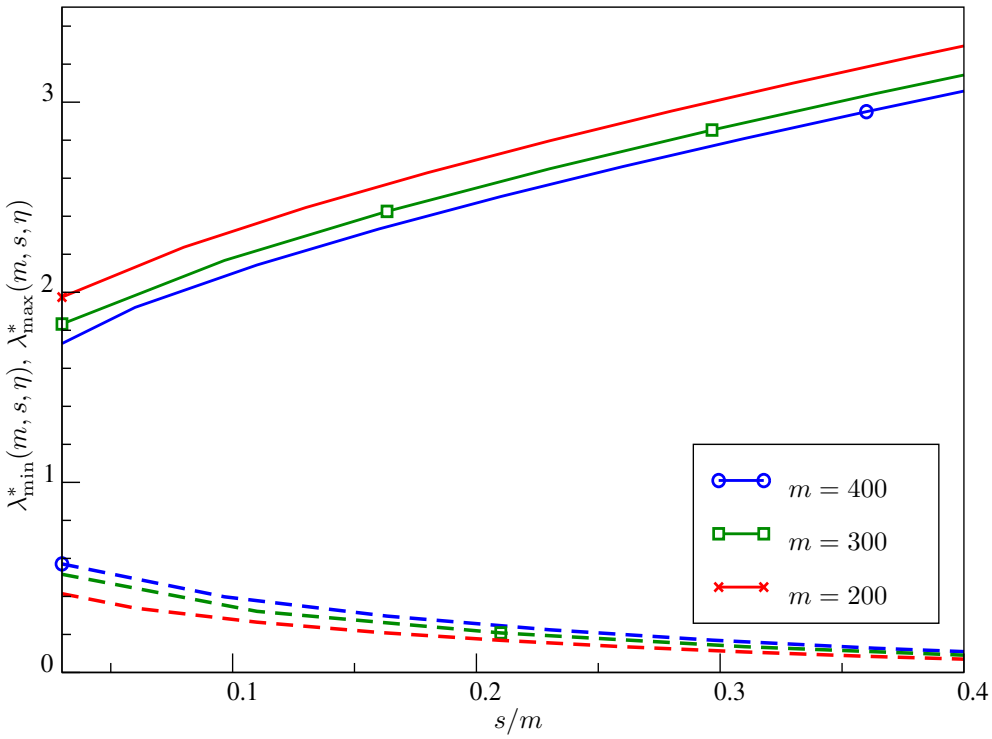

Figure 2.1: The asymmetric extreme eigenvalues thresholds of the Wishart matrix $\mathbf{W}$ as a function of s/m, for $\eta = 10^{-10}$. The lower threshold $\lambda^*_{\min}(m,s,\eta)$ and the upper threshold $\lambda^*_{\max}(m,s,\eta)$ are represented by dashed and solid lines, respectively.

for small values of m the deviation of the extreme eigenvalues from unity is more significant, i.e., the RIC should be larger, the asymptotic tail behavior of the eigenvalues distributions in [62–64] cannot be used for upper bounding the RICs in the finite case.

Definition 2 (ARIC [50,62])**.** The lower restricted isometry constant (LRIC) of order s of $\mathbf{A}$, $\underline{\delta}_s(\mathbf{A})$, is defined as the smallest constant larger than zero that satisfies

$$1-\underline{\delta}_s(\mathbf{A}) \leq \frac{\|\mathbf{A}_S\,\mathbf{c}\|^2}{\|\mathbf{c}\|^2} \quad \forall\,\mathbf{c}\in\mathbb{R}^s, \forall\, S\subset\Omega : \mathrm{card}(S)=s \tag{2.18}$$

and the upper restricted isometry constant (URIC) of order s of $\mathbf{A}$, $\overline{\delta}_s(\mathbf{A})$, is defined as the smallest constant larger than zero that satisfies

$$\frac{\|\mathbf{A}_S\,\mathbf{c}\|^2}{\|\mathbf{c}\|^2} \leq 1+\overline{\delta}_s(\mathbf{A}) \quad \forall\,\mathbf{c}\in\mathbb{R}^s, \forall\, S\subset\Omega : \mathrm{card}(S)=s. \tag{2.19}$$

Clearly, the relation with the symmetric RIC is $\delta_s(\mathbf{A}) = \max\{\underline{\delta}_s(\mathbf{A}), \overline{\delta}_s(\mathbf{A})\}$. Moreover, from Definition 2 and (2.5), we can represent the ARICs as

$$\underline{\delta}_s(\mathbf{A}) = 1 - \min_{\substack{S\subset\Omega \\ \mathrm{card}(S)=s}} \lambda_{\min}(\mathbf{W}) \tag{2.20}$$

$$\overline{\delta}_s(\mathbf{A}) = \max_{\substack{S\subset\Omega \\ \mathrm{card}(S)=s}} \lambda_{\max}(\mathbf{W}) - 1. \tag{2.21}$$

2.4 Symmetric and Asymmetric RICs

The symmetric and asymmetric RICs of a Gaussian matrix can be seen as functions of the extreme eigenvalues of Wishart matrices as in (2.20) and (2.21), and hence are themselves random variables (r.v.s). In this section, we derive at first lower bounds on the probability of satisfying RIP for finite dimensional Gaussian random matrices using the exact eigenvalues distribution, and then a lower bound on the RIC. Additionally, the CDFs of the ARICs are lower bounded using the CDFs of the extreme eigenvalues. Finally, thresholds for ARICs that are not exceeded with a target probability are deduced.

In the following, the analysis derived starting from the exact eigenvalues statistic (2.16) will be referred as the exact eigenvalues distribution (EED) based approach.

2.4.1 RIP Analysis for Gaussian Matrices

A Gaussian matrix is said to satisfy the RIP of order s if its RIC, $\delta_s(\mathbf{A})$, is less than a constant δ with high probability on a random draw of $\mathbf{A}$. In other words, if a sufficient condition for perfect reconstruction using a sparse recovery algorithm is satisfied with high probability. This probability can be lower bounded from (2.8) and (2.16) as

$$\beta(\delta, m, n, s) \geq 1 - \binom{n}{s} \Big[1 - \psi_{ms}\left(m(1-\delta), m(1+\delta)\right) \Big]. \tag{2.22}$$

The expression (2.22) gives, to the best of our knowledge, the tightest lower bound on the probability of satisfying the RIP, $\beta(\delta)$, for finite dimensional Gaussian matrices. This is attributed to employing the exact joint distribution of the extreme eigenvalues of Wishart matrices, providing a quantitatively sharper estimates compared to the concentration bound and the asymptotic approaches.

When applying CS, it is important to estimate the RIC to assess the recovery property of the measurement matrix. Let us define $\delta^*_{s,\min}(m,n,\epsilon)$ as the RIC which is exceeded with probability ϵ, such that

$$\mathbb{P}\{\delta_s(\mathbf{A}) \leq \delta^*_{s,\min}(m,n,\epsilon)\} = 1-\epsilon\,. \tag{2.23}$$

Using (2.22) we can upper bound this value as

$$\delta^*_{s,\min}(m,n,\epsilon) \leq \delta^*_s(m,n,\epsilon) \triangleq \psi^{-1}_{ms}\left(1-\epsilon/\binom{n}{s}\right) \tag{2.24}$$

where $\psi^{-1}_{ms}(y)$ is the inverse of $\psi_{ms}(m(1-x),m(1+x))$. In the following we will refer to $\delta^*_s(m,n,\epsilon)$ in (2.24) as the restricted isometry constant threshold (RICt), where from (2.23) and (2.24) we have

$$\mathbb{P}\{\delta_s(\mathbf{A}) \leq \delta^*_s(m,n,\epsilon)\} \geq 1-\epsilon\,. \tag{2.25}$$

2.4.2 Asymmetric RIP Analysis for Gaussian Matrices

Let $\underline{\delta}_s(\mathbf{A})$ be the LRIC as defined in (2.20). The cumulative distribution function (CDF) of the LRIC, $F_{\ell\text{RIC}}(x)$, is lower bounded as

$$\mathbb{P}\left\{\underline{\delta}_s(\mathbf{A}) \leq x\right\} \geq 1-\binom{n}{s}\left[1-\psi_{ms}\left(m(1-x),\infty\right)\right]. \tag{2.26}$$

In fact, from (2.20) the CDF of the LRIC $\underline{\delta}_s(\mathbf{A})$ is

$$\begin{aligned} F_{\ell\text{RIC}}(x) &= \mathbb{P}\left\{1-\min_{\substack{S\subset\Omega\\ \text{card}(S)=s}} \lambda_{\min}(\mathbf{W}) \;\leq x\right\} \\ &\geq 1-\binom{n}{s}\mathbb{P}\left\{\lambda_{\min}(\mathbf{W}) \leq 1-x\right\} \\ &= 1-\binom{n}{s}\left[1-\psi_{ms}(m\,(1-x),\infty)\right]. \end{aligned} \tag{2.27}$$

Let us define $\underline{\delta}^*_{s,\min}(m,n,\epsilon)$ as the LRIC which is exceeded with probability ϵ, such that

$$\mathbb{P}\{\underline{\delta}_s(\mathbf{A}) \leq \underline{\delta}^*_{s,\min}(m,n,\epsilon)\} = 1-\epsilon\,.$$

This quantity is upper bounded as follows

$$\underline{\delta}^*_{s,\min}(m,n,\epsilon) \leq \underline{\delta}^*_s(m,n,\epsilon) = \psi^{-1}_{ms,\text{lower}}\left(1-\epsilon/\binom{n}{s}\right) \tag{2.28}$$

where $\psi^{-1}_{ms,\text{lower}}(y)$ is the inverse of $\psi_{ms}(m(1-x),\infty)$. In the following we will refer to $\underline{\delta}^*_s(m,n,\epsilon)$ as the lower restricted isometry constant threshold (LRICt).

Similarly, for the CDF of the URIC, $F_{\text{uRIC}}(x)$, we have

$$\begin{aligned}\mathbb{P}\left\{\overline{\delta}_s(\mathbf{A}) \leq x\right\} &\geq 1 - \binom{n}{s}\mathbb{P}\left\{\lambda_{\max}(\mathbf{W}) \geq 1+x\right\} \\ &= 1 - \binom{n}{s}\left[1 - \psi_{ms}(0, m\,(1+x))\right].\end{aligned} \tag{2.29}$$

Then, we can compute a threshold such that $\mathbb{P}\{\overline{\delta}_s(\mathbf{A}) \leq \overline{\delta}^*_{s,\min}(m,n,\epsilon)\} = 1-\epsilon$, which leads to

$$\overline{\delta}^*_{s,\min}(m,n,\epsilon) \leq \overline{\delta}^*_s(m,n,\epsilon) = \psi^{-1}_{ms,\text{upper}}\left(1 - \frac{\epsilon}{\binom{n}{s}}\right) - 1 \tag{2.30}$$

where $\psi^{-1}_{ms,\text{upper}}(y)$ is the inverse of $\psi_{ms}(0, m(1+x))$. In the following we will refer to $\overline{\delta}^*_s(m,n,\epsilon)$ as the upper restricted isometry constant threshold (URICt).

Note that, while previously known approaches refer to infinite dimensional matrices, our analysis accounts for the (always finite) true dimensions of the problem.

2.5 Conditions For Perfect Recovery

In this section, the estimated thresholds for the RICs (both symmetric and asymmetric) of finite matrices are used to quantify the maximum allowed signal sparsity order for various recovery algorithms.

Definition 3 (The maximum sparsity order)**.** Let $\mathbf{A}$ be a random $m \times n$ measurement matrix, s be the signal sparsity order, and $0 < \epsilon < 1$ be an arbitrary constant. The maximum sparsity order, s^*, is the value such that every s-sparse vector with $s < s^*$ can be recovered perfectly with probability P_{PR} at least $1-\epsilon$ on a random draw of $\mathbf{A}$. Then the maximum oversampling ratio, a finite regime version of the asymptotic phase transition function, is defined as s^*/m.

The maximum sparsity order is used to compare the performance of different recovery algorithms and their associated sufficient conditions. As mentioned before, the perfect reconstruction conditions for many sparse recovery algorithms are stated in terms of the RICs [5, 49, 51–60]. We now exploit these conditions to provide a probabilistic framework for the recovery problem.

2.5.1 Symmetric RIC Based Sparse Recovery

About the symmetric RIC, the sufficient condition for perfect signal recovery via ℓ_1-minimization can be represented in a generic form as $\delta_{ks}(\mathbf{A}) < \delta$, where k is a positive integer and δ is a constant. As a consequence, the probability of perfect recovery can be bounded as

$$P_{\mathrm{PR}} \geq \mathbb{P}\left\{\delta_{ks}(\mathbf{A}) < \delta\right\} = \beta(\delta, m, n, ks) \tag{2.31}$$

with the proposed (2.22). Sufficient recovery condition of this class are, e.g., $\delta_s(\mathbf{A}) < 1/3$ [54], $\delta_{2s}(\mathbf{A}) < 0.6246$ [6], etc. Also, the design of the measurements matrix is possible through (2.31), where the minimum number of measurements m can be calculated to ensure perfect recovery with a guaranteed probability. The inverse problem is the calculation of the maximum sparsity order, for a given m and a given n, such that the P_{PR} is at least $1-\epsilon$. For this target we have

$$s^* = \max\left\{s : \beta(\delta, m, n, ks) \geq 1-\epsilon\right\}. \tag{2.32}$$

2.5.2 Asymmetric RIC Based Sparse Recovery

Although the asymmetric RICs are less investigated, it is known that the conditions stated in terms of them lead to tighter bounds for the maximum sparsity order [62]. This is attributed to the asymmetric behavior of the extreme eigenvalues for Wishart matrices as analyzed in section 2.3.3.

A general class of sufficient recovery conditions based on the ARICs has the form

$$\mu(s, \mathbf{A}) \triangleq f\left(\underline{\delta}_{k_1 s}(\mathbf{A}), \overline{\delta}_{k_2 s}(\mathbf{A})\right) < 1 \tag{2.33}$$

where k_1 and k_2 are arbitrary positive integers and $f\left(\underline{\delta}_{k_1 s}(\mathbf{A}), \overline{\delta}_{k_2 s}(\mathbf{A})\right)$ is a non-decreasing function in both $\underline{\delta}_{k_1 s}(\mathbf{A})$ and $\overline{\delta}_{k_2 s}(\mathbf{A})$. In this regard, we propose a generalization of the symmetric RIC based condition, $\delta_s(\mathbf{A}) < \frac{1}{3}$, to an asymmetric one. In particular, if the following condition is satisfied

$$\mu_{\mathrm{ECG}}(s, \mathbf{A}) \triangleq 2\,\underline{\delta}_s(\mathbf{A}) + \overline{\delta}_s(\mathbf{A}) < 1 \tag{2.34}$$

then all s-sparse vectors can be recovered perfectly using ℓ_1-minimization. The condition is obtained by extending the analysis in [54] to account for the asymmetric RICs, as detailed in Appendix A. Other sufficient conditions in the form of (2.33) are found in [50, 67]. For example, it is shown in [50] that if

$$\mu_{\mathrm{FL}}(s, \mathbf{A}) \triangleq \frac{1}{4}\left(1+\sqrt{2}\right)\left(\frac{1+\overline{\delta}_{2s}(\mathbf{A})}{1-\underline{\delta}_{2s}(\mathbf{A})} - 1\right) < 1 \tag{2.35}$$

and in [67] that if

$$\mu_{\text{BT}}(s,\mathbf{A}) \triangleq \underline{\delta}_{2s}(\mathbf{A}) + \frac{1}{4}\left(\underline{\delta}_{6s}(\mathbf{A}) + \overline{\delta}_{6s}(\mathbf{A})\right) < 1$$

then perfect reconstruction is also guaranteed.

Therefore, for random measurement matrices, the probability of perfect recovery by incorporating the ARICs can be bounded as

$$P_{\text{PR}} \geq \mathbb{P}\left\{\mu(s,\mathbf{A}) < 1\right\}. \tag{2.36}$$

For the design problem of calculating the maximum sparsity order, by exploiting the monotonicity of the function $f(\cdot,\cdot)$, we have

$$\begin{aligned}\mathbb{P}\left\{\mu(s,\mathbf{A}) \leq 1\right\} &\geq \mathbb{P}\left\{\underline{\delta}_{k_1 s}(\mathbf{A}) \leq \underline{\delta}^*_{k_1 s}, \overline{\delta}_{k_2 s}(\mathbf{A}) \leq \overline{\delta}^*_{k_2 s}\right\} \\ &\geq 1 - \mathbb{P}\left\{\underline{\delta}_{k_1 s}(\mathbf{A}) \geq \underline{\delta}^*_{k_1 s}\right\} - \mathbb{P}\left\{\overline{\delta}_{k_2 s}(\mathbf{A}) \geq \overline{\delta}^*_{k_2 s}\right\} \end{aligned} \tag{2.37}$$

for any $\underline{\delta}^*_{k_1 s}$ and $\overline{\delta}^*_{k_2 s}$ such that $f\left(\underline{\delta}^*_{k_1 s}, \overline{\delta}^*_{k_2 s}\right) < 1$. Equation (2.37) is due to the union bound, (2.20), and (2.21). Setting the bound (2.37) to $1-\eta$ and distributing equally the probability on the lower and upper RICs, we get

$$\mathbb{P}\left\{\overline{\delta}_{k_2 s}(\mathbf{A}) \leq \overline{\delta}^*_{k_2 s}\right\} = \mathbb{P}\left\{\underline{\delta}_{k_1 s}(\mathbf{A}) \leq \underline{\delta}^*_{k_1 s}\right\} = 1 - \frac{\eta}{2}. \tag{2.38}$$

Finally, the maximum sparsity order s^* is the maximum s compatible with $f\left(\underline{\delta}^*_{k_1 s}, \overline{\delta}^*_{k_2 s}\right) < 1$, where $\underline{\delta}^*_{k_1 s}, \overline{\delta}^*_{k_2 s}$ are calculated from (2.28) and (2.30) with $\epsilon = \eta/2$ to satisfy (2.38). Then, every sparse vector with $s < s^*$ can be perfectly recovered with probability at least $1-\eta$ on a random draw of $\mathbf{A}$.

Although we focused on ℓ_1-minimization based recovery, the same approach can be used to estimate the maximum sparsity order using greedy or thresholding algorithms. For example, sufficient conditions on the RIC for perfect recovery using compressive sampling matching pursuit (CoSaMP), orthogonal matching pursuit (OMP), and IHT are $\delta_{4s}(\mathbf{A}) < 0.4782$ [6], $\delta_{13s}(\mathbf{A}) < 0.1666$ [6,60], and $\delta_{3s}(\mathbf{A}) < 0.5773$ [68], respectively. Additionally, asymmetric RIC based conditions have been obtained in [69] for CoSaMP, IHT, and subspace pursuit (SP). For example,

$$\mu_{\text{BCTT}}(s,\mathbf{A}) \triangleq 2\sqrt{2}\left(\frac{\overline{\delta}_{3s}(\mathbf{A}) + \underline{\delta}_{3s}(\mathbf{A})}{2 + \overline{\delta}_{3s}(\mathbf{A}) - \underline{\delta}_{3s}(\mathbf{A})}\right) < 1$$

is a sufficient condition for perfect recovery using IHT [69].

2.6 Robust Recovery of Compressible Signals

Up to now, we have studied the case of perfect recovery of sparse data in noiseless setting. However, in practice signals can also be not exactly sparse, but rather compressible, i.e., the data is well approximated by a sparse signal. Moreover, noise can be present during the acquisition process.

A measure of the discrepancy between a compressible signal and its sparse representation is the ℓ_1-error of best s-term approximation $\sigma_s(\mathbf{x})_1$, defined as

$$\sigma_s(\mathbf{x})_1 \triangleq \inf\{\|\mathbf{x}-\mathbf{x}_s\|_1, \quad \mathbf{x}_s \in \mathbb{R}^n \text{ is } s\text{-sparse}\}\,. \tag{2.39}$$

Hence, a signal is well approximated by an s-sparse vector if $\sigma_s(\mathbf{x})_1$ is small [6]. Besides considering compressible signals, we can also include the measurement noise in the model, so that the measured vector can be written as

$$\mathbf{y} = \mathbf{A}\mathbf{x} + \mathbf{z} \tag{2.40}$$

where $\mathbf{z}$ is a bounded noise with $\|\mathbf{z}\| \leq \kappa$. Assuming κ is known, we can account for the noise term by modifying the constraint in the ℓ_1-minimization problem (2.3) as

$$\hat{\mathbf{x}} = \arg\min \|\mathbf{x}\|_1 \text{ subject to } \|\mathbf{y}-\mathbf{A}\mathbf{x}\| \leq \kappa\,. \tag{2.41}$$

This algorithm is called quadratically constrained ℓ_1-minimization [70]. There are also other algorithms for sparse recovery in noisy cases, e.g., Dantzig selector [71], basis pursuit denoising [72], denoising-orthogonal approximate message passing [73], etc.

For the model illustrated in (2.40), we cannot guarantee perfect signal recovery, but rather an approximate reconstruction can be assured with bounded error. For example, it was shown in [54] that if $\delta_s(\mathbf{A}) < 1/3$, the error after recovery can be bounded by a weighted combination of κ and $\sigma_s(\mathbf{x})_1$, i.e.,

$$\|\hat{\mathbf{x}}-\mathbf{x}\| \leq C_1\kappa + C_2\frac{\sigma_s(\mathbf{x})_1}{\sqrt{s}} \tag{2.42}$$

where

$$C_1\left(\delta_s(\mathbf{A})\right) = \frac{\sqrt{8\left(1+\delta_s(\mathbf{A})\right)}}{1-3\delta_s(\mathbf{A})} \tag{2.43}$$

$$C_2\left(\delta_s(\mathbf{A})\right) = \frac{\sqrt{8}\left(2\delta_s(\mathbf{A}) + \sqrt{\left(1-3\delta_s(\mathbf{A})\right)\delta_s(\mathbf{A})}\right)}{1-3\delta_s(\mathbf{A})} + 2\,. \tag{2.44}$$

The constants C_1 and C_2 give an insight about both the robustness (ability to handle noise) and the stability (ability to handle compressible signals) of the recovery algorithm, respectively.

When $\mathbf{A}$ is a random matrix, both C_1 and C_2 are random variables. To characterize their statistical distribution, we propose to find a bound on the threshold $C^*_{i,\min}$, with $i = 1, 2$, which is not exceeded with a predefined probability ϵ_i, i.e.,

$$\mathbb{P}\left\{C_i\left(\delta_s(\mathbf{A})\right) \leq C^*_{i,\min}\right\} = 1 - \epsilon_i\,. \tag{2.45}$$

Noting that $C_i\left(\delta_s(\mathbf{A})\right)$ is monotonically increasing in $\delta_s(\mathbf{A})$, we have

$$\mathbb{P}\left\{C_i\left(\delta_s(\mathbf{A})\right) \leq C_i\left(\delta^*_s(m,n,\epsilon_i)\right)\right\} = \mathbb{P}\left\{\delta_s(\mathbf{A}) \leq \delta^*_s(m,n,\epsilon_i)\right\} \geq 1-\epsilon_i \tag{2.46}$$

where the RICt $\delta^*_s(m,n,\epsilon_i)$ can be calculated from (2.24). Consequently, from (2.45) and (2.46) we upper bound $C^*_{i,\min}$ as

$$C^*_{i,\min} \leq C^*_i \triangleq C_i\left(\delta^*_s(m,n,\epsilon_i)\right). \tag{2.47}$$

The inverse problem is finding the maximum sparsity order, for a given m and a given n, such that the r.v. C_i, with $i = 1, 2$, is less than a targeted constant c_i with probability at least $1 - \epsilon_i$. For this aim we have

$$s^* = \max\left\{s : C_i\left(\delta^*_s(m,n,\epsilon_i)\right) \leq c_i\right\}.$$

Analogous results relating the recovery error with $\sigma_s(\mathbf{x})_1$ and κ have been obtained for different algorithms under suitable symmetric and asymmetric RIC based sufficient conditions [50, 69, 74–76]. By following the same approach, the proposed methodology can be applied to describe the statistics of the stability and robustness constants also for these cases.

2.7 Tracy-Widom Based RIC Analysis

Although the proposed framework based on the exact distribution of the eigenvalues (2.16) provides tight bounds on the RICs, it could be computationally expensive for large matrices, for which easier approaches are preferred.

In this section, we derive approximations for the RICs of finite matrices based on the TW distribution, much tighter than those obtained from concentration of measure inequalities. Also, we study the convergence rate of the distribution of extreme eigenvalues to those based on the TW by exploiting the small deviation analysis of the extreme eigenvalues around their mean.

In particular, we prove that TW based distributions approximate the eigenvalues statistics of finite Gaussian matrices with exponentially small error in m, leading to accurate estimation of the RICs.

In fact, it is well known that the distribution of the smallest and largest eigenvalues of Wishart matrices tend, under some conditions, to a properly scaled and shifted TW distributions [77–83]. Specifically, it has been shown that for the real Wishart matrix $\mathbf{M}$ when $m, s \to \infty$ and $m/s \to \gamma \in (0, \infty)$

$$\frac{\lambda_{\max}(\mathbf{M}) - \mu_{ms}}{\sigma_{ms}} \xrightarrow{\mathcal{D}} \mathcal{TW}_1 \tag{2.48}$$

where $\mathcal{TW}_1$ is a Tracy-Widom r.v. of order 1 with complementary cumulative distribution function (CCDF) $\Psi_{\text{TW1}}(t)$, $\mu_{ms} = \left(\sqrt{m} + \sqrt{s}\right)^2$, and $\sigma_{ms} = \sqrt{\mu_{ms}}(1/\sqrt{s} + 1/\sqrt{m})^{1/3}$ [79]. More precisely, from the convergence in distribution definition and letting $\rho \triangleq s/m$ we have

$$\begin{aligned}
&\lim_{m \to \infty} \mathbb{P}\left\{\lambda_{\max}(\mathbf{M}) \geq \mu_{ms} + t\,\sigma_{ms}\right\} = \\
&\lim_{m \to \infty} \mathbb{P}\left\{\lambda_{\max}(\mathbf{W}) \geq (1 + \sqrt{\rho})^2 + t\, m^{-\frac{2}{3}}\, \rho^{-\frac{1}{6}}\, (1 + \sqrt{\rho})^{\frac{4}{3}}\right\} = \Psi_{\text{TW1}}(t).
\end{aligned} \tag{2.49}$$

Similarly, for the smallest eigenvalue, when $m, s \to \infty$ and $m/s \to \gamma \in (1, \infty)$ [82]

$$-\frac{\ln \lambda_{\min}(\mathbf{M}) - v_{ms}}{\tau_{ms}} \xrightarrow{\mathcal{D}} \mathcal{TW}_1 \tag{2.50}$$

with scaling and centering parameters

$$\tau_{ms} = \frac{\left((s - 1/2)^{-1/2} - (m - 1/2)^{-1/2}\right)^{1/3}}{\sqrt{m - 1/2} - \sqrt{s - 1/2}}$$

$$v_{ms} = 2 \ln\left(\sqrt{m - 1/2} - \sqrt{s - 1/2}\right) + \frac{1}{8}\tau_{ms}^2.$$

Regarding the RIC analysis for finite Gaussian matrices, let $\overline{\delta}_s^*(m, n, \epsilon)$, $\underline{\delta}_s^*(m, n, \epsilon)$, and $\delta_s^*(m, n, \epsilon)$ be the restricted isometry constant thresholds as defined in (2.30), (2.28), and (2.24), respectively. We will show that they can be approximated as

$$\overline{\delta}_s^*(m, n, \epsilon) \simeq \overline{\delta}_{\text{TW}}^* \triangleq \rho + 2\sqrt{\rho} + m^{-\frac{2}{3}} \rho^{-\frac{1}{6}} (1 + \sqrt{\rho})^{\frac{4}{3}}\, \Psi_{\text{TW1}}^{-1}\left(\epsilon / \binom{n}{s}\right) \tag{2.51}$$

$$\underline{\delta}_s^*(m, n, \epsilon) \simeq \underline{\delta}_{\text{TW}}^* \triangleq 1 - \frac{1}{m} \exp\left(v_{ms} - \tau_{ms} \Psi_{\text{TW1}}^{-1}\left(\epsilon / \binom{n}{s}\right)\right) \tag{2.52}$$

$$\delta_s^*(m, n, \epsilon) \simeq \delta_{\text{TW}}^* \triangleq \widetilde{P}_{sw}^{-1}\left(1 - \epsilon / \binom{n}{s}\right) \tag{2.53}$$

for $\overline{\delta}^*_{\rm TW}$, $\underline{\delta}^*_{\rm TW}$, and $\delta^*_{\rm TW}$ less than one, where $\Psi^{-1}_{\rm TW1}(y)$ is the inverse of the TW's CCDF and $\widetilde{P}^{-1}_{sw}(y)$ is the inverse of

$$\widetilde{P}_{sw}(x) \triangleq 1 - \Psi_{\rm TW1}\left(\frac{v_{ms} - \ln m(1-x)}{\tau_{ms}}\right) - \Psi_{\rm TW1}\left(\frac{m(1+x)-\mu_{ms}}{\sigma_{ms}}\right). \quad (2.54)$$

In order to prove these formulas, at first the convergence rate of the extreme eigenvalue distributions to those based on the TW is provided. For the URIC, it has been shown in [84, Theorem 2] that there exists a constant $c > 0$, depending only on ρ, such that

$$\mathbb{P}\left\{\lambda_{\max}(\mathbf{M}) \geq \mu_{ms}(1+z)\right\} \leq c \exp\left(-\frac{1}{c}\, s\, z^{\frac{3}{2}}\right) \quad (2.55)$$

for all $m > s \geq 1$ and $0 < z \leq 1$. This small deviation analysis provides tighter bounds compared to the concentration inequality (2.10) and Edelman bound [65, Lemma 4.2] used for large m in [62–64]. From (2.55), the L.H.S. of (2.49) can be tightly bounded for finite m and for $t \leq m^{2/3}\rho^{1/6}\left(1+\sqrt{\rho}\right)^{2/3}$ as

$$\mathbb{P}\left\{\lambda_{\max}(\mathbf{W}) \geq (1+\sqrt{\rho})^2 + t\, m^{-\frac{2}{3}}\, \rho^{-\frac{1}{6}}\, (1+\sqrt{\rho})^{\frac{4}{3}}\right\} \leq c \exp\left(-\, c_1\, t^{\frac{3}{2}}\right) \quad (2.56)$$

where $c_1 \triangleq c^{-1}\, \rho^{3/4}\left(1+\sqrt{\rho}\right)^{-1}$. Regarding the R.H.S, for sufficiently large t we have

$$\Psi_{\rm TW1}(t) \leq c_2 \exp\left(-c_3\, t^{\frac{3}{2}}\right) \quad (2.57)$$

where $c_2 > 0$ and $c_3 > 0$ are constants [85, eq. (2)], [86]. Now the error in using the TW can be bounded as

$$\left|\mathbb{P}\left\{\lambda_{\max}(\mathbf{W}) \geq (1+\sqrt{\rho})^2 + t\, m^{-\frac{2}{3}}\, \rho^{-\frac{1}{6}}\, (1+\sqrt{\rho})^{\frac{4}{3}}\right\} - \Psi_{\rm TW1}(t)\right| \leq c_4 \exp\left(-c_5\, t^{\frac{3}{2}}\right) \quad (2.58)$$

where $c_4 = \max\{c, c_2\}$ and $c_5 = \min\{c_1, c_3\}$. Therefore, the error due to approximating $\mathbb{P}\left\{\lambda_{\max}(\mathbf{W}) \geq 1+x\right\}$ in (2.29) by that of the TW can be bounded from (2.58) as

$$\left|\mathbb{P}\left\{\lambda_{\max}(\mathbf{W}) \geq 1+x\right\} - \Psi_{\rm TW1}\left(\left(x - 2\sqrt{\rho} - \rho\right) m^{\frac{2}{3}}\, \rho^{\frac{1}{6}}\, (1+\sqrt{\rho})^{-\frac{4}{3}}\right)\right| \leq c_4 \exp\left(-m\left(x - 2\sqrt{\rho} - \rho\right)^{\frac{3}{2}} c_5\, \rho^{\frac{1}{4}}\, (1+\sqrt{\rho})^{-2}\right) \quad (2.59)$$

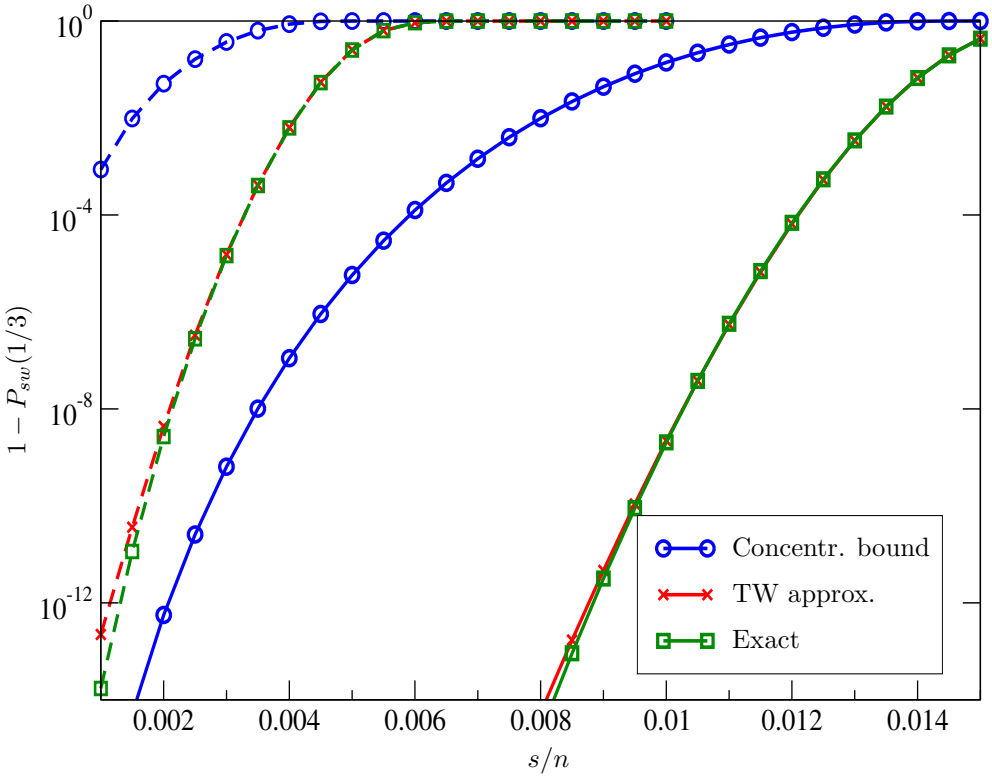

Figure 2.2: The probability that a measurement submatrix $\mathbf{A}_S$ is ill conditioned, $1-\mathbb{P}\left\{1-\delta\leq\lambda_{\min}(\mathbf{A}_S^T\mathbf{A}_S),\lambda_{\max}(\mathbf{A}_S^T\mathbf{A}_S)\leq 1+\delta\right\}$, with $\delta=1/3$, as a function of the sparsity ratio, s/n, for compression ratios $m/n=0.2$ (dashed) and $m/n=0.6$ (solid). The signal dimension is $n=10^4$.

for $x\leq 2\left(1+\sqrt{\rho}\right)^2-1$.[1] Hence, the absolute error in approximating the exact probability with that based on the TW distribution is exponentially small in m and the URICt can be approximated by (2.51). A similar reasoning can be used to derive the thresholds for the lower and symmetric RICs (the proof is not reported here for the sake of conciseness).

Finally, we would like to remark that Tracy-Widom based approaches could be used not only for Gaussian ensembles, but also for a wider class of matrices like those drawn from some sub-Gaussian distributions, e.g., Rademacher and Bernoulli measurement matrices. This is motivated by the universality of the TW laws for the extreme eigenvalues of large random matrices [87, 88], although further research is required to investigate such extensions.

[1]Note that $x\leq 1$ is a stronger condition than $x\leq 2\left(1+\sqrt{\rho}\right)^2-1$.

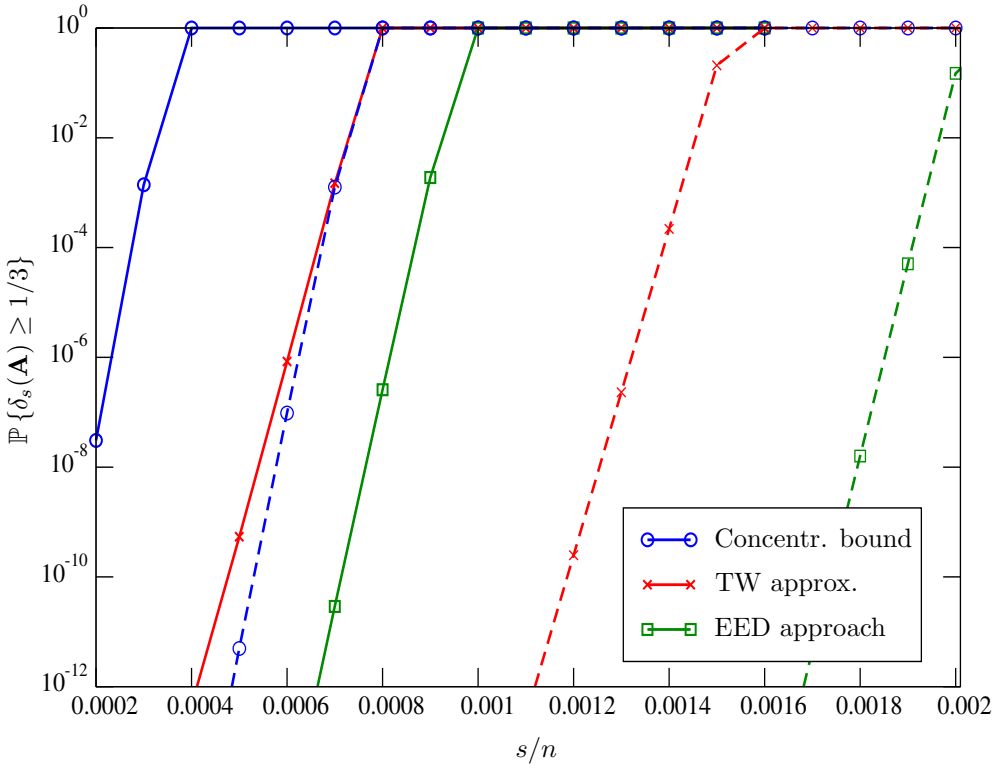

Figure 2.3: Symmetric RIP: upper bounds on the probability of not satisfying the RIP, $\mathbb{P}\{\delta_s(\mathbf{A}) \geq 1/3\}$, for $m/n = 0.4$ (solid) and $m/n = 0.8$ (dashed). The signal dimension is $n = 10^4$. Curves obtained through the concentration bound, (2.8) and (2.12), the EED, (2.22), and the TW approximation, (2.8) and (2.54).

2.8 Numerical Results

In this section, numerical results are presented to compare the proposed exact and TW approaches with the concentration inequalities, for analyzing at first the probability that the measurement submatrices are well conditioned, and then that the RIP is satisfied. Moreover, the statistics of the RICs, the probability of perfect reconstruction, the maximum sparsity order for various recovery algorithms, and the robustness and stability constants are also investigated. In all numerical results, the signal dimension has been fixed to $n = 10^4$, unless otherwise stated.

First, the dependence between the probability that a submatrix is ill conditioned, $1 - P_{sw}(\delta)$, and the sparsity ratio, s/n, is examined. In particular, in Fig. 2.2 the exact probability obtained from Theorem 1 (2.16), TW approximation (2.54), and concentration of measure bound (2.12) are compared

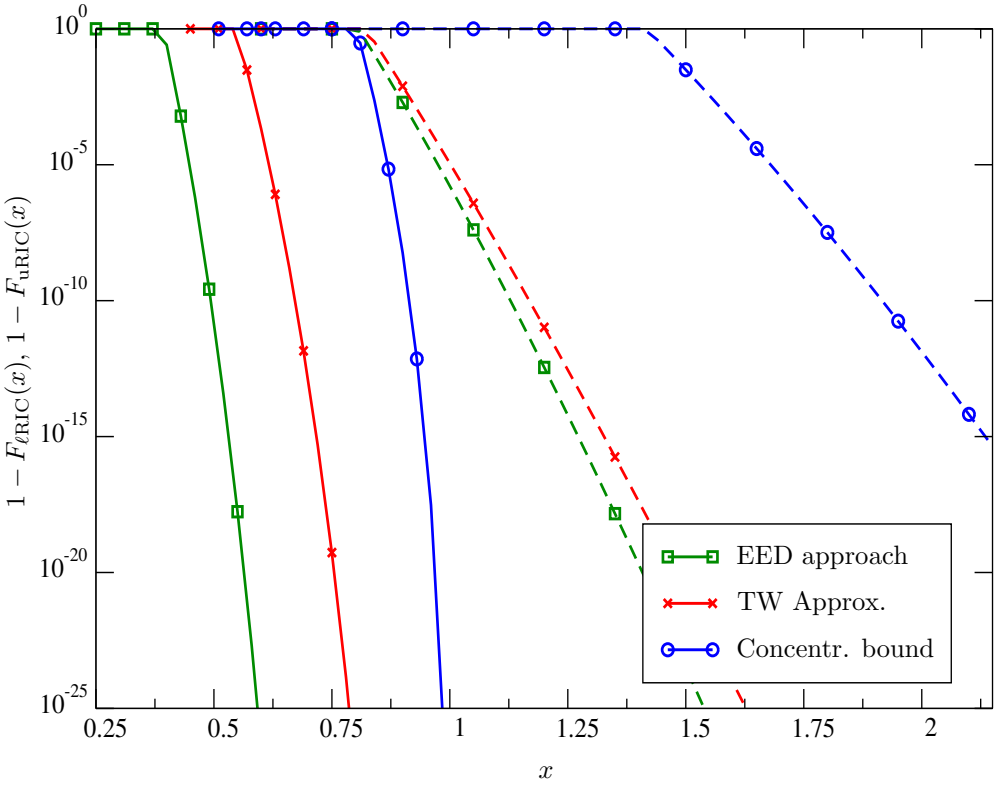

Figure 2.4: Asymmetric RICs: upper bounds on the CCDFs of the LRIC (solid) and URIC (dashed), for $m = 300$, $n = 600$, and $s = 5$.

as a function of the sparsity ratio. We observe that the TW approximation is almost coincident with the exact probability, while the well-known concentration bound is quite loose (about 8 orders of magnitude at $s/n = 0.002$ and $m/n = 0.2$).

Fig. 2.3 shows upper bounds on the probability of not satisfying the RIP, $\mathbb{P}\{\delta_s(\mathbf{A}) \geq 1/3\}$, using the EED based approach (2.22), the TW approximation (2.8), (2.54), and the concentration bound (2.8), (2.12). Note that when the sparsity level is beyond some threshold value, the probability of not satisfying the RIP rapidly increases from zero to one. This figure also illustrates the limit on the maximum sparsity ratio that still permits satisfying the RIP with a targeted probability. We can see that the EED based approach indicates higher sparsity ratios (less sparse vectors) compared to those estimated by the concentration bound (more than 250% increase in s/n when the probability is 10^{-6} and $m/n = 0.4$).

Considering the statistics of the ARICs, upper bounds on their complementary CDFs (CCDFs) are shown in Fig. 2.4, for $m = 300$, $n = 600$, and $s = 5$, using the EED, TW approximation, and concentration bound. Note

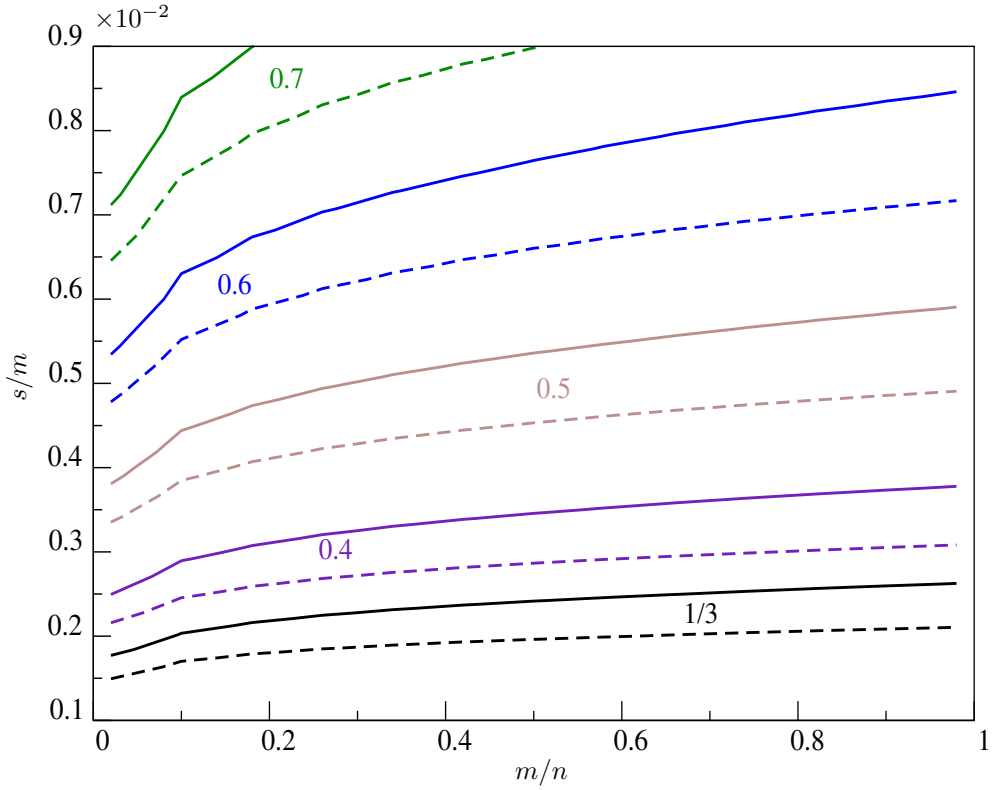

Figure 2.5: Level sets of the symmetric restricted isometry constant threshold, using the EED, $\delta_s^*(m,n,\epsilon)$ (solid), for $m = 2000$ and $\epsilon = 10^{-2}$, and the asymptotic bound in [63] $\delta_{\text{BT}}\,(s/m, m/n)$ (dashed).

that the proposed methods provide tighter bounds compared to the concentration inequality (more than 20 orders of magnitude).

In Fig. 2.5, we compare the asymptotic RIC, $\delta_{\text{BT}}\,(s/m, m/n)$, presented in [63, Definition 2.2] with that obtained by the proposed method (2.24), for $\epsilon = 10^{-2}$, $m = 2000$, and n from 10^5 to 2000. We can see that the asymptotic approach overestimates the RIC, with respect to the proposed EED analysis, and consequently leads to pessimistic results for the maximum allowable sparsity order. For example, this sparsity underestimation is in the order of 20% for the sufficient condition $\delta_s(\mathbf{A}) < 1/3$ (black curves).

Regarding the ARICs, the URIC thresholds, $\overline{\delta}_s^*(m,n,\epsilon)$, computed by means of (2.30) and (2.51), are plotted in Fig. 2.6 for an excess probability $\epsilon = 10^{-3}$, as a function of the compression ratio, m/n, and the oversampling ratio, s/m. In this figure, we set $m = 4000$ and vary n from $2 \cdot 10^5$ to 4000. As can be noticed the TW approximation is quite accurate.

In Fig. 2.7 we report the proposed lower restricted isometry constant

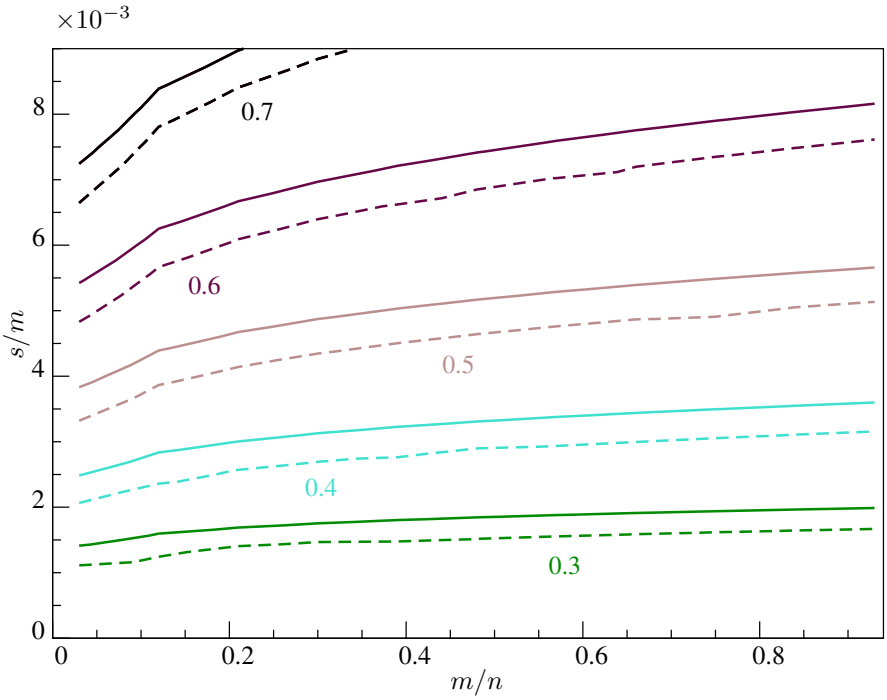

Figure 2.6: Level sets of the URICt $\overline{\delta}_s^*(m, n, \epsilon) \in \{0.3, 0.4, 0.5, 0.6, 0.7\}$, using the EED (solid) and TW (dashed), for $m = 4000$ and $\epsilon = 10^{-3}$.

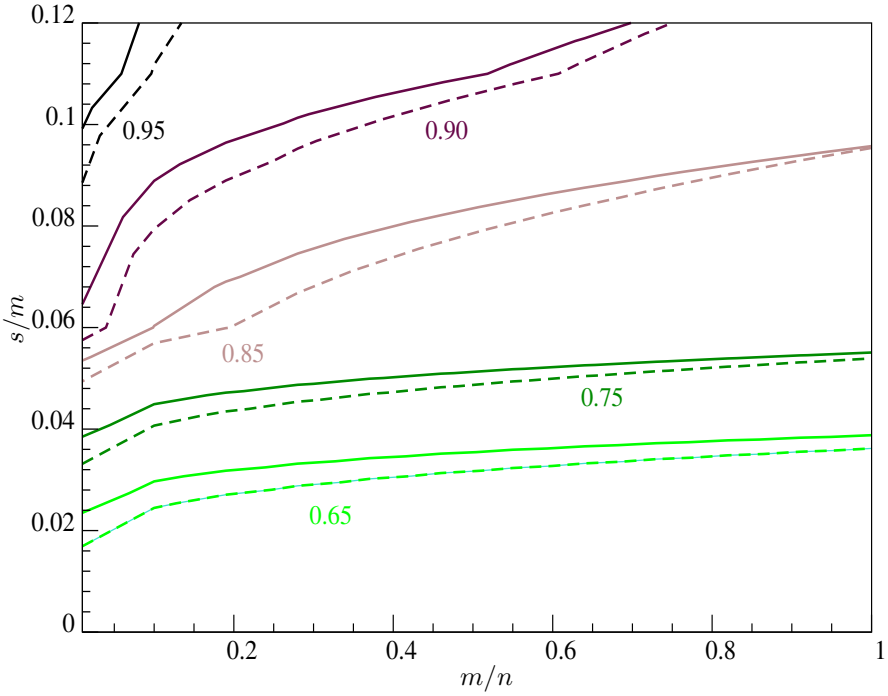

Figure 2.7: Level sets of the LRICt using the EED (solid) and TW (dashed) approaches, for $m = 200$ and $\epsilon = 10^{-3}$.

Table 2.1: The RIC thresholds using the EED bound and TW approximation for $\epsilon = 10^{-2}$, empirical averaged lower bounds [89], BCT [62], and BT [63] approaches, for $m = 2000$ and $s = 4$. For each m/n, the two rows give the upper and lower RIC.

$m/n \downarrow$	Finite			Asymptotic	
	EED upper bounds (2.30), (2.28)	TW approx. (2.51), (2.52)	Empirical lower bounds [89]	BCT [62]	BT [63]
0.4	0.3071	0.3395	0.2703	0.3408	0.3402
	0.2561	0.2846	0.2322	0.2777	0.2772
0.6	0.3000	0.3304	0.2626	0.3344	0.3337
	0.2512	0.2778	0.2268	0.2734	0.2729
0.8	0.2949	0.3239	0.2580	0.3297	0.3291
	0.2477	0.2729	0.2214	0.2703	0.2698

thresholds using EED and TW based methods given by (2.28) and (2.52). We can see that the TW approximation provides accurate results also for this case.

To further investigate the RIC bounds, we report in Table 2.1 both the LRIC and URIC thresholds for different m/n using various approaches: the proposed EED (2.28), (2.30), the TW approximation (2.52), (2.51), the empirical lower bounds in [89], and the asymptotic bounds in [62], [63]. We can see that the upper bounds on the RICs obtained from the EED approach is sharp, with small differences from the empirical lower bounds (averaged over 100 different realizations) indicated by [89].

With the aim of comparing different sufficient recovery conditions via ℓ_1-minimization, IHT, and CoSaMP algorithms, in Fig. 2.8 we report the maximum oversampling ratio, s^*/m, such that $P_{\text{PR}} \geq 0.999$. All curves have been obtained by using the EED based approach. Specifically, for ℓ_1-minimization we consider the symmetric RIC condition $\delta_s(\mathbf{A}) \leq 1/3$ [54], its relaxed asymmetric extension $\mu_{\text{ECG}}(s, \mathbf{A}) < 1$ proposed in Section 2.5.2,

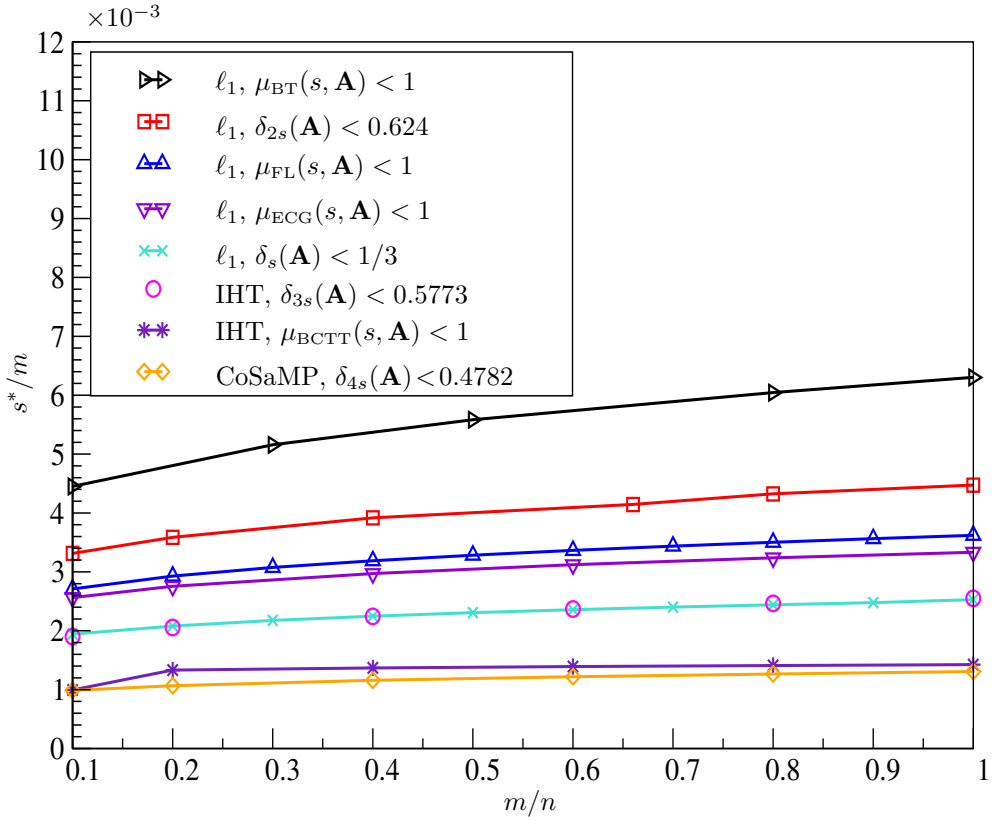

Figure 2.8: The maximum oversampling ratio, s^*/m, for various recovery algorithms and their associated sufficient conditions using the proposed EED based approach, for $m = 4000$ and $P_{\text{PR}} \geq 0.999$ ($\eta = 10^{-3}$).

$\delta_{2s}(\mathbf{A}) < 0.624$ [6], $\mu_{\text{FL}}(s, \mathbf{A}) < 1$ [50], and $\mu_{\text{BT}}(s, \mathbf{A}) < 1$ [67]. For IHT we used the conditions $\delta_{3s}(\mathbf{A}) < 0.5773$ [68] and $\mu_{\text{BCTT}}(s, \mathbf{A}) < 1$ [69], while for the CoSaMP we considered $\delta_{4s}(\mathbf{A}) < 0.4782$ [6]. We can see that the asymmetric conditions provide higher estimates of the sparsity which can be handled by compressed sensing, compared to the symmetric conditions (more than 40% increase in s). As known, the ℓ_l-minimization and IHT algorithms allow higher oversampling ratios than the CoSaMP algorithm.

Moreover, we provide in Fig. 2.9 the maximum oversampling ratio, for uniform recovery, indicated by our proposed approach along with those obtained from the polytope [47], Null space [6, Theorem 9.29], geometric functional [45, Theorem 4.1], and RIP [6, Theorem 9.27] analyses for finite matrices with $m = 4000$ and $P_{\text{PR}} \geq 0.5$. However, we would like to note that the polytope based approach suggests tighter bounds on the maximum sparsity order, as it fully exploits the geometry of the ℓ_1-minimization for signal

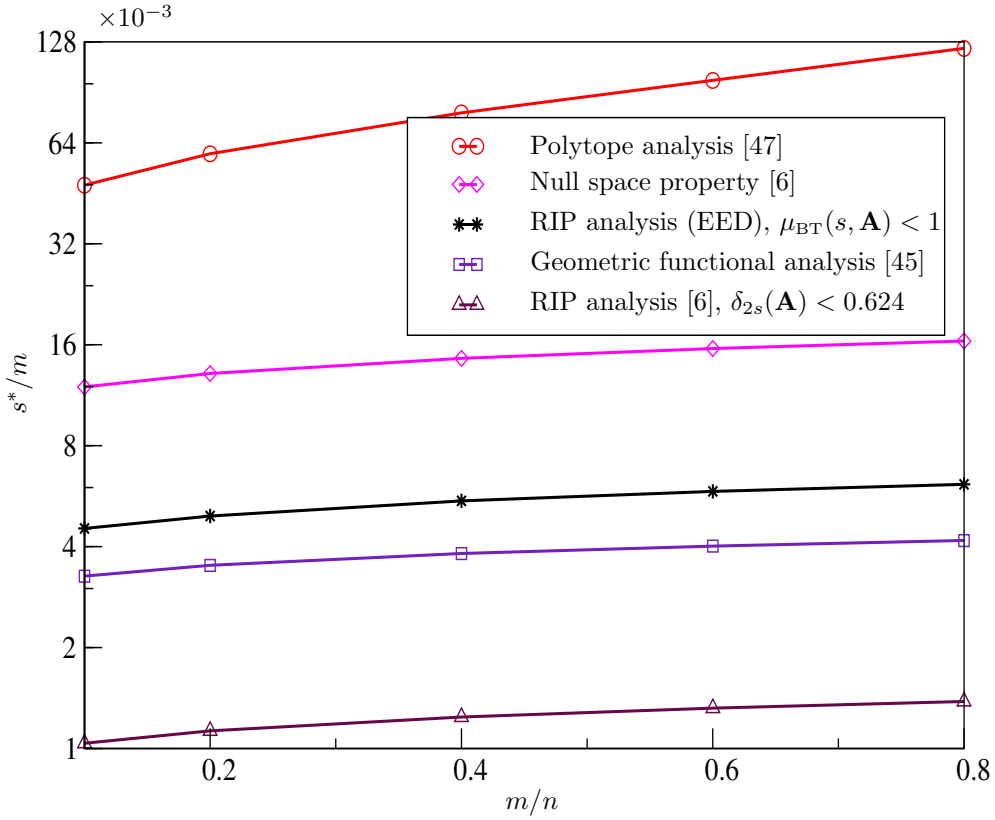

Figure 2.9: The maximum oversampling ratio, s^*/m, for perfect recovery via ℓ_1-minimization, estimated by the proposed RIP based approach (EED) along with the RIP [6], polytope [47], Null space [6], and geometric functional [45] analyses, for $m = 4000$ and $P_{\text{PR}} \geq 0.5$.

recovery from Gaussian measurements. On the other hand, the RIP is suitable for analyzing the robust and stable reconstruction with several sparse recovery algorithms, such as optimization, greedy, and thresholding.

Finally, regarding the analysis for compressible signals in noise, the contours for robustness and stability thresholds C_1^* and C_2^* are shown in Fig. 2.10. As can be seen for small s/m the thresholds are small, indicating that the more sparse is the signal, the more robust and stable is the reconstruction process. Therefore, a compromise between sparsity and robustness/stability should be considered when designing the acquisition system. This figure also gives the maximum oversampling ratio for a given m and n, such that the minimization program (2.41) can approximately recover the measured signal with a predefined discrepancy.

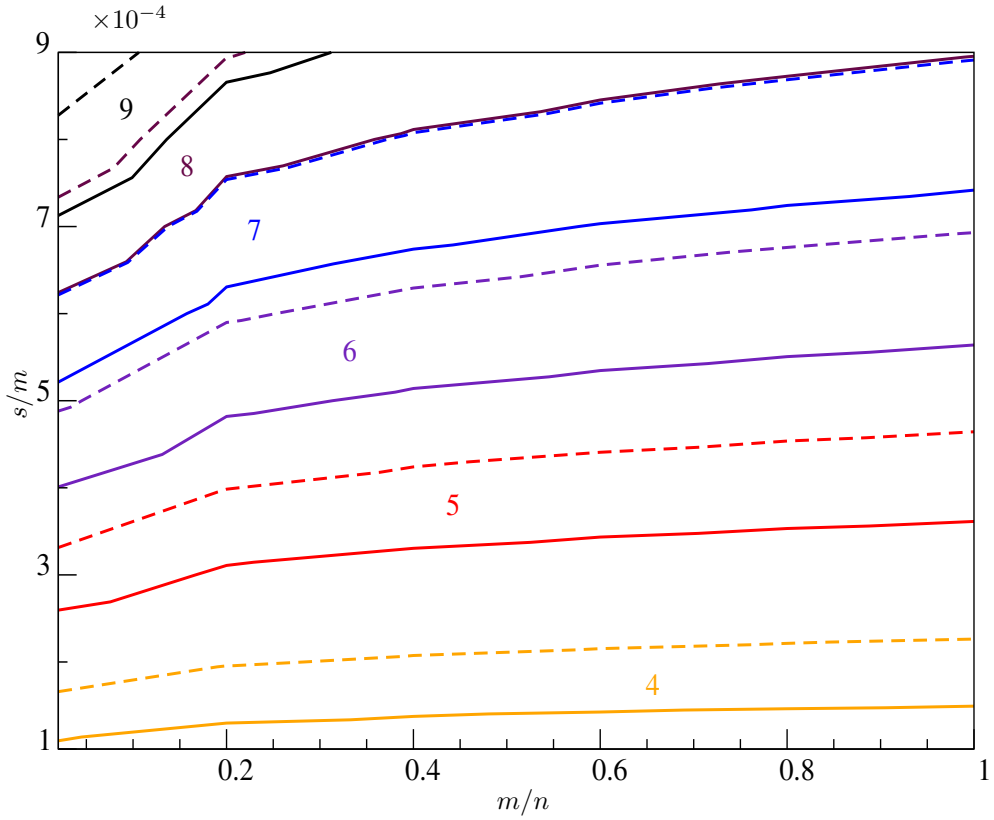

Figure 2.10: Level sets of robustness and stability thresholds in Section 2.6, C_1^* (solid) and C_2^* (dashed), with C_1^*, $C_2^* \in \{4, 5, 6, 7, 8, 9\}$, for $m = 2 \cdot 10^4$ and $\epsilon_1 = \epsilon_2 = 10^{-3}$, using the EED based approach.

2.9 Conclusion

For sparse data acquisition we have found that the concentration of measure inequality provides a loose upper bound on the probability that a measurement submatrix is ill conditioned. For example, in some cases it overestimate the maximum sparsity ratio by over 250% with respect to the proposed exact eigenvalues based approach. For finite matrices, by tightly bounding the symmetric and asymmetric RICs, the best current lower bound on the maximum sparsity order guaranteeing successful recovery has been provided, for various sparse reconstruction algorithms. For stable and robust recovery of compressible data, we have noticed that when the sparsity order decreases the discrepancy between the recovered and original signals reduces. Finally, we have shown that simple approximations for the RICs can be obtained based on TW distributions.

Chapter 3

Weak RIC Analysis of Finite Gaussian Matrices for Joint Sparse Recovery

3.1 Introduction

The problem of simultaneously acquiring multiple signals is important for IoT networks, where a huge number of nodes are involved. It has been shown that a significant performance gain can be achieved by exploiting additional signal structure, besides the traditional sparsity of signals in some domain discussed in Chapter 2 [90,91]. For example, the data generated from multiple sensors within dense IoT networks tend to be jointly sparse, i.e., different sparse signals share a common support.

On the contrary of the reconstruction of a sparse signal from a SMV analyzed in Chapter 2, CS for multiple measurement vectors (MMV) considers the acquisition and the recovery of an s-row sparse matrix $\mathbf{X} \in \mathbb{R}^{n\times\ell}$ with support S (i.e., only $s \ll n$ rows of $\mathbf{X}$ indexed by S are nonzero) from $\mathbf{Y} \in \mathbb{R}^{m\times\ell}$ linear measurements

$$\mathbf{Y} = \mathbf{A}\mathbf{X} \tag{3.1}$$

where $\mathbf{A} \in \mathbb{R}^{m\times n}$ is the measurement matrix and $m < n$ [90–103]. There exists a unique s-row sparse matrix satisfying (3.1) under the sufficient and necessary condition $m \geq 2s + 1 - \text{rank}(\mathbf{X})$ [102]. This matrix can be found by minimizing the ℓ_0 quasi-norm of $\mathbf{X}$, but this problem has been shown to be NP-hard [104]. Nevertheless, for the special full rank case with $\ell \geq s$, $\mathbf{X}$ can be recovered from the same minimum sufficient measurements, $s+1$, via the polynomial time algorithm MUSIC [95, 105, 106].

Regarding the rank defective case $\ell < s$, $\mathbf{X}$ can be uniquely recovered, from a larger number of measurements, using greedy algorithms [95–101] or via the following mixed $\ell_{2,1}$-minimization program

$$\text{minimize} \|\mathbf{X}\|_{2,1} \qquad \text{subject to} \quad \mathbf{AX} = \mathbf{Y} \tag{3.2}$$

where $\|\mathbf{X}\|_{2,1} = \sum_{j=1}^{n} \|\mathbf{x}^j\|$ with $\|\mathbf{x}^j\|$ indicating the ℓ_2 norm of the jth row of $\mathbf{X}$ [92–94]. Sufficient conditions for joint sparse recovery in terms of the RIC are provided in [100, 101]. The RIC indicates how well a linear transformation preserves distances between sparse vectors, as illustrated in Chapter 2. Unfortunately, the RIC based approach provides a worst case analysis, which does not depend on ℓ.[1] Therefore, it cannot explain the advantage due to the availability of multiple measurements. Instead, an average case guarantee was proposed in [94], where the probability of recovery failure is exponentially small in ℓ when a condition on the so-called weak restricted isometry constant (WRIC) is satisfied. For instance, considering $\mathbf{A}_S$ as the submatrix of $\mathbf{A}$ with columns indexed by the matrix support S, the WRIC tells how close is the column space of $\mathbf{A}_S$ to that spanned by another disjoint set of columns with cardinality r [31]. The WRIC can provide statements considering the recovery of *a random sparse vector*, e.g., the probability that a random vector can be recovered. Hence, it falls within the framework of average-case (non-uniform) analysis.

In fact, sufficient recovery conditions for various joint reconstruction algorithms are based on the WRIC, e.g., $\ell_{2,1}$-minimization [94], SA-Music [95], and OSMP [96]. The WRIC for Gaussian matrices has been bounded using concentration of measure inequalities and the union bound [94–96]. However, this approach results in a large overestimation of the WRIC leading to an underestimation of the maximum achievable s.

This chapter provides a probabilistic analysis of the WRIC for finite Gaussian matrices. The proposed approach relies on the exact distribution of the extreme eigenvalues for Wishart matrices or on its gamma approximation based on TW's laws. In particular, we derive a tight lower bound on the CDF of the WRICs and on the probability of satisfying an arbitrary recovery condition, much tighter than those based on the concentration inequalities. Moreover, we propose a unified framework to quantify the recovery limits of joint sparse reconstruction algorithms with WRIC based sufficient conditions, for both noiseless and noisy measurements. More precisely, the analysis estimates the maximum support cardinality of row sparse matrices (jointly sparse signals), such that a target probability of recovery is assured.

[1] The RIC based methods are considered as worst-case (uniform) analysis, providing the recovery guarantee for *all* sparse vectors.

Then, the unified approach is applied to theoretically assess the reconstruction through three algorithms, i.e., $\ell_{2,1}$, SA-Music, and OSMP. Finally, we provide sufficient conditions in terms of the asymmetric WRICs permitting recovery with higher s, compared to those obtained through the symmetric WRIC.

Throughout the chapter, $|\cdot|$ denotes the cardinality of a set, $\|\cdot\|$ indicates the ℓ_2-norm of a vector or the spectral norm of a matrix, $\mathbf{a}_k$ is the kth column of a matrix $\mathbf{A}$, $P(a,x) = 1/\Gamma(a)\int_0^x t^{a-1}e^{-t}dt$ is the regularized lower incomplete gamma function, $(\cdot)^\dagger$ is the pseudoinverse, and $\mathbf{P}_{\mathcal{X}}$ denotes the projection matrix on the subspace $\mathcal{X}$.

3.2 WRIC and Eigenvalues Statistics

In this section, we describe the problem and provide the mathematical tools needed to analyze the WRICs. In particular, a generalization of the WRIC considering lower and upper asymmetric constants is reported below.

Definition 4 (The asymmetric weak restricted isometry constants [31, 95])**.** Let $\mathbf{A}$ be an $m \times n$ matrix, $S \subset \Omega \triangleq \{1, 2, ..., n\}$ be a set of indexes with $|S| = s$, the lower weak restricted isometry constant (LWRIC) and the upper weak restricted isometry constant (UWRIC), $\underline{\delta}_1(\mathbf{A}, s)$ and $\overline{\delta}_1(\mathbf{A}, s)$, are the smallest constants such that the inequalities

$$1 - \underline{\delta}_1(\mathbf{A}, s) \leq \frac{\|\mathbf{A}\mathbf{v}\|^2}{\|\mathbf{v}\|^2} \leq 1 + \overline{\delta}_1(\mathbf{A}, s) \tag{3.3}$$

are satisfied for all $\mathbf{v} \in \mathbb{R}^n$ with support $S \cup T$ where $T \subset \Omega/S$ is any set with $|T| \leq r$. The symmetric WRIC defined as $\delta_1(\mathbf{A}, s) \triangleq \max\{\underline{\delta}_1(\mathbf{A}, s), \overline{\delta}_1(\mathbf{A}, s)\}$ simultaneously satisfies both inequalities.

We aim to upper bound the WRICs of Gaussian measurement matrices, so that joint sparse recovery is guaranteed with predefined probability. Hence, the statistics of WRICs should be calculated. Let us start from the Rayleigh quotient inequality for the ratio in (3.3), for a fixed set T

$$\lambda_{\min}(\mathbf{A}_Z^T\mathbf{A}_Z) \leq \frac{\|\mathbf{A}_Z\,\mathbf{v}_Z\|^2}{\|\mathbf{v}\|^2} \leq \lambda_{\max}(\mathbf{A}_Z^T\mathbf{A}_Z) \tag{3.4}$$

where $Z \triangleq S \cup T$, $\mathbf{A}_Z$ is the $m \times z$ submatrix with $z \triangleq |Z| = s + r$, and $\lambda_{\min}(\mathbf{A}_Z^T\mathbf{A}_Z)$ and $\lambda_{\max}(\mathbf{A}_Z^T\mathbf{A}_Z)$ are the minimum and maximum eigenvalues

of the Wishart matrix, respectively. Therefore, from (3.4) and accounting for all possible sets of T, the asymmetric WRICs can be

$$\underline{\delta}_1(\mathbf{A}, s) = 1 - \min_{T,|T|=r} \lambda_{\min}(\mathbf{A}_Z^T \mathbf{A}_Z) \tag{3.5}$$

$$\overline{\delta}_1(\mathbf{A}, s) = \max_{T,|T|=r} \lambda_{\max}(\mathbf{A}_Z^T \mathbf{A}_Z) - 1. \tag{3.6}$$

The WRICs of Gaussian matrices are functions of the extreme eigenvalues of the corresponding Wishart matrices, and thus are themselves r.v.s.

In order to study the exact distribution of extreme eigenvalues we use the framework developed in [66]. Hereafter, we consider $\mathbf{A}$ with i.i.d. entries drawn from a zero-mean Gaussian distribution with variance $1/m$. The exact CDFs of the extreme eigenvalues of $\mathbf{A}_Z^T \mathbf{A}_Z$ are calculated as

$$\mathbb{P}\left\{\lambda_{\min}(\mathbf{A}_Z^T \mathbf{A}_Z) \le x\right\} = 1 - \psi\left(m\,x, \infty\right) \tag{3.7}$$

$$\mathbb{P}\left\{\lambda_{\max}(\mathbf{A}_Z^T \mathbf{A}_Z) \le x\right\} = \psi\left(0, m\,x\right) \tag{3.8}$$

where $\psi(a, b)$ is the probability that all eigenvalues of a Wishart matrix are within the interval (a, b), computed by Algorithm 1 in Chapter 2. The exact expressions (3.7) and (3.8) are computationally easy for moderate matrix dimensions. For larger dimensions, the exact CDFs can be approximated, based on TW's laws [79], by shifted and scaled gamma distributions [66]

$$\begin{aligned}\mathbb{P}\left\{\lambda_{\min}(\mathbf{A}_Z^T \mathbf{A}_Z) \le x\right\} &\simeq \tilde{\psi}_{\text{lower}}(x) \\ &\triangleq 1 - P\left(k, \frac{(\alpha - (\ln(m\,x) - v)/\tau)^+}{\theta}\right)\end{aligned} \tag{3.9}$$

$$\mathbb{P}\left\{\lambda_{\max}(\mathbf{A}_Z^T \mathbf{A}_Z) \le x\right\} \simeq \tilde{\psi}_{\text{upper}}(x) \triangleq P\left(k, \frac{(\alpha + (m\,x - \mu)/\sigma)^+}{\theta}\right) \tag{3.10}$$

where $k = 46.446$, $\theta = 0.186$, $\alpha = 9.848$, $\mu = \left(\sqrt{m} + \sqrt{z}\right)^2$, $\sigma = \sqrt{\mu}(1/\sqrt{z} + 1/\sqrt{m})^{1/3}$, $x^+ = \max\{x, 0\}$, and

$$\tau = \frac{\left((z - 1/2)^{-1/2} - (m - 1/2)^{-1/2}\right)^{1/3}}{\sqrt{m - 1/2} - \sqrt{z - 1/2}}$$

$$v = 2\ln\left(\sqrt{m - 1/2} - \sqrt{z - 1/2}\right) + \tau^2/8\,.$$

Alternatively, since the TW distribution can also be approximated by its asymptotic tail expansion [107], $P(k, z)$ in (3.9) and (3.10) can be replaced by

$$\widetilde{P}\,(z) \triangleq 1 - \frac{1}{4\sqrt{\pi}}(z\theta - \alpha)^{\frac{3}{4}} e^{-\frac{2}{3}(z\theta - \alpha)^{\frac{3}{2}}} \quad \text{for } z > \frac{\alpha}{\theta}$$

whenever simpler expressions for WRICs are preferable.

It can be verified from the exact distributions that the extreme eigenvalues asymmetrically deviate from unity. Hence, the asymmetric analysis leads to more accurate description of the WRICs, as previously noticed for the RIC in Chapter 2.

3.3 WRIC Analysis for Gaussian Matrices

We derive at first lower bounds on the CDFs of the WRICs using the exact distributions of the extreme eigenvalues and their gamma approximation. Then, we deduce the weak restricted isometry constant thresholdss which are not exceeded with a target probability.

Specifically, the CDF of the LWRIC is lower bounded from (3.5) and (3.7) by[2]

$$F_{\mathrm{LWRIC}}(x) \triangleq 1 - \binom{n-s}{r} \left[1 - \psi\left(m\ (1-x), \infty\right)\right] \tag{3.11a}$$

$$\simeq 1 - \binom{n-s}{r} \tilde{\psi}_{\mathrm{lower}}(1-x) \tag{3.11b}$$

where the binomial coefficient is from the union bound to account for all possible sets T with $|T| = r$, and (3.11b) is based on (3.9). Let us define the LWRIC threshold (LWRICt), $\underline{\delta}_r^*(s,\epsilon)$, such that

$$\mathbb{P}\{\underline{\delta}_r(\mathbf{A}, s) \leq \underline{\delta}_r^*(s,\epsilon)\} \geq 1 - \epsilon \tag{3.12}$$

is satisfied. Then, from (3.11) and (3.12), it can be estimated as

$$\underline{\delta}_r^*(s,\epsilon) = \psi_{mz,\mathrm{lower}}^{-1}\left(1 - \frac{\epsilon}{\binom{n-s}{r}}\right) \tag{3.13a}$$

$$\simeq 1 - \frac{1}{m}\exp\left(\tau\left[\alpha - \theta P^{-1}\left(k, 1 - \frac{\epsilon}{\binom{n-s}{r}}\right)\right] + v\right) \tag{3.13b}$$

where $\psi_{\mathrm{lower}}^{-1}(y)$ is the inverse of $\psi(m(1-x), \infty)$.

Similarly, the CDF of the UWRIC is lower bounded by

$$F_{\mathrm{UWRIC}}(x) \triangleq 1 - \binom{n-s}{r}[1 - \psi\left(0, m(1+x)\right)] \tag{3.14a}$$

$$\simeq 1 - \binom{n-s}{r}[1 - \tilde{\psi}_{\mathrm{upper}}(1+x)]. \tag{3.14b}$$

[2]The set S is replaced by s in the notation, as the WRICs of i.i.d. random matrices statistically depend on the cardinality rather than the set itself.

Accordingly, the UWRIC threshold (UWRICt) is

$$\overline{\delta}_r^*(s,\epsilon) = \psi_{mz,\text{upper}}^{-1}\left(1 - \frac{\epsilon}{\binom{n-s}{r}}\right) \tag{3.15a}$$

$$\simeq \frac{\sigma}{m}\left[\theta\, P^{-1}\left(k, 1 - \frac{\epsilon}{\binom{n-s}{r}}\right) - \alpha\right] + \frac{\mu}{m} - 1 \tag{3.15b}$$

where $\psi_{mz,\text{upper}}^{-1}(y)$ is the inverse of $\psi(0, m(1+x))$.

Analogously, the CDF of the symmetric WRIC can be lower bounded by

$$F_{\text{WRIC}}(x) \triangleq 1 - \binom{n-s}{r}\left[1 - \psi\left(m(1-x), m(1+x)\right)\right] \tag{3.16a}$$

$$\simeq 1 - \binom{n-s}{r}\left[1 + \tilde{\psi}_{\text{lower}}(1-x) - \tilde{\psi}_{\text{upper}}(1+x)\right] \tag{3.16b}$$

where for (3.16b) we applied the union bound to $1 - \psi(a,b)$. Following the same reasoning, the symmetric weak restricted isometry constant thresholds can be derived as $\delta_r^*(s,\epsilon) = F_{\text{WRIC}}^{-1}(1-\epsilon)$.

3.4 Unified Framework for Recovery Assessment

In this section, the WRIC thresholds are used to quantify the maximum s, denoted $\widehat{s}$, permitting recovery with a target probability. Let us consider the recovery of a random row sparse matrix $\mathbf{X}$ with support cardinality s, acquired through a random measurement matrix $\mathbf{A}$. In general, for a given $\mathbf{A}$, if a sufficient condition stated usually in the form [31, 94–96]

$$f_{\text{c}}\left(\underline{\delta}_1(\mathbf{A}, s), \overline{\delta}_1(\mathbf{A}, s)\right) < 1 \tag{3.17}$$

is fulfilled, then recovery is guaranteed with probability $P_{\text{r|c}}$ depending on the distribution of $\mathbf{X}$.[3] Since $\mathbf{A}$ is random, the sufficient condition (3.17) is satisfied with some probability $P_{\text{c}}^{\mathbf{A}}$, and recovery is ensured with probability at least

$$P_{\text{r}} = P_{\text{r|c}}\, P_{\text{c}}^{\mathbf{A}}. \tag{3.18}$$

In order to find $\widehat{s}$ satisfying $P_{\text{r}} \geq \eta$ for a given $P_{\text{r|c}}$, we need to ensure that $P_{\text{c}}^{\mathbf{A}} \geq \eta / P_{\text{r|c}}$. Hence, we propose to substitute the WRICs in (3.17) with

[3] Note that $f_{\text{c}}\left(\underline{\delta}_1, \overline{\delta}_1\right)$ is a non-decreasing function in both $\underline{\delta}_1$ and $\overline{\delta}_1$.

the WRICts (3.13) and (3.15). Then, $\widehat{s}$ can be calculated as the maximum s compatible with $f_{\rm c}(\underline{\delta}_1^*(\mathbf{A},s,\epsilon),\overline{\delta}_1^*(\mathbf{A},s,\epsilon))<1$, where ϵ is derived to meet the required $P_{\rm c}^{\mathbf{A}}$. By exploiting the monotonicity of $f_{\rm c}(\cdot,\cdot)$ and the union bound, $1-P_{\rm c}^{\mathbf{A}}$ can be upper bounded by

$$\begin{aligned}\mathbb{P}\left\{f_{\rm c}\left(\underline{\delta}_1(\mathbf{A},\widehat{s}),\overline{\delta}_1(\mathbf{A},\widehat{s})\right)\geq f_{\rm c}\left(\underline{\delta}_1^*(\widehat{s},\epsilon),\overline{\delta}_1^*(\widehat{s},\epsilon)\right)\right\}\\ \leq \mathbb{P}\left\{\underline{\delta}_1(\mathbf{A},\widehat{s})\geq\underline{\delta}_1^*(\widehat{s},\epsilon)\right\}+\mathbb{P}\left\{\overline{\delta}_1(\mathbf{A},\widehat{s})\geq\overline{\delta}_1^*(\widehat{s},\epsilon)\right\}\leq 2\,\epsilon.\end{aligned}$$

So the goal $P_{\rm r}\geq\eta$ is fulfilled for

$$\epsilon=\epsilon\big(\eta,P_{\rm r|c}\big)=\frac{1}{2}-\frac{\eta}{2\,P_{\rm r|c}}. \tag{3.19}$$

In the following, we investigate the performance of three reconstruction methods (i.e., $\ell_{2,1}$-minimization, SA-Music, and OSMP), when $\mathbf{X}$ is a sparse Gaussian matrix and $\mathbf{A}$ is Gaussian with normalized columns [94–96].[4]

3.4.1 Perfect Recovery from Noiseless Measurements

The first example considers the reconstruction via $\ell_{2,1}$-minimization program, for which it has been proved that if

$$\left\|\mathbf{A}_S^{\dagger}\,\mathbf{a}_k\right\|<\alpha<1,\qquad\forall k\notin S \tag{3.20}$$

then the matrix $\mathbf{X}$ can be recovered via (3.2) with probability at least $P_{\rm r|c}(\alpha)\triangleq 1-n\exp(-\ell(\alpha^{-2}+2\log\alpha)/2-1)$ [94]. Condition (3.20) is expressed in terms of the WRIC as [94]

$$\frac{\delta_1(\mathbf{A},s)}{1-\delta_1(\mathbf{A},s)}<\alpha. \tag{3.21}$$

We propose relaxing condition (3.21) to a milder one (i.e., easily satisfied for larger s). Applying properties of the spectral norm to (3.20) and considering (3.5), we get

$$\begin{aligned}\left\|\mathbf{A}_S^{\dagger}\,\mathbf{a}_k\right\|\leq\delta_1(\mathbf{A},s)\,\left\|(\mathbf{A}_S^*\mathbf{A}_S)^{-1}\right\|&\leq\frac{\delta_1(\mathbf{A},s)}{\lambda_{\min}(\mathbf{A}_S^*\mathbf{A}_S)}\\ &\leq\frac{\delta_1(\mathbf{A},s)}{1-\underline{\delta}_0(\mathbf{A},s)}<\alpha.\end{aligned} \tag{3.22}$$

[4]For large m, the ℓ_2-norm of each column of $\mathbf{A}$ is approximately one.

Since $\underline{\delta}_0(\mathbf{A}, s) \leq \underline{\delta}_1(\mathbf{A}, s) \leq \delta_1(\mathbf{A}, s)$, the left hand side of (3.22) is less than that of (3.21), leading to higher estimates of $\widehat{s}$.

Now, following the outlined procedure, the maximum s satisfying the sufficient condition

$$\frac{\delta_1^* \left(\mathbf{A}, s, \epsilon \left(\eta, P_{\mathrm{r|c}}(\alpha)\right)\right)}{1 - \underline{\delta}_0^* \left(\mathbf{A}, s, \epsilon \left(\eta, P_{\mathrm{r|c}}(\alpha)\right)\right)} < \alpha$$

denoted by $\breve{s}(\alpha)$, can be found for a given α. Finally, a tighter upper bound on the maximum support cardinality is obtained by maximizing over α as

$$\widehat{s} = \max_{0<\alpha<1} \breve{s}(\alpha).$$

3.4.2 Robust Support Estimation from Noisy Measurements

In the presence of noisy measurements, (3.1) becomes

$$\mathbf{Y} = \mathbf{A}\mathbf{X} + \mathbf{Z} \tag{3.23}$$

where $\mathbf{Z}$ represents the noise. Approximate recovery of $\mathbf{X}$ may consist of a joint support estimation followed by signal reconstruction through the resulting overdetermined system.

For example, the support can be estimated via SA-Music algorithm given that a sufficient condition on WRICs, on the form of (3.17), is satisfied [95]. More precisely, denoting the signal subspace by $\mathcal{X}$, let $\widehat{\mathcal{R}}$ and $\widehat{\mathcal{X}}$ be $\hat{\ell}$-dimensional subspaces of $\mathbb{R}^m$ and $\mathcal{X}$, respectively, with $\|\mathbf{P}_{\widehat{\mathcal{R}}} - \mathbf{P}_{\widehat{\mathcal{X}}}\| \leq \kappa$.[5] Then, SA-Music applied to $\widehat{\mathcal{R}}$ recovers the support if

$$\sqrt{\frac{1 - \underline{\delta}_1(\mathbf{A}, s)}{1 + \overline{\delta}_1(\mathbf{A}, s)}} \, \frac{\sqrt{\hat{\ell}/s}\,\sqrt{1 - \underline{\delta}_1(\mathbf{A}, s)} - \sqrt{\underline{\delta}_1(\mathbf{A}, s)}}{2 + \sqrt{\hat{\ell}/s}\,\sqrt{1 - \underline{\delta}_1(\mathbf{A}, s)} - \sqrt{\underline{\delta}_1(\mathbf{A}, s)}} > \kappa\,. \tag{3.24}$$

Alternatively, if support estimation is performed via OSMP, the sufficient condition is [96]

$$\underline{\delta}_1(\mathbf{A}, s) < 1 - \max\left\{4\,\kappa(1-\kappa), \left[\frac{1}{1 + \hat{\ell}/s}\left(2\kappa\sqrt{\hat{\ell}/s} + \sqrt{1 + \hat{\ell}/s - 4\,\kappa^2}\right)\right]^2\right\}. \tag{3.25}$$

[5] $\|\mathbf{P}_{\widehat{\mathcal{R}}} - \mathbf{P}_{\widehat{\mathcal{X}}}\|$ is bounded with high probability for Gaussian noise [95].

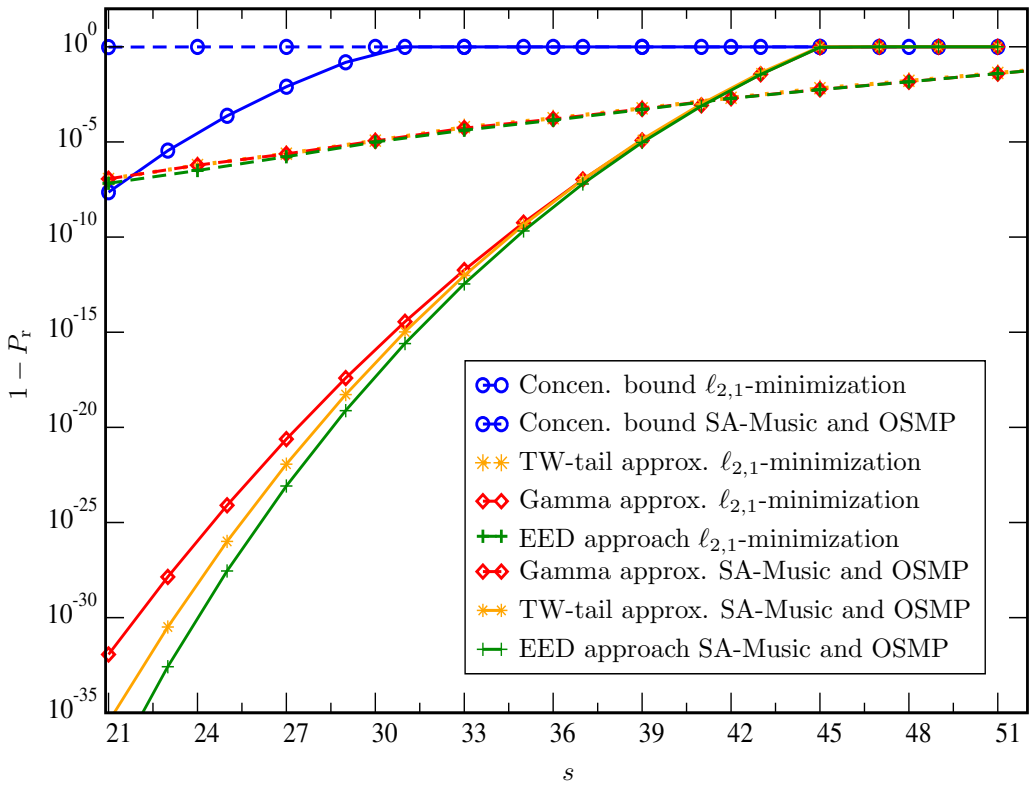

Figure 3.1: Upper bounds on the probability of recovery failure using the proposed approaches and concentration bound for various algorithms, with $n = 2m = 6000$, $\ell = 20$, and $\kappa = 0$.

Note that the probability of exact support recovery via SA-Music and OSMP is greater than the probability of satisfying (3.24) and (3.25), respectively (i.e., $P_{\mathrm{r|c}} = 1$). We would like to note also that (3.24) and (3.25) relax the recovery conditions in [95] and [96] by utilizing the asymmetric WRICs. The original formulas in [95] and [96] can be obtained by substituting $\underline{\delta}_1(\mathbf{A}, s)$ and $\overline{\delta}_1(\mathbf{A}, s)$ with $\delta_1(\mathbf{A}, s)$.

3.5 Numerical Results

In this section, numerical results are presented to investigate the WRICs and the estimated maximum sparsity order for various recovery algorithms. Note that the analysis based on the exact extreme eigenvalue statistics (3.7) and (3.8) will be referred as the EED.

Fig. 3.1 shows upper bounds on the probability of reconstruction failure derived from the concentration of measure in [95, Proposition 6.1], along with

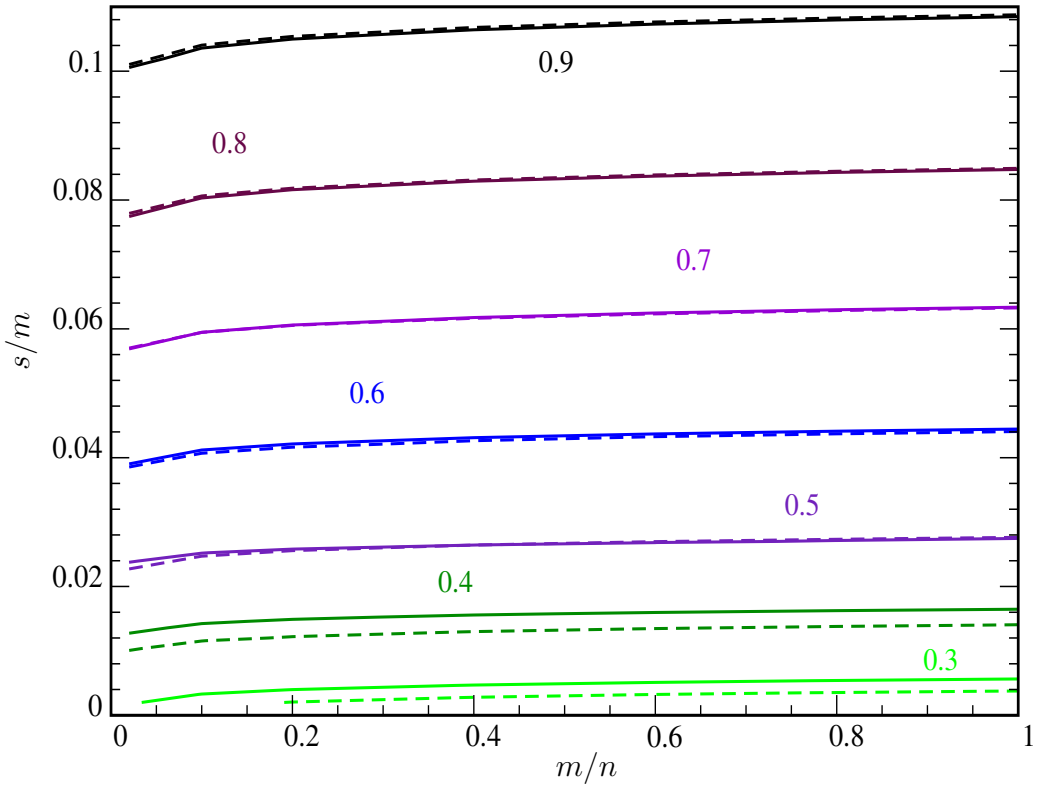

Figure 3.2: Level sets of the UWRIC threshold $\overline{\delta}_1(\mathbf{A}, s, 10^{-3}) \in \{0.3, \ldots, 0.9\}$ using the EED (solid) and gamma approximation (dashed), for $m = 3000$.

the EED bound and gamma and TW tail expansion based approximations. The analysis is based on the sufficient recovery conditions via SA-Music and OSMP and via $\ell_{2,1}$-minimization (3.21). It results that the proposed methods provide tighter bounds compared to the concentration inequalities (many orders of magnitude). Also, the gamma and TW approximations well describe the exact eigenvalues based analysis (overlapped for $1 - P_{\mathrm{r}} \geq 10^{-10}$). Moreover, the theoretical performance of SA-Music and OSMP are coincident, as they have the same condition for the noiseless case.[6] Additionally, they have better performance for small s, while the $\ell_{2,1}$-minimization is superior at higher s.

Fig. 3.2 plots the contours of the UWRIC thresholds calculated by means of the EED and gamma approximation (3.15). As can be seen the gamma approximation is quite accurate, and provides tight upper bounds on the UWRIC thresholds for small values, relevant to sparse recovery.

[6]Note that both the conditions in (3.24) and (3.25) reduce to $\delta_1(\mathbf{A}, s) \leq \ell/(s + \ell)$ in the noiseless case ($\kappa = 0$, $\hat{\ell} = \ell$).

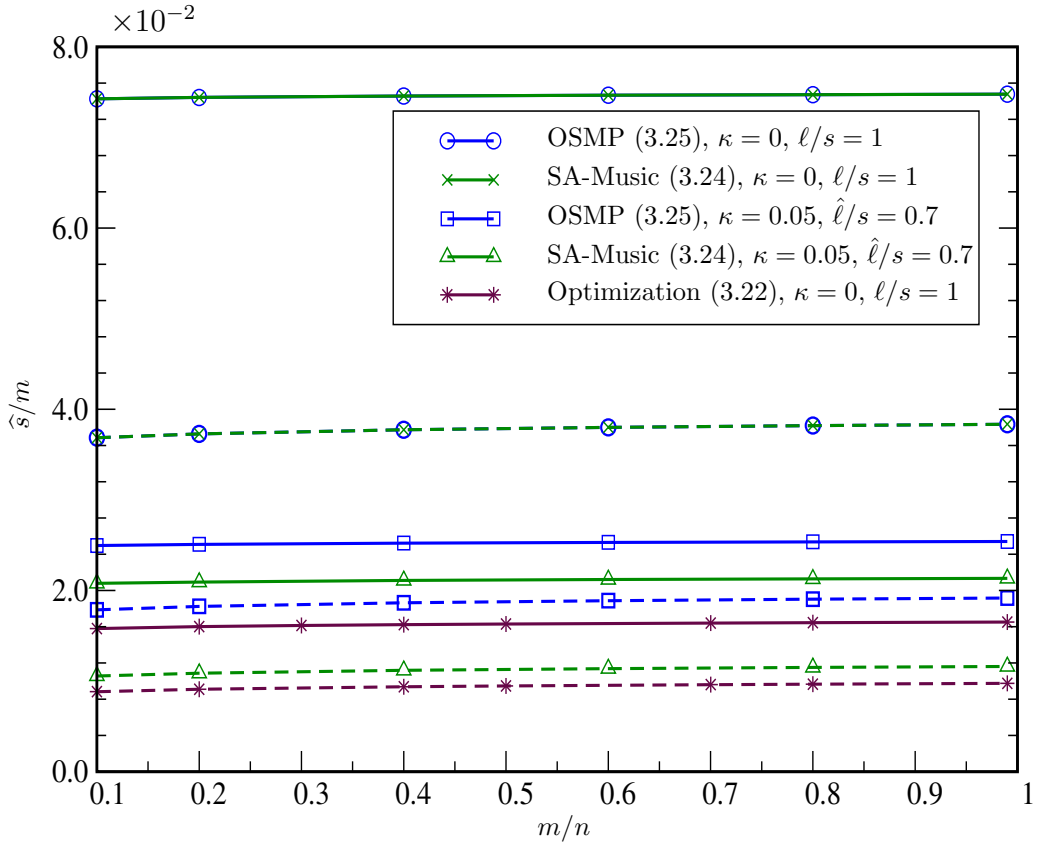

Figure 3.3: The normalized $\widehat{s}$ via the three recovery methods through asymmetric (solid) and symmetric (dashed) conditions, with $P_{\rm r} \geq 0.999$ and $m = 3000$.

Finally, the normalized maximum sparsity order, $\widehat{s}/m$, for various recovery algorithms is shown in Fig 3.3. In particular, $\widehat{s}$ has been estimated using the associated asymmetric and symmetric conditions, where the WRICs are calculated by the EED, for various noise parameters κ and probability of correct support estimation at least 0.999.[7] As can be noticed, OSMP allows recovery of less sparse signals, compared to SA-Music, for noisy measurements. In the noiseless case, for the set of chosen parameters, the mixed norm minimization indicates lower $\widehat{s}$. Additionally, it is evident that the proposed asymmetric conditions provide higher estimates of $\widehat{s}$ compared to the symmetric ones (up to 100% increase in s).

[7]Support estimation is sufficient for perfect recovery in the noiseless case.

3.6 Conclusion

We have studied the weak restricted isometry constant of Gaussian matrices, which is particularly important for MMV problem arising in many applications, e.g., data gathering from IoT devices, localization, imaging, and multivariate regression. The proposed analysis provides tighter bounds on the probability of recovery, several orders of magnitude compared to the concentration bounds. Additionally, the suggested framework allows comparing various joint sparse recovery algorithms in terms of the maximum allowable support cardinality. Finally, the analysis indicates that the derived asymmetric WRIC based conditions are preferable over those based on WRIC, as they result in better performance bounds.

Chapter 4

Lossy Compression of Noisy Sparse Sources Based on Syndrome Encoding

4.1 Introduction

The problem of designing efficient compression schemes is gaining increasing interest [108–111]. More precisely, the growing challenge in transform coding theory is to represent a compressible signal with a minimum number of bits while limiting the distortion due to quantization and sparse approximation [3, 112, 113].

The key objectives considered while designing lossy source encoders for sparse sources are:

1. developing a practical source encoder which exploits sparsity to minimize the average rate and energy consumption also in the presence of noise;

2. analyzing the theoretical performance of encoders in terms of operational distortion-rate (ODR) and operational distortion-energy (ODE), which are particularly important, e.g., to design efficient networks in IoT scenarios and for optimal bit allocation among sub-bands in wavelet based schemes [114–116].

Let us start by considering a signal, $\mathbf{x} \in \mathbb{R}^N$, emitted by a discrete-time continuous-valued source. The target is to encode $\mathbf{x}$ at the minimum rate which still guarantees a predefined average distortion, when it is know a-priori that at most k_0 elements of $\mathbf{x}$ are non-zero, i.e., $\mathbf{x}$ is a sparse vector with sparsity order k_0. The first intuitive approach, which we name address coding

(AC), is to separately quantize the k_0 non-zero components using a uniform scalar quantizer with b bit/sample, then encode each of their locations with a fixed number of bits $\lceil \log_2 N \rceil$. The total number of required bits per sample (i.e., the rate) is calculated as

$$r_{\mathrm{AC}} = \frac{1}{N}\big(k_0 \lceil \log_2 N \rceil + k_0\, b\big) \qquad [\text{bit/sample}]\,. \tag{4.1}$$

This approach is simple, but it requires the transmission of both the values and locations separately, and also there exist more efficient encoders, in terms of the compression gain. For example, it is possible to represent the signal support by encoding all the $\sum_{i=0}^{k_0} \binom{N}{i}$ possible supports which have at most k_0 ones. However, this approach is not practical, as the number of configurations is exponentially large in N.

Another method is based on CS, as discussed in previous Chapters, where one can collect $M < N$ linear observations from $\mathbf{x}$, i.e., $\mathbf{y} = \mathbf{A}\,\mathbf{x}$, through an $M \times N$ measurement matrix $\mathbf{A}$. In fact, considering Gaussian measurement matrices, perfect recovery is guaranteed with high probability for $M \geq c\, k_0 \log(N/k_0)$ [4, 5, 117].[1] One important advantage of CS is that the knowledge about the basis at which the signal is sparse is required only at the decoder side and not the encoder. Moreover, it has been proven to be stable with respect to compressible (non-strictly sparse) signals, as shown in Section 2.6. On the other hand, the number of measurements is still considerably higher than the signal sparsity and there is no efficient practical scheme to accurately multiply the random measurement matrix with the signal in the analog domain, except for Rademacher and Bernoulli matrices [8].

Regarding the performance analysis, the ODR of scalar quantizers have been analyzed for sources with uniform, Generalized Gaussian, and exponential distributions [118–121]. An increasing attention has been given to mixed distributed sources (MDSs), adopted for sparse representation of piecewise smooth data including images and wireless sensor network (WSN) signals in the wavelet domain [112, 122, 123]. In particular, asymptotic formulations of the information distortion-rate (IDR) for a class of MDSs have been given in [124, 125]. Moreover, an approximation for the entropy of quantized noiseless Bernoulli-Generalized Gaussian sources is derived in [126]. Assuming coding at the entropy rate of the quantized sources, an approximation for the optimal ODR of uniform quantizers with infinite number of levels is provided in [126], while asymptotic formulas are given in [123].

In this chapter, we provide two practical approaches for lossy source compression of noisy sparse sources. At first, we derive a blind estimator for the

[1] Explicit bounds on the required number of measurements can be found from Chapter 2.

sparsity order based on a model order selection rule to detect the non-zero elements of sparse signals embedded in noise. Alternatively, an excision filter to differentiate signal entries from noise by thresholding is designed and analyzed. Then, two novel schemes based on exploiting the syndromes associated with channel block codes, i.e., Reed-Solomon (RS) and Bose, Chaudhuri, and Hocquenghem (BCH) codes, are proposed as lossless source encoders of quantized sparse signals.[2]

With respect to previous works, this chapter provides an accurate performance measure of the proposed lossy source encoder (i.e., signal denoising and uniform quantizer followed by syndrome encoding) for MDSs encompassing Bernoulli and an arbitrary continuous distribution. In particular, our setting includes some important features:

- noisy sources with additive pre-quantization noise, which fits also the case of not exactly sparse (compressible) sources [112];
- quantizers with finite number of levels and saturation effect;
- accounting for the pre-quantization noise and the sparsity estimator behavior in analyzing the encoder performance.

Furthermore, an accurate performance measure of the proposed lossy source encoder (i.e., signal denoising and uniform quantizer followed by syndrome encoding) is provided for MDSs encompassing Bernoulli and an arbitrary continuous distribution. In particular, we derive the distortion due to both quantization and input noise for Bernoulli-uniform (BU) and Bernoulli-Gaussian (BG) sources. Then, a closed-form expression for the ODR is derived for finite rates, accounting also for the pre-quantization noise and the proposed denoising approach. Moreover, considering a power profile for an implementation of the presented encoder, its ODE is analyzed.

Finally, we address a case study for the compression of signals from a WSN network, deployed in Torgiovannetto (Assisi, Italy). The performance of the proposed encoders for these signals are also investigated in terms of the ODR and ODE, showing that the proposed approach achieves better performance when compared to CS. Thus, employing such approach for IoT scenarios can increase the network lifetime and the accuracy of the recovered data.

Throughout this chapter, we denote with $\|\cdot\|_0$ the ℓ_0 quasi-norm of a vector indicating the number of its non-zero entries, with $\delta(\cdot)$ the Dirac-delta

[2]Source encoders based on channel coding theory have been used for the different purpose of approaching the Slepian-Wolf/Wyner-Ziv bounds for the problems of lossless/lossy distributed source coding with side information only at the receiver [127–136], and also for the lossy compression of binary symmetric sources [137].

distribution, with bold small letters vectors, with bold capital letters matrices, with $\mathbf{I}_N$ the N-dimensional identity matrix, with $\mathbb{F}_q$ the Galois field of order q, with $\mathcal{N}(\boldsymbol{\mu}, \mathbf{C})$ the multivariate Gaussian distribution with mean $\boldsymbol{\mu}$ and covariance matrix $\mathbf{C}$, with $f(x; \sigma^2)$ the probability density function (PDF) of the zero mean Gaussian r.v. with variance σ^2, with $\mathcal{N}(\mu, \sigma^2, a, b)$ the univariate Gaussian distribution with mean μ and variance σ^2 truncated between a and b, with calligraphic letters, e.g., $\mathcal{S}$, r.v.s, with $f_{\mathcal{S}}(s)$ the PDF of $\mathcal{S}$, with $\mathrm{erf}(\cdot)$ the error function, with $\mathrm{erfc}(\cdot)$ the complementary error function, and with $\mathbf{1}_A$ an indicator function which equals one when the condition A is satisfied and zero otherwise.

4.2 Signal Model

Let us consider memoryless sparse sources modeled as MDSs, a model which fits images, sounds, medical data, and sensor signals in appropriate transform domains [123, 126, 138]. More precisely, the source emits i.i.d. r.v.s arranged into a vector $\mathbf{s} \in \mathbb{R}^N$. Each source symbol $\mathcal{S}$ is generated as a multiplication of a Bernoulli r.v. $\mathcal{Z} \in \{0, 1\}$ with $\mathbb{P}\{\mathcal{Z} = 1\} = p$, where p represents the average sparsity ratio, and $\mathcal{Y}$ drawn from some continuous distribution $f_{\mathcal{Y}}(y)$, i.e.,

$$\mathcal{S} = \mathcal{Z}\,\mathcal{Y} \tag{4.2}$$

whose PDF is then given by

$$f_{\mathcal{S}}(s) = p\, f_{\mathcal{Y}}(s) + (1 - p)\delta(s). \tag{4.3}$$

This MDS is referred as Bernoulli-Gaussian (BG) and Bernoulli-uniform (BU), considering the continuous distribution as Gaussian and uniform, respectively. MDSs are usually adopted within the framework of sparse representation for wavelet coefficients of piecewise smooth signals including images. Also, such model fits the distribution of wavelet coefficients for low rate (high distortion) region [112, 138].

The acquisition device may add noise to the input signal, thus the noisy vector at the sampler output can be represented as

$$\mathbf{x} = \mathbf{s} + \mathbf{w} \tag{4.4}$$

where $\mathbf{w} \sim \mathcal{N}(\mathbf{0}, \sigma_{\mathrm{n}}^2 \mathbf{I}_N)$ represents the noise. This model fits also the case of compressible sources, where the signal is not exactly sparse, and the Gaussian vector $\mathbf{w}$ accounts for the insignificant components [112].

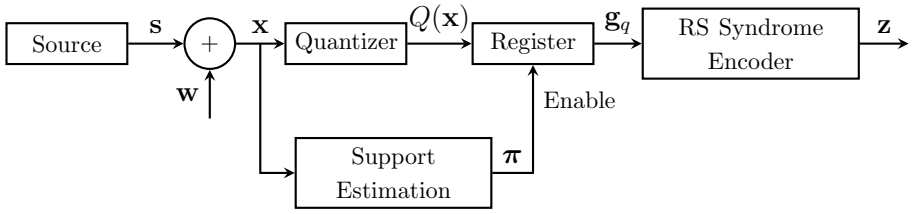

(a) RS based source encoder.

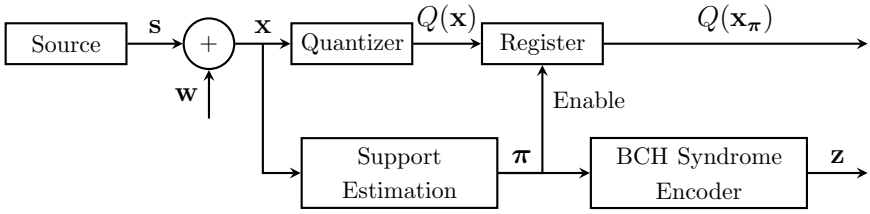

(b) BCH based source encoder.

Figure 4.1: The block diagram of the proposed compression schemes for noisy sparse sources.

4.3 Compression Schemes based on Syndrome Encoding

In this section, we describe two novel schemes for efficient lossy compression shown in Fig. 4.1. Let us consider a random realization of the noiseless source, $\mathbf{s}$, with k_0 non-zero elements in locations identified by $\boldsymbol{\pi}$. At first, the locations of the non-zero elements is estimated from $\mathbf{x}$. Then, the data is compressed by calculating the syndromes using the parity-check matrix of RS or BCH code. In the following, we will separately illustrate each part of the proposed scheme.

4.3.1 Support Detection and Signal Denoising

We propose two methods that can be used for support estimation. In particular, the first approach exploits model order selection based on generalized information criterion (GIC), while the second method relies on an excision thresholding filter. The GIC does not require the knowledge of the statistical distribution of the source nor the noise power (i.e., it is universal), but its performance analysis is quite involving [139]. On the contrary, the excision filter needs the statistical distributions of the source and noise to be known, however, the design and analysis of this filter can be tractable. In the following these techniques are discussed in detail.

Support detection by model order selection

A novel estimator is derived for the number and locations of the non-zero elements in the noisy sparse signal, based on model order selection theory [139–142]. At first, the vector $\mathbf{x}$ is sorted in descending order, according to the absolute values of its entries, $|x_i|$, such that $|x_{\pi_1}| \geq |x_{\pi_2}| \geq \cdots \geq |x_{\pi_N}|$ where $\boldsymbol{\pi} = (\pi_1, \pi_2, \cdots, \pi_N)$ is the permutation vector. We denote by $\tilde{\mathbf{x}} \triangleq (x_{\pi_1}, x_{\pi_2}, \cdots, x_{\pi_N})$ the ordered vector, which can be represented as a concatenation of two vectors $(\tilde{\mathbf{x}}_{1:k_0}, \tilde{\mathbf{w}}_{k_0+1:N})$, where the first one, $\tilde{\mathbf{x}}_{1:k_0}$, contains signal-plus-noise elements, while $\tilde{\mathbf{w}}_{k_0+1:N}$ includes noise-only terms. Hence, the estimated signal support can be denoted by the set of indexes $\hat{\boldsymbol{\pi}}(k_0) = \{\pi_1, \pi_2, \cdots, \pi_{k_0}\}$. Therefore, detecting the location of the non-zero elements of $\mathbf{s}$ is equivalent to estimating k_0, i.e., the signal sparsity. To pursue this goal, we propose to reformulate detection as a model order selection problem where the order of the model to be estimated can be related with the unknown signal sparsity. A powerful solution to model order estimation is based on information-theoretic criteria, where the model order is determined by minimizing a penalized likelihood [140,143]. In particular, we consider the GIC because of its versatility in controlling the estimation accuracy [139,142].

Considering that the sparse signal, $\mathbf{s}$, is unknown and deterministic, the PDF of $\tilde{\mathbf{x}}$ can be expressed from (4.4) as

$$f(\tilde{\mathbf{x}}) = \frac{1}{(2\pi\,\sigma_{\mathrm{n}}^2)^{\frac{N}{2}}} \exp\left(-\frac{\sum_{i=1}^{N}(\tilde{x}_i - \tilde{s}_i)^2}{2\,\sigma_{\mathrm{n}}^2}\right) \tag{4.5}$$

where $\tilde{\mathbf{s}} \triangleq (s_{\pi_1}, s_{\pi_2}, \cdots, s_{\pi_N})$. Let us define a family of models to fit the measured data with the kth model representing the case where the last signal-plus-noise sample is the kth one, i.e., $\tilde{\mathbf{s}}_{k+1:N} = \mathbf{0}$. The likelihood function can be derived from (4.5), where the noise variance, σ_{n}^2, and the sparse signal, $\tilde{\mathbf{s}}_{1:k}$, are unknown parameters denoted by $\boldsymbol{\Theta}_{(k)} \triangleq (\sigma_{\mathrm{n}}^2, \tilde{s}_1, \tilde{s}_2, \cdots, \tilde{s}_k)$, while $\widehat{\boldsymbol{\Theta}}_{(k)} \triangleq (\hat{\sigma}_{(k)}^2, \hat{\tilde{s}}_1, \hat{\tilde{s}}_2, \cdots, \hat{\tilde{s}}_k)$ denotes their estimate. As a consequence, the number of degrees of freedom (the model order) in the kth model is $k+1$. In the kth hypothesis, the maximum likelihood (ML) estimate of the signal amplitudes are $\hat{\tilde{\mathbf{s}}}_{1:k} = \tilde{\mathbf{x}}_{1:k}$, while the remaining components are set to zero, i.e., $\hat{\tilde{\mathbf{s}}}_{k+1:N} = \mathbf{0}_{k+1:N}$. For the noise variance, the ML estimate is

$$\hat{\sigma}_{(k)}^2 = \underset{\sigma_{\mathrm{n}}^2>0}{\arg\max} \log f(\tilde{\mathbf{x}}; \sigma_{\mathrm{n}}^2) = \frac{1}{N}\sum_{i=k+1}^{N} \tilde{x}_i^2\,. \tag{4.6}$$

Then, the log-likelihood function (LLF) of the kth model can be written from

(4.5) and (4.6) as

$$\log f\left(\tilde{\mathbf{x}}; \widehat{\boldsymbol{\Theta}}_{(k)}\right) = -\frac{N}{2}\log\left(\frac{2\pi}{N}\sum_{i=k+1}^{N}\tilde{x}_i^2\right) - \frac{N}{2}$$

from which the estimated sparsity order, $\hat{k}_0$ can be found by the GIC as

$$\hat{k}_0 = \underset{k\in[0,N-1]}{\arg\min}\left\{N\,\log\left(\sum_{i=k+1}^{N}\tilde{x}_i^2\right) + \nu\,k\right\} \tag{4.7}$$

where ν is a penalty factor which will be investigated in Section 4.7.

The estimated support can now be identified as $\hat{\boldsymbol{\pi}}(\hat{k}_0) = \{\pi_1, \pi_2, \cdots, \pi_{\hat{k}_0}\}$, and the corresponding filtered sparse signal becomes

$$x_i^* = \begin{cases} x_i, & i \in \hat{\boldsymbol{\pi}}(\hat{k}_0) \\ 0, & \text{otherwise.} \end{cases} \tag{4.8}$$

We will show in Section 4.7 that this blind estimator performs well for high signal-to-noise ratio (SNR). Nevertheless, its theoretical performance analysis is quite complex so the parameter ν needs to be calculated numerically. In the following, we present an alternative method for support recovery, useful when that the distributions of $\mathbf{s}$ and $\mathbf{w}$ along with their parameters are known a-priori.

Support detection using excision filter

The support detection problem of the embedded signal in noise is reformulated here as hypothesis testing. At first, the detector goal is to discriminate, for each noisy source sample x_i, between two hypothesis[3]

$$\begin{aligned} \mathcal{H}_0 &: x = w \\ \mathcal{H}_1 &: x = y + w\,. \end{aligned}$$

The corresponding likelihood ratio test is given by

$$\Lambda(x) = \frac{f_{\mathcal{X}|\mathcal{H}_1}(x|\mathcal{H}_1)}{f_{\mathcal{X}|\mathcal{H}_0}(x|\mathcal{H}_0)} \underset{\mathcal{D}_0}{\overset{\mathcal{D}_1}{\gtrless}} \lambda \tag{4.9}$$

where $f_{\mathcal{X}|\mathcal{H}_1}(x|\mathcal{H}_1)$ and $f_{\mathcal{X}|\mathcal{H}_0}(x|\mathcal{H}_0)$ are the PDFs of the noisy source, $\mathcal{X}$, given the hypothesis $\mathcal{H}_1$ and $\mathcal{H}_0$, respectively.

[3]Since the source is i.i.d., the subscript i is dropped here.

For BG sources with $\mathcal{Y} \sim \mathcal{N}(0, \sigma_{\rm s}^2)$, the log-likelihood ratio test (LLRT) can be written as

$$\log \Lambda(x) = \frac{\sigma_{\rm n} \exp(-x^2/2\sigma_{\rm x}^2)}{\sigma_{\rm x} \exp(-x^2/2\sigma_{\rm n}^2)} \underset{\mathcal{D}_0}{\overset{\mathcal{D}_1}{\gtrless}} \lambda \tag{4.10}$$

with $\sigma_{\rm x} \triangleq \sqrt{\sigma_{\rm n}^2 + \sigma_{\rm s}^2}$, leading to

$$x^2 \underset{\mathcal{D}_0}{\overset{\mathcal{D}_1}{\gtrless}} \eta \tag{4.11}$$

where the threshold η is chosen to minimize the ODR, as will be illustrated later. Therefore, the support estimation turns into an energy detection problem to declare the presence/absence of the non-zero elements. Then, as illustrated before, the encoder nulls out the samples declared as $\mathcal{D}_0$ to obtain the denoised signal $\mathbf{x}^*$. The two important metrics that determine the performance of such detector are the probability of miss-detection, $\mathrm{P_{MD}}$, and the probability of false alarm, $\mathrm{P_{FA}}$, derived as

$$\mathrm{P_{MD}} = \mathbb{P}\left\{\mathcal{X}^2 < \eta | \, \mathcal{H}_1\right\} = \mathrm{erf}\left(\sqrt{\frac{\eta}{2\sigma_{\rm x}^2}}\right) \tag{4.12}$$

$$\mathrm{P_{FA}} = \mathbb{P}\left\{\mathcal{X}^2 \geq \eta | \, \mathcal{H}_0\right\} = \mathrm{erfc}\left(\sqrt{\frac{\eta}{2\sigma_{\rm n}^2}}\right). \tag{4.13}$$

Regarding the BU sources, where the non-zero elements are drawn from a uniform distribution with

$$f_{\mathcal{Y}}(y) = \begin{cases} \frac{1}{2A}, & |y| \leq A \\ 0, & \text{otherwise} \end{cases} \tag{4.14}$$

we have

$$f_{\mathcal{X}|\mathcal{H}_1}(x|\mathcal{H}_1) = \frac{1}{4A}\left[\mathrm{erf}\left(\frac{A-x}{\sqrt{2}\sigma_{\rm n}}\right) + \mathrm{erf}\left(\frac{A+x}{\sqrt{2}\sigma_{\rm n}}\right)\right] \tag{4.15}$$

leading to the LLRT

$$\log \Lambda(x) = \log \frac{\sqrt{2\pi}}{4A}\sigma_{\rm n} + \log\left[\mathrm{erf}\left(\frac{A-x}{\sqrt{2}\sigma_{\rm n}}\right) + \mathrm{erf}\left(\frac{A+x}{\sqrt{2}\sigma_{\rm n}}\right)\right] + \frac{x^2}{2\sigma_{\rm n}^2} \underset{\mathcal{D}_0}{\overset{\mathcal{D}_1}{\gtrless}} \eta\,. \tag{4.16}$$

The test metric (4.16) can be approximated, for high SNR, using the Taylor series expansion around $x = 0$ as

$$\log\Lambda(x) \simeq \log\left[\frac{\sigma_{\rm n}}{\sqrt{2}A}\,\mathrm{erf}\left(\frac{A}{\sqrt{2}\sigma_{\rm n}}\right)\right] + x^2\left(\frac{1}{2\sigma_{\rm n}^2} - \frac{Ae^{-\frac{A^2}{2\sigma_{\rm n}^2}}}{\sqrt{2\pi}\sigma_{\rm n}^3\mathrm{erf}\left(\frac{A}{\sqrt{2}\sigma_{\rm n}}\right)}\right) \quad (4.17)$$

which is equivalent to the energy detection in (4.11) with the same false alarm (4.13). The probability of miss-detection is given as

$$\begin{aligned}\mathrm{P_{MD}} = \; & 2\int_0^{\sqrt{\eta}} f_{\mathcal{X}|\mathcal{H}_1}(x|\mathcal{H}_1)dx = -\frac{\sigma_{\rm n}}{\sqrt{2\pi}A}e^{-\frac{(A+\sqrt{\eta})^2}{2\sigma_{\rm n}^2}}\left(e^{\frac{2A\sqrt{\eta}}{\sigma_{\rm n}^2}} - 1\right) \\ & + \frac{1}{2A}\left[\left(\sqrt{\eta} - A\right)\mathrm{erf}\left(\frac{A-\sqrt{\eta}}{\sqrt{2}\sigma_{\rm n}}\right) + \left(A + \sqrt{\eta}\right)\mathrm{erf}\left(\frac{A+\sqrt{\eta}}{\sqrt{2}\sigma_{\rm n}}\right)\right]. \quad (4.18)\end{aligned}$$

4.3.2 Scalar Uniform Quantizer

Due to the large number of zero elements in $\mathbf{x}^*$, we consider a scalar mid-tread uniform quantizer, whose zero-valued level prevents the introduction of additional quantization noise out of the signal support [144]. This quantizer maps each element x_i^* of $\mathbf{x}^*$ to a discrete quantization index

$$Q : \mathbb{R} \to \{0, 1, \cdots, 2^b - 2\}$$

where b is the quantization depth indicating the number of bits per sample. More precisely, the signal $\mathbf{x}^*$ is uniformly partitioned into $2^b - 1$ levels with a step size

$$\Delta = \frac{2A}{2^b - 1} \quad (4.19)$$

where the number of levels is odd in mid-tread uniform quantizers and $[-A, A]$ is the supported range beyond which the output is saturated.[4] Considering $q \triangleq 2^b$, the index vector of the quantized signal is

$$\mathbf{g}_q \triangleq Q(\mathbf{x}^*) = (Q(x_1^*), Q(x_2^*), \cdots, Q(x_N^*)) \in \mathbb{F}_q^N.$$

4.3.3 Syndrome Based Source Encoder

We propose a source encoder for quantized sparse vectors in $\mathbb{F}_q^N$ based on the syndrome vector of a RS code. Firstly, let us consider the *dual channel coding* problem, assuming that the transmitter sends a codeword, $\mathbf{c} \in \mathbb{F}_q^N$, from the RS code with minimum distance $2k_0 + 1$. If the channel changes at

[4]For BU sources A is selected to match the support of $\mathcal{Y}$, while, e.g., it can be chosen as $A = 4\,\sigma_{\rm s}$ for BG [144].

most k_0 symbols, then the received vector can be represented as $\mathbf{r} = \mathbf{c} + \mathbf{g}_q$, where $\mathbf{g}_q \in \mathbb{F}_q^N$ is the error vector with a maximum sparsity order k_0, and the summation is in $\mathbb{F}_q$. Hence, the receiver can estimate the error vector, which is the sparsest vector satisfying the computed syndrome.

Regarding the *source coding* problem, $\mathbf{g}_q$ is compressed by calculating its syndrome vector through the parity check matrix of the k_0-error-correcting RS code at the encoder. Consequently, the receiver can perfectly reconstruct $\mathbf{g}_q$ from the syndromes, provided that the sparsity order is at most k_0. More precisely, the syndrome $\mathbf{z} \in \mathbb{F}_q^{2\hat{k}_0}$ is computed by the source encoder as

$$\mathbf{z} = \mathbf{g}_q \, \mathbf{H}^T \tag{4.20}$$

where all the operations are performed in $\mathbb{F}_q$, $\hat{k}_0$ is the estimated sparsity order, and

$$\mathbf{H} = \begin{bmatrix} 1 & \alpha & \alpha^2 & \cdots & \alpha^{N-1} \\ 1 & \alpha^2 & (\alpha^2)^2 & \cdots & (\alpha^2)^{N-1} \\ \vdots & \vdots & \vdots & \vdots & \vdots \\ 1 & \alpha^{2\hat{k}_0} & (\alpha^{2\hat{k}_0})^2 & \cdots & (\alpha^{2\hat{k}_0})^{N-1} \end{bmatrix} \tag{4.21}$$

is the $2\,\hat{k}_0 \times N$ parity-check matrix for the $\hat{k}_0$-error-correcting RS code with $N = 2^b - 1$ and $b \geq 3$, while α is a primitive element in $\mathbb{F}_q$ [111, 145]. The syndrome symbols can also be computed using efficient hardware [109, 111].

The resulting rate required for encoding the sparse vector using RS syndrome coding is

$$r_{\text{RS}} = 2\,b\,\frac{\hat{k}_0}{N} = 2\,\log_2(N+1)\,\frac{\hat{k}_0}{N} \qquad \text{[bit/sample]}. \tag{4.22}$$

A further compression gain can be achieved by separately sending the $\hat{k}_0$ quantized non-zero elements, then compressing the binary vector which determines their locations using the syndrome of a BCH code (Fig.4.1b).[5] Since for BCH code the number of parity check bits $m(N, \hat{k}_0) \leq \hat{k}_0 \log_2(N+1)$, the required rate is

$$r_{\text{BCH}} = \frac{1}{N}\left(m(N, \hat{k}_0) + \hat{k}_0\, b\right) \tag{4.23}$$

$$\leq \frac{\hat{k}_0}{N}\,\log_2(N+1) + b\,\frac{\hat{k}_0}{N} \qquad \text{[bit/sample]} \tag{4.24}$$

[5]Note that the ones in the N-bit location vector indicate the locations of the non-zero elements.

where $m(N, \hat{k}_0)$ is calculated from the design table of the BCH code, for a given sparsity order (i.e., error correcting capability) and dimension [109, Appendix C]. Clearly, from (4.22) and (4.23) the rate of this scheme is upper-bounded by the RS based approach, but the non-zero values and the syndrome vector should be transmitted separately. In the following the proposed schemes in Fig. 4.1a and Fig.4.1b will be referred as RS based source coding (RSSC) and BCH based source coding (BCHSC), respectively.

4.3.4 Source Decoder

Regarding the RSSC approach, the locations and the values of the non-zero elements can be estimated at the receiver from the syndrome vector $\mathbf{z}$ using Berlekamp's iterative algorithm [146]. Due to the minimum distance properties of the RS code and the maximum sparsity order of $\mathbf{g}_q$, the vector of the quantization indexes $\mathbf{g}_q$ is exactly recovered at the receiver.

Finally, the mapper $Q^{-1} : \{0, 1, \cdots, q-2\} \rightarrow \{i\,\Delta\}_{i=-2^{b-1}+1}^{2^{b-1}-1}$ reconstructs the quantized signal from its indexes, and the reconstructed signal $\hat{\mathbf{x}}$ is then

$$\hat{\mathbf{x}} = Q^{-1}(\mathbf{g}_q) \triangleq \left(Q^{-1}(\Gamma_1), Q^{-1}(\Gamma_2), \cdots, Q^{-1}(\Gamma_N)\right). \tag{4.25}$$

The proposed RSSC scheme requires only $2\,\hat{k}_0$ words ($2\,\hat{k}_0\,b$ bits). Hence, it can achieve a compression gain of $N/(2\,\hat{k}_0)$ over the non-compressed version.[6] Moreover, the complexity for both the transmitter and receiver are low, as there are efficient devices for encoding and decoding the signal, and the location vector is implicitly embedded in the data.

Considering the BCHSC approach, the binary location vector can be recovered using also the Berlekamp's algorithm, and the quantized non-zero entries are reconstructed from the quantization indexes as usual.

4.4 Theoretical Performance Analysis with Genie-Aided Support

In this section, we derive the ODR of the proposed schemes in Fig. 4.1, assuming perfect support estimation.[7] The ODR, $D(R)$, is a function that maps the expected rate R at which the system is working (i.e., the average number of bits required to describe a single source sample) to the average

[6] For $\hat{k}_0 \geq N/2$, the signal is not considered sparse, hence syndrome encoding is no longer efficient.

[7] Perfect support estimation assumption will be relaxed in Section 4.5.

distortion. More precisely,

$$D(R) = \mathbb{E}_{\mathcal{S},\mathcal{W}} \left\{ d\left(\hat{\mathcal{S}}(\mathcal{S}, \mathcal{W}, R) - \mathcal{S} \right) \right\} = \int_{-\infty}^{\infty} d\left(\tau\right)\, f_{\mathcal{T}}(\tau)\, d\tau \tag{4.26}$$

where $d(\cdot)$ is the distortion function, $\mathcal{S}$, $\mathcal{W}$, $\hat{\mathcal{S}}$, and $\mathcal{T} \triangleq \hat{\mathcal{S}} - \mathcal{S}$ are r.v.s representing the source output, pre-quantization noise, decoder output, and error due to both the quantization and pre-quantization noise, respectively. Hence, finding the PDF of the error, $f_{\mathcal{T}}(\tau)$, is essential for deriving the ODR. Considering perfect denoising outside the signal support, the decoder output $\hat{\mathcal{S}}$ can be obtained from (4.2), (4.4), and (4.8), as

$$\hat{\mathcal{S}} = Q^{-1}(Q\left(\mathcal{X}^*\right)) = Q^{-1}(Q\left(\mathcal{Z}\mathcal{Y} + \mathcal{Z}\mathcal{W}\right)) \triangleq \mathcal{S} + \mathcal{T} \tag{4.27}$$

where $\mathcal{X}^*$ is the r.v. representing the filtered signal, $\mathcal{Z}$ is the Bernoulli r.v. defined in Section 4.2, $\mathcal{W} \sim \mathcal{N}(0, \sigma_{\mathrm{n}}^2)$, and $Q^{-1}\left(Q\left(x\right)\right)$ accounts for the scalar mid-tread uniform quantizer with bounded range described in Section 4.3.2, i.e.,

$$Q^{-1}(Q\left(x\right)) = \begin{cases} -A + \Delta/2, & x \leq -A + \Delta \\ i\,\Delta, & (i - \frac{1}{2})\Delta \leq x \leq (i + \frac{1}{2})\Delta \\ A - \Delta/2, & x \geq A - \Delta \end{cases} \tag{4.28}$$

for $i \in \{i_{\min} + 1, i_{\min} + 2, ..., i_{\max} - 1\}$, where $i_{\max} = -i_{\min} = 2^{b-1} - 1 = A/\Delta - 1/2$.

The PDF of the error $\mathcal{T}$ can be written as

$$f_{\mathcal{T}}(\tau) = p\, f_{\mathcal{T}|\mathcal{Z}}(\tau|1) + (1-p)\, f_{\mathcal{T}|\mathcal{Z}}(\tau|0) = p\, f_{\mathcal{T}|\mathcal{Z}}(\tau|1) + (1-p)\, \delta(\tau) \tag{4.29}$$

where the error vanishes for $\mathcal{Z} = 0$, as the support is perfectly estimated at the encoder and mid-tread quantizers do not introduce distortion to the zero valued source symbol. Hence, only the non-zero elements are subject to distortion.

Given that the source symbol is non-zero and conditioned to the noise $\mathcal{W} = w$, the function $g(\cdot)$ which maps the source $\mathcal{Y}$ into the error $\mathcal{T}$ can be written from (4.27) and (4.28) as

$$g(y) = \begin{cases} \frac{\Delta}{2} - A - y, & y < -w - A \\ i\Delta - y, & (i - \frac{1}{2})\Delta - w \leq y \leq (i + \frac{1}{2})\Delta - w \\ A - \frac{\Delta}{2} - y, & y > A - w. \end{cases} \tag{4.30}$$

The PDF of the error $f_{\mathcal{T}|\mathcal{Z},\mathcal{W}}(\tau|1,w)$ is then

$$f_{\mathcal{T}|\mathcal{Z},\mathcal{W}}(\tau|1,w) = \sum_j \frac{g(\widetilde{y}_j)}{|g'(\widetilde{y}_j)|} \tag{4.31}$$

where $\{\widetilde{y}_1, \widetilde{y}_2, \cdots\}$ indicate the solutions of $g(y) = \tau$ and $g'(\widetilde{y}_j)$ is the derivative of $g(y)$ at $\widetilde{y}_j$. Considering that the solutions $\widetilde{y}_j$ depend on the value of τ and that $|g'(\widetilde{y}_j)| = 1$, then

$$\begin{aligned} f_{\mathcal{T}|\mathcal{Z},\mathcal{W}}(\tau|1,w) = &\sum_{i=i_{\min}}^{i_{\max}} f_{\mathcal{Y}}\left(i\Delta - \tau\right) \operatorname{rect}\left(\frac{\tau - w}{\Delta}\right) + f_{\mathcal{Y}}\left(\frac{\Delta}{2} - A - \tau\right) \\ &\times u\left(\tau - w - \frac{\Delta}{2}\right) + f_{\mathcal{Y}}\left(A - \frac{\Delta}{2} - \tau\right) u\left(w - \tau - \frac{\Delta}{2}\right) \end{aligned} \tag{4.32}$$

where $\operatorname{rect}(x)$ and $u(x)$ are the unit rectangle between $[-1/2, 1/2]$ and unit step functions, respectively. Therefore, the PDF of the error can be derived by averaging over $\mathcal{W}$, i.e.,

$$\begin{aligned} f_{\mathcal{T}|\mathcal{Z}}(\tau|1) = &\mathbb{E}_{\mathcal{W}}\left\{f_{\mathcal{T}|\mathcal{Z},\mathcal{W}}(\tau|1,w)\right\} = \Phi(\tau) \sum_{i=i_{\min}}^{i_{\max}} f_{\mathcal{Y}}\left(i\Delta - \tau\right) \\ &+ \phi(\tau)\, f_{\mathcal{Y}}\left(A - \frac{\Delta}{2} - \tau\right) + \phi(-\tau)\, f_{\mathcal{Y}}\left(\frac{\Delta}{2} - A - \tau\right) \end{aligned} \tag{4.33}$$

where

$$\begin{aligned} \Phi(x) &\triangleq \frac{1}{2}\left[\operatorname{erf}\left(\frac{x + \Delta/2}{\sqrt{2}\,\sigma_{\mathrm{n}}}\right) - \operatorname{erf}\left(\frac{x - \Delta/2}{\sqrt{2}\,\sigma_{\mathrm{n}}}\right)\right] \\ \phi(x) &\triangleq \frac{1}{2}\left[1 - \operatorname{erf}\left(\frac{x + \Delta/2}{\sqrt{2}\,\sigma_{\mathrm{n}}}\right)\right]. \end{aligned}$$

Altogether, (4.29)-(4.33) give the error density function for an arbitrary distribution of the non-zero elements, $f_{\mathcal{Y}}(y)$, as

$$\begin{aligned} f_{\mathcal{T}}(\tau) = (1-p)\,\delta(\tau) + p\Bigg(&\underbrace{\phi(\tau)\, f_{\mathcal{Y}}\left(A - \frac{\Delta}{2} - \tau\right)}_{f_{\mathrm{L}}(\tau)} + \underbrace{\phi(-\tau)\, f_{\mathcal{Y}}\left(\frac{\Delta}{2} - A - \tau\right)}_{f_{\mathrm{U}}(\tau)} \\ &+ \underbrace{\Phi(\tau) \sum_{i=i_{\min}}^{i_{\max}} f_{\mathcal{Y}}\left(i\Delta - \tau\right)}_{f_{\mathrm{M}}(\tau)}\Bigg). \end{aligned} \tag{4.34}$$

We now specialize (4.34) for two important distributions of the source. First, let us consider BU sources where the non-zero elements are drawn from a uniform distribution with PDF defined in (4.14). The most important consideration while substituting (4.14) into (4.34) is to find the proper intervals according to the support of $\mathcal{Y}$. In particular, $f_{\mathrm{L}}(\tau)$ and $f_{\mathrm{U}}(\tau)$ can be found such that $|\Delta/2 - A - \tau| \leq A$ and $|A - \Delta/2 - \tau| \leq A$, respectively, as

$$f_{\mathrm{L}}(\tau) = \begin{cases} \frac{1}{2A}\,\phi(\tau), & -2\,A + \frac{\Delta}{2} \leq \tau \leq \frac{\Delta}{2} \\ 0\,, & \text{otherwise} \end{cases} \tag{4.35}$$

$$f_{\mathrm{U}}(\tau) = \begin{cases} \frac{1}{2A}\,\phi(-\tau), & -\frac{\Delta}{2} \leq \tau \leq 2A - \frac{\Delta}{2} \\ 0\,, & \text{otherwise.} \end{cases} \tag{4.36}$$

Regarding $f_{\mathrm{M}}(\tau)$, two conditions should be satisfied while finding the range of τ such that $f_{\mathrm{M}}(\tau)$ is non-zero, i.e., $|i\Delta - \tau| \leq A$, leading to

$$\lceil (\tau - A)/\Delta \rceil \leq i \leq \lfloor (A + \tau)/\Delta \rfloor$$

and the summation limits in (4.34): $i_{\min} \leq i \leq i_{\max}$. By considering these inequalities, we get

$$f_{\mathcal{Y}}(i\Delta - \tau) = \begin{cases} \frac{1}{2A}, & -2A + \frac{\Delta}{2} \leq \tau \leq 2A - \frac{\Delta}{2} \\ 0, & \text{otherwise} \end{cases}$$

with $i \in \{i_{\mathrm{L}}(\tau), \cdots, i_{\mathrm{H}}(\tau)\}$, where

$$\begin{aligned} i_{\mathrm{L}}(\tau) &\triangleq \max\left\{\lceil (\tau - A)/\Delta \rceil, -A/\Delta + 1/2\right\} \\ i_{\mathrm{H}}(\tau) &\triangleq \min\left\{\lfloor (A + \tau)/\Delta \rfloor, A/\Delta - 1/2\right\}. \end{aligned}$$

Since the distribution is uniform, the summation in (4.34) reduces to $\left(i_{\mathrm{H}}(\tau) - i_{\mathrm{L}}(\tau) + 1\right)/2A$, and $f_{\mathrm{M}}(\tau)$ can be represented as

$$f_{\mathrm{M}}(\tau) = \frac{\Phi(\tau)}{2A} \times \begin{cases} \left\lfloor \frac{\tau}{\Delta} + \frac{1}{2} \right\rfloor + \frac{2A}{\Delta}, & -2\,A + \frac{\Delta}{2} \leq \tau < -\frac{\Delta}{2} \\ \frac{2\,A}{\Delta}, & -\frac{\Delta}{2} \leq \tau < \frac{\Delta}{2} \\ \left\lfloor \frac{1}{2} - \frac{\tau}{\Delta} \right\rfloor + \frac{2A}{\Delta}, & \frac{\Delta}{2} \leq \tau \leq 2\,A - \frac{\Delta}{2} \\ 0, & \text{otherwise.} \end{cases} \tag{4.37}$$

From (4.34) to (4.37), the PDF of pre-quantization plus quantization error can be written as

$$f_{\mathcal{T}}^{\mathrm{BU}}(\tau) = (1-p)\delta(\tau) + \frac{p}{2A} \times \begin{cases} 1 + \Phi(\tau)\left(\frac{2A}{\Delta} - 1\right), & |\tau| < \frac{\Delta}{2} \\ \Phi(\tau)\left(\left\lfloor \frac{1}{2} - \frac{|\tau|}{\Delta} \right\rfloor + \frac{2A}{\Delta}\right) + \phi(|\tau|), & \frac{\Delta}{2} \le |\tau| \le 2A - \frac{\Delta}{2} \\ 0, & \text{otherwise.} \end{cases} \quad (4.38)$$

Similarly, the PDF of pre-quantization plus quantization noise with BG sources, $f_{\mathcal{T}}^{\mathrm{BG}}(\tau)$, can be obtained by substituting the PDF of the Gaussian distribution into (4.34).

In order to derive the ODR for BU and BG sources, we first analyze the distortion at the decoder output. For example, considering the squared error distortion $d(\tau) = \tau^2$, the mean distortion can be calculated from (4.26), (4.34), and (4.38) as

$$D^{\mathrm{BU/BG}}(\Delta) = \int_{-\infty}^{\infty} \tau^2 \, f_{\mathcal{T}}^{\mathrm{BU/BG}}(\tau) \, d\tau. \quad (4.39)$$

For BU sources, it is also possible to give an approximation in closed-form as

$$D^{\mathrm{BU}}(\Delta) \simeq p\left(\frac{\Delta^2}{12} + \sigma_{\mathrm{n}}^2\right) + \frac{p}{24A}\left(-\sqrt{\frac{2}{\pi}}\sigma_{\mathrm{n}} e^{-\frac{\Delta^2}{2\sigma_{\mathrm{n}}^2}}\left(\Delta^2 + 5\sigma_{\mathrm{n}}^2\right) - 12\Delta\sigma_{\mathrm{n}}^2 + \frac{9\sigma_{\mathrm{n}}^4}{\Delta}\left(\mathrm{erf}\left(\frac{\Delta}{\sqrt{2}\sigma_{\mathrm{n}}}\right) - \mathrm{erf}\left(\frac{\sqrt{2}\Delta}{\sigma_{\mathrm{n}}}\right)\right)\right) \quad (4.40)$$

as illustrated in Appendix B. Regarding BG sources, the integration (4.39) cannot be found in closed-form. However, in the low distortion region, i.e., $A \gg \sigma_{\mathrm{n}}$ and $\Delta \ll \sigma_{\mathrm{s}}$, the error due to quantization can be modeled as additive and uniformly distributed, independent from both the source and the pre-quantization noise [147]. Therefore, the distortion can be approximated as

$$D^{\mathrm{BG}}(\Delta) \simeq \widehat{D}^{\mathrm{BG}}(\Delta) \triangleq p\left(\frac{\Delta^2}{12} + \sigma_{\mathrm{n}}^2\right). \quad (4.41)$$

For noiseless BG sources, an upper bound on the distortion is derived in Appendix D.

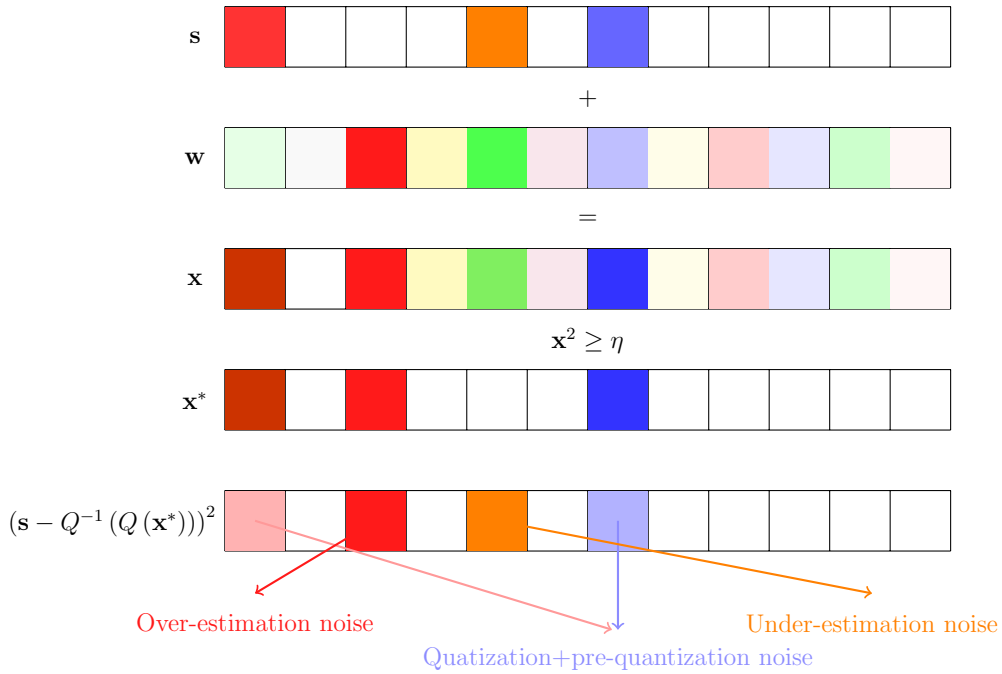

Figure 4.2: An example for imperfect support estimation and the corresponding distortion.

Now, the ODR for RSSC in Fig. 4.1a can be derived by reformulating the distortion in terms of the average rate. At first, the expected rate is calculated from (4.22) as

$$R = \mathbb{E}\left[\mathcal{R}_{\mathrm{RS}}\right]/N = 2\,b\,\mathbb{E}\left[\mathcal{K}_0\right]/N = 2\,b\,p \qquad \text{[bit/sample]} \tag{4.42}$$

where $\mathcal{K}_0$ is a binomial r.v. with mean pN which represents the number of non-zero elements. Finally, the ODR can be written from (4.19), (4.39), (4.42), and (B.2) as

$$\begin{aligned} D_{\mathrm{RS}}^{\mathrm{BU/BG}}(R) &= D^{\mathrm{BU/BG}}\left(\frac{2A}{2^{R/(2p)}-1}\right) \\ &\simeq \widehat{D}_{\mathrm{RS}}^{\mathrm{BU/BG}}(R) \triangleq \widehat{D}^{\mathrm{BU/BG}}\left(\frac{2A}{2^{R/(2p)}-1}\right). \end{aligned} \tag{4.43}$$

Similarly, the ODR of the BCH based scheme $D_{\mathrm{BCH}}^{\mathrm{BU/BG}}(R)$ can be found, where

$$R = p\,b + m(N, pN)/N \leq p\,(b + \log_2(N+1)) \qquad \text{[bit/sample]}\,. \tag{4.44}$$

4.5 Operational Distortion-Rate with Imperfect Support Estimation

In this section, the ODR of the proposed schemes for BG/BU sources is analyzed when the signal support is estimated by the excision filter. The optimal threshold that minimizes the ODR is then derived.

In fact, since the signal support is not estimated perfectly, i.e., $\mathrm{P_{MD}} > 0$ and $\mathrm{P_{FA}} > 0$, the distortion at the decoder output is due to three types of error, as shown in figure 4.2:

1. under-estimation distortion because of erroneously filtering some samples due to miss-detection;

2. over-estimation distortion because of not properly zeroing some noise components due to false alarm;

3. distortion due to quantization and pre-quantization noise for the correctly detected samples.

Taking into account these contributions, the overall distortion can be written

$$\begin{aligned} D^{\mathrm{t}}(\Delta,\eta) &= \sum_{i=0}^{1}\sum_{j=0}^{1} \mathbb{P}_{\mathcal{D}|\mathcal{H}}\left\{\mathcal{D}_j|\mathcal{H}_i\right\}\mathbb{P}_{\mathcal{H}}\left\{\mathcal{H}_i\right\}\mathbb{E}\left\{\left(\mathcal{S}-\hat{\mathcal{S}}\right)^2\Big|\mathcal{H}_i,\mathcal{D}_j\right\} \\ &= (1-p)\,\mathrm{P_{FA}}(\eta)\,\mathbb{E}\left\{\left(Q^{-1}\left(Q\left(\mathcal{W}\right)\right)\right)^2\Big|\mathcal{W}^2\geq\eta\right\} \\ &\quad + p\,\mathrm{P_{MD}}(\eta)\,\mathbb{E}\left\{\mathcal{Y}^2\Big|(\mathcal{Y}+\mathcal{W})^2<\eta\right\} + p\,\left(1-\mathrm{P_{MD}}(\eta)\right) \\ &\quad \times\mathbb{E}\left\{\left(Q^{-1}\left(Q\left(\mathcal{Y}+\mathcal{W}\right)\right)-\mathcal{Y}\right)^2\Big|(\mathcal{Y}+\mathcal{W})^2\geq\eta\right\}. \end{aligned} \tag{4.45}$$

For the over-estimation distortion the encoder treats noise samples as if they belong to the sparse signal. Firstly, the probability mass function (PMF) of the quantized noise given that over-estimation event occurred is derived as

$$\mathbb{P}\left\{Q^{-1}\left(Q\left(\mathcal{W}\right)\right)=i\Delta|\mathcal{W}^2\geq\eta\right\}=\frac{1}{2\,\mathrm{erfc}\left(\sqrt{\frac{\eta}{2\sigma_{\mathrm{n}}^2}}\right)}$$

$$\times\begin{cases}2\,\mathrm{erfc}\left(\dfrac{\sqrt{\eta}}{\sqrt{2}\sigma_{\mathrm{n}}}\right)-2\,\mathrm{erfc}\left(\dfrac{\Delta\left(|i|+\frac{1}{2}\right)}{\sqrt{2}\sigma_{\mathrm{n}}}\right), & |i|=\left\lceil\dfrac{\sqrt{\eta}}{\Delta}-\dfrac{1}{2}\right\rceil \text{ and } \eta\leq\dfrac{\Delta^2}{4}\\ \mathrm{erfc}\left(\dfrac{\sqrt{\eta}}{\sqrt{2}\sigma_{\mathrm{n}}}\right)-\mathrm{erfc}\left(\dfrac{\Delta\left(|i|+\frac{1}{2}\right)}{\sqrt{2}\sigma_{\mathrm{n}}}\right), & |i|=\left\lceil\dfrac{\sqrt{\eta}}{\Delta}-\dfrac{1}{2}\right\rceil \text{ and } \eta>\dfrac{\Delta^2}{4}\\ \mathrm{erfc}\left(\dfrac{\Delta\left(|i|-\frac{1}{2}\right)}{\sqrt{2}\sigma_{\mathrm{n}}}\right)-\mathrm{erfc}\left(\dfrac{\Delta\left(|i|+\frac{1}{2}\right)}{\sqrt{2}\sigma_{\mathrm{n}}}\right), & \left\lceil\dfrac{\sqrt{\eta}}{\Delta}-\dfrac{1}{2}\right\rceil+1\leq|i|\leq\dfrac{A}{\Delta}-\dfrac{3}{2}\\ \mathrm{erfc}\left(\dfrac{A-\Delta}{\sqrt{2}\sigma_{\mathrm{n}}}\right), & |i|=\dfrac{A}{\Delta}-\dfrac{1}{2}\\ 0, & \text{otherwise.}\end{cases}$$

Then, the over-estimation distortion can be given for BG and BU sources as

$$\mathbb{E}\left\{\left(Q^{-1}\left(Q\left(\mathcal{W}\right)\right)\right)^2|\mathcal{W}^2\geq\eta\right\}=\sum_{i=\left\lceil\frac{\sqrt{\eta}}{\Delta}-\frac{1}{2}\right\rceil}^{\frac{A}{\Delta}-\frac{1}{2}}(i\Delta)^2\,\mathbb{P}\left\{Q^{-1}\left(Q\left(\mathcal{W}\right)\right)=i\Delta|\mathcal{W}^2\geq\eta\right\}. \quad (4.46)$$

In the low distortion region, i.e., $b\geq 6$ bit/sample and $A\gg\sigma_{\mathrm{n}}$, equation (4.46) can be approximated in closed-form considering a continuous un-quantized noise model. In fact, the distribution of $|\widetilde{\mathcal{W}}|$, where $\widetilde{\mathcal{W}}\triangleq\{\mathcal{W}|\mathcal{W}^2\geq\eta\}$, follows that of a truncated Gaussian, i.e., $|\widetilde{\mathcal{W}}|\sim\mathcal{N}(0,\sigma_{\mathrm{n}}^2,\sqrt{\eta},\infty)$. Hence, the distortion can be simply approximated as

$$\mathbb{E}\left\{\left(Q^{-1}\left(Q\left(\mathcal{W}\right)\right)\right)^2|\mathcal{W}^2\geq\eta\right\}\simeq\mathbb{E}\left\{\widetilde{\mathcal{W}}^2\right\}=\sigma_{\mathrm{n}}^2+\sigma_{\mathrm{n}}e^{-\frac{\eta}{2\sigma_{\mathrm{n}}^2}}\sqrt{\frac{2\eta}{\pi}}\frac{1}{\mathrm{erfc}\left(\sqrt{\frac{\eta}{2\sigma_{\mathrm{n}}^2}}\right)}. \quad (4.47)$$

Then, the usual distortion due to quantization and pre-quantization noise can be approximated from (4.39) as

$$\mathbb{E}\left\{\left(Q^{-1}\left(Q\left(\mathcal{Y}+\mathcal{W}\right)\right)-\mathcal{Y}\right)^2\Big|(\mathcal{Y}+\mathcal{W})^2\geq\eta\right\}\simeq\mathbb{E}\left\{\left(\widehat{\mathcal{Y}}(\mathcal{Y},\mathcal{W},R)-\mathcal{Y}\right)^2\right\}=\frac{1}{p}D^{\mathrm{BG/BU}}(\Delta) \quad (4.48)$$

since the threshold η is usually designed to minimize the probability of miss-detection leading to $\mathbb{P}\{(\mathcal{Y}+\mathcal{W})^2 \geq \eta\} \simeq 1$.

For the under-estimation distortion, we have

$$\mathbb{E}\left\{\mathcal{Y}^2 | (\mathcal{Y}+\mathcal{W})^2 < \eta\right\} = \mathbb{E}_{\mathcal{W}}\left\{\mathbb{E}_{\mathcal{Y}|\mathcal{W}}\left\{\mathcal{Y}^2 | \sqrt{\eta} - w \leq \mathcal{Y} \leq \sqrt{\eta} - w\right\}\right\}. \quad (4.49)$$

Clearly, (4.49) depends on the distribution of the continuous source, i.e., Gaussian or uniform. For BG, substituting the inner expectation by the second moment of the truncated Gaussian distribution yields

$$\begin{aligned}
&\mathbb{E}_{\mathcal{W}}\left\{\mathbb{E}_{\mathcal{Y}|\mathcal{W}}\left[\mathcal{Y}^2 | \sqrt{\eta} - w \leq \mathcal{Y} \leq \sqrt{\eta} - w\right]\right\} = \\
&\mathbb{E}_{\mathcal{W}}\left\{\sqrt{\frac{8}{\pi}}\sigma_{\mathrm{s}} e^{-\frac{\eta+\mathcal{W}^2}{2\sigma_{\mathrm{s}}^2}} \frac{\mathcal{W}\sinh\left(\frac{\sqrt{\eta}\mathcal{W}}{\sigma_{\mathrm{s}}^2}\right) - \sqrt{\eta}\cosh\left(\frac{\sqrt{\eta}\mathcal{W}}{\sigma_{\mathrm{s}}^2}\right)}{\mathrm{erf}\left(\frac{\sqrt{\eta}-\mathcal{W}}{\sqrt{2}\sigma_{\mathrm{s}}}\right) + \mathrm{erf}\left(\frac{\sqrt{\eta}+\mathcal{W}}{\sqrt{2}\sigma_{\mathrm{s}}}\right)} + \sigma_{\mathrm{s}}^2\right\} \simeq \sigma_{\mathrm{s}}^2 \quad (4.50) \\
&- \frac{\sqrt{\frac{2}{\pi}}\sqrt{\eta}\sigma_{\mathrm{s}} e^{-\frac{\eta}{2\sigma_{\mathrm{s}}^2}}}{\mathrm{erf}\left(\frac{\sqrt{\eta}}{\sqrt{2}\sigma_{\mathrm{s}}}\right)} - \sigma_{\mathrm{n}}^2 \frac{e^{-\frac{\eta}{\sigma_{\mathrm{s}}^2}}\left(2\eta\sigma_{\mathrm{s}} + \sqrt{2\pi}\sqrt{\eta}e^{\frac{\eta}{2\sigma_{\mathrm{s}}^2}}\left(\eta - 3\sigma_{\mathrm{s}}^2\right)\mathrm{erf}\left(\frac{\sqrt{\eta}}{\sqrt{2}\sigma_{\mathrm{s}}}\right)\right)}{2\pi\sigma_{\mathrm{s}}^3 \mathrm{erf}\left(\frac{\sqrt{\eta}}{\sqrt{2}\sigma_{\mathrm{s}}}\right)^2} \quad (4.51)
\end{aligned}$$

where the approximation (4.51) is due to the Taylor series expansion of the argument inside the expectation in (4.50) around $\mathcal{W} = 0$, which is accurate for high SNR. Similarly, for BU we have

$$\begin{aligned}
&\mathbb{E}_{\mathcal{Y}|\mathcal{W}}\left\{\mathcal{Y}^2 | \sqrt{\eta} - w \leq \mathcal{Y} \leq \sqrt{\eta} - w\right\} \\
&= \frac{1}{12}\begin{cases} 3\left(A - \sqrt{\eta} - w\right)^2 + \left(A - \sqrt{\eta} + w\right)^2, & -A - \sqrt{\eta} < w \leq \sqrt{\eta} - A \\ 4\,\eta + 12\,w^2, & \sqrt{\eta} - A < w \leq A - \sqrt{\eta} \\ 3\left(-A + \sqrt{\eta} - w\right)^2 + \left(A + \sqrt{\eta} - w\right)^2, & A - \sqrt{\eta} < w \leq A + \sqrt{\eta} \\ 0, & \text{otherwise.} \end{cases}
\end{aligned}$$

So, the corresponding distortion becomes

$$\begin{aligned}
\mathbb{E}\left\{\mathcal{Y}^2 | (\mathcal{Y}+\mathcal{W})^2 < \eta\right\} = \frac{\sigma_{\mathrm{n}}}{3\sqrt{2\pi}} e^{-\frac{(A+\sqrt{\eta})^2}{2\sigma_{\mathrm{n}}^2}} &\left(\left(\sqrt{\eta} - 2A\right) e^{\frac{2A\sqrt{\eta}}{\sigma_{\mathrm{n}}^2}} - 4A + \sqrt{\eta}\right) \\
&+ \frac{1}{6}\left(\left(-2A^2 + 3A\sqrt{\eta} + 4\sigma_{\mathrm{n}}^2\right)\mathrm{erf}\left(\frac{A - \sqrt{\eta}}{\sqrt{2}\sigma_{\mathrm{n}}}\right)\right. \\
&\left. + \left(2A^2 - 3A\sqrt{\eta} + 2\left(\eta + \sigma_{\mathrm{n}}^2\right)\right)\mathrm{erf}\left(\frac{A + \sqrt{\eta}}{\sqrt{2}\sigma_{\mathrm{n}}}\right)\right). \quad (4.52)
\end{aligned}$$

Finally, the overall distortion can be approximated by substituting (4.46), (4.48), and (4.51) or (4.52) into (4.45).

In order to derive the ODR, accounting for imperfect support recovery using the excision filer, firstly, the expected rate for RSSC is calculated as

$$R = \frac{2\,b}{N}\mathbb{E}\left\{\hat{\mathcal{K}}_0\right\} \tag{4.53}$$

where $\hat{\mathcal{K}}_0$ is a r.v. representing the number of non-zero elements at the output of the excision filter, so $\mathbb{E}\left\{\hat{\mathcal{K}}_0\right\} = N\,p\,(1-\mathrm{P_{MD}}) + N\,(1-p)\,\mathrm{P_{FA}}$. Similarly, the average rate for BCH can be derived as

$$R = \frac{1}{N}\,\mathbb{E}\left\{b\,\hat{\mathcal{K}}_0 + m(N,\,\hat{\mathcal{K}}_0)\right\} = b\left(p\,(1-\mathrm{P_{MD}}) + (1-p)\,\mathrm{P_{FA}}\right) + \frac{1}{N}\,m\Big(N,\,N\,p\,(1-\mathrm{P_{MD}}) + N\,(1-p)\,\mathrm{P_{FA}}\Big). \tag{4.54}$$

Then, the corresponding ODR can be approximated from (4.45), (4.46), (4.48), (4.51), (4.52), and (4.53) as

$$D^{\mathrm{t}}_{\mathrm{RS/BCH}}(R,\eta) = D^{\mathrm{t}}\left(\frac{2A}{2^{b(R)}-1},\eta\right) \tag{4.55}$$

where

$$b(R) = \frac{R}{2\,p\,(1-\mathrm{P_{MD}}) + 2\,(1-p)\,\mathrm{P_{FA}}}$$

$$b(R) = \frac{NR - m\left(N,\,\mathbb{E}\left\{\hat{\mathcal{K}}_0\right\}\right)}{\mathbb{E}\left\{\hat{\mathcal{K}}_0\right\}}$$

for RSSC and BCHSC, respectively.

The threshold η is crucial for the encoder performance, because as η increases the rate decreases, but at the same time the distortion could increase due to missing significant samples. Therefore, the optimal value of the threshold η such that the distortion is minimized for a given rate can be calculated from (4.55) as

$$\widehat{\eta}_{\mathrm{RS/BCH}}(R) = \arg\min_{\eta>0} D^{\mathrm{t}}_{\mathrm{RS/BCH}}(R,\eta). \tag{4.56}$$

4.6 Operational Distortion-Energy of Syndrome Encoding Schemes

In some applications, the ODR is not sufficient to fully describe the behavior of source encoders. In fact, for IoT scenarios the energy spent during acquisition, compression, and transmission is a critical aspect. In this regard, we

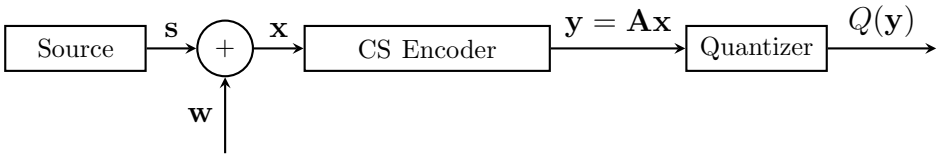

Figure 4.3: The block diagram of the CS based source encoder [8, 39].

derive a new metric for the evaluation of the system performance relating the expected distortion with the average consumed energy in the sensor, which is called operational distortion-energy (ODE).

Let us start with the energy consumption of the proposed approach along with the CS based encoder in Fig. 4.3. For example, we consider a possible energy model similar to that in [148, 149]. The total energy consumption in the sensor node can be calculated as a sum of the computational and communication energy

$$E_t(r) = E_{\text{comp}} + E_{\text{comm}}(r) \tag{4.57}$$

where the computational energy, $E_{\text{comp}} = E_{\text{acq}} + E_{\text{bck}} + E_{\text{sp}}$, is a combination of the acquisition, background, and signal processing energy, while the communication energy $E_{\text{comm}}(r) = E_{\text{tx}}(r) + E_{\text{tx}}$ is the consumption occurred during transmitting and receiving data, and r is the distance between the transmitter and receiver. More precisely, the energy spent in acquisition and background operations are given by $E_{\text{acq}} = N\epsilon_{\text{ack}}T_{\text{ins}}$ and $E_{\text{bck}} = T_{\text{ins}}n_o\epsilon_{\text{bck}}$, where ϵ_{ack} is the acquisition power, T_{ins} is the instruction executing time, ϵ_{bck} is the background power consumption, and n_o is the number of performed operations. With this model, the total spent energy during data acquisition, compression, and transmission can be calculated for our approach and compared with CS as follows.

For the proposed RSSC, the signal is first sparsified using, e.g., the discrete cosine transform (DCT).[8] Then, it is compressed using the proposed syndrome encoding method. Let ϵ_{rd}, ϵ_{add}, ϵ_{mul}, ϵ_{cmp}, and ϵ_{wr} be the energy consumed during reading, addition, multiplication, comparing, and writing, respectively. The computational energy consumption due to vector reading, DCT, support detection through thresholding, and syndrome calculation can be found as

[8]Real signals from WSNs may not be sparse in time, but rather in other domains such as DCT.

$$E_{\rm sp} = \overbrace{N\epsilon_{\rm rd}}^{\text{Reading}} + \overbrace{\frac{N}{2}\log_2(N)\epsilon_{\rm mul} + \left(\frac{3N}{2}\log_2(N) - N + 1\right)\epsilon_{\rm add}}^{\text{DCT}} +$$
$$\overbrace{N(\epsilon_{\rm cmp} + \epsilon_{\rm wr})}^{\text{Thresholding}} + \overbrace{2\,\mathbb{E}\left\{\hat{\mathcal{K}}_0\right\}\left(\epsilon_{\rm add}\left(\mathbb{E}\left\{\hat{\mathcal{K}}_0\right\} - 1\right) + \mathbb{E}\left\{\hat{\mathcal{K}}_0\right\}\epsilon_{\rm mul} + \epsilon_{\rm wr}\right)}^{\text{Syndrome Calculation}} \quad (4.58)$$

while the background power consumption is calculated as

$$E_{\rm bck} = \epsilon_{\rm bck}\, T_{\rm ins}\Big(2\,N + 2\,N\log_2(N) + 1 + 4\,\left(\mathbb{E}\left\{\hat{\mathcal{K}}_0\right\}\right)^2\Big). \quad (4.59)$$

The energy consumed during transmission is a function of the distance and can be found as

$$E_{\rm comm}(b_{\rm SE}) = 2\,\mathbb{E}\left\{\hat{\mathcal{K}}_0\right\}\, b_{\rm SE}\,\big(\,(1+h_{oh})\,E_{\rm tx}(r) + h_{ack}E_{\rm tx}\big) \quad (4.60)$$

where p_{oh} and p_{ack} represent the percentage of overhead and acknowledgment with respect to the maximum payload. The total consumed power using the syndrome encoding scheme is written from (4.58), (4.59), and (4.60) as

$$E_{\rm SE}(b_{\rm SE}) = E_{\rm acq} + E_{\rm sp} + E_{\rm bck} + E_{\rm comm}(b_{\rm SE}). \quad (4.61)$$

Regarding the CS encoder, the total consumed energy is

$$E_{\rm CS}(b_{\rm CS}) = E_{\rm acq} + N\epsilon_{\rm rd} + M((N-1)\epsilon_{\rm add} + N\epsilon_{\rm mul}) + M\epsilon_{\rm wr}$$
$$+ \epsilon_{\rm bck}T_{\rm ins}\,(N + 2NM) + Mb_{\rm CS}\big(\,(1+h_{oh})\,E_{\rm tx}(r) + h_{ack}E_{\rm tx}\big). \quad (4.62)$$

Finally, the ODE function can be derived from (4.45) as

$$D_{\rm SE/CS}(E) = D^{\rm t}\left(\frac{2A}{2^{b_{\rm SE/CS}(E)} - 1}, \eta\right) \quad (4.63)$$

where $b_{\rm SE/CS}$ can be found from (4.61) and (4.62) for syndrome encoding and CS based approaches, respectively.

4.7 Numerical Results

In this section, numerical results and Monte Carlo simulations are presented to illustrate the performance of the proposed RSSC and BCHSC schemes. We also compare the ODR of such encoders with the entropy bound. The

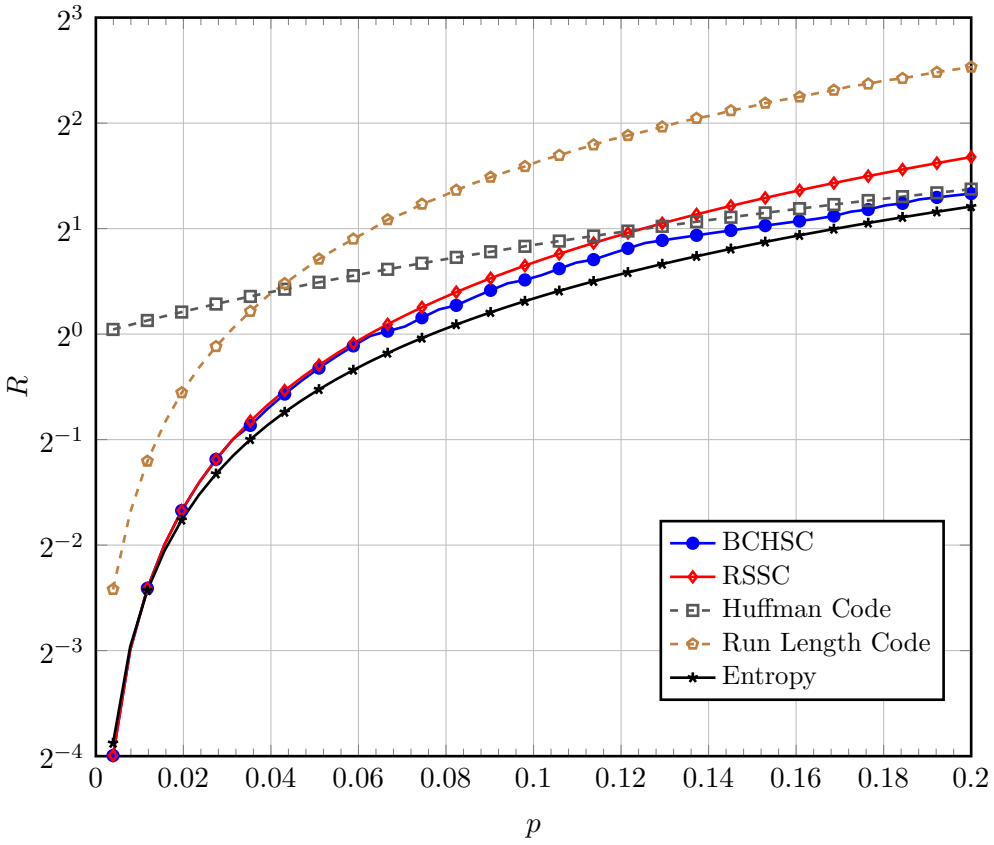

Figure 4.4: Average rate for encoding sparse BU sources quantized with $b = 8$ bit/sample, for $A = 4$ and $N = 255$.

SNR is defined as the signal power to the pre-quantization noise power at the encoder, i.e., SNR $\triangleq \mathbb{E}\left\{\mathbf{s}\,\mathbf{s}^T\right\}/\mathbb{E}\left\{\mathbf{w}\,\mathbf{w}^T\right\}$. In all numerical results $p = 0.15$, $A = 1$, and $N = 2^b - 1$, unless otherwise stated. As a benchmark, the entropy of quantized BU and BG sources and the optimal ODR of the quantizer are derived in Appendices C and D.

In Fig. 4.4, we report the average rate needed to encode the noiseless quantized BU source using AC (4.1), RSSC (4.22), BCHSC (4.23), Huffman encoder, and run length encoding, plus the Shannon's lower bound (C.2), as a function of the average sparsity ratio p, for $b = 8$ bit/sample, $A = 4$, and $N = 255$. It is noted that the rates indicated by both RSSC and AC are coincident, while the BCHSC can achieve a higher compression gain (up to 15% compared to RSSC). Also, the proposed approaches are superior to run length coding and Huffman coding for $p < 0.13$, while the gap between the entropy bound and syndrome encoders is small for low sparsity ratios.

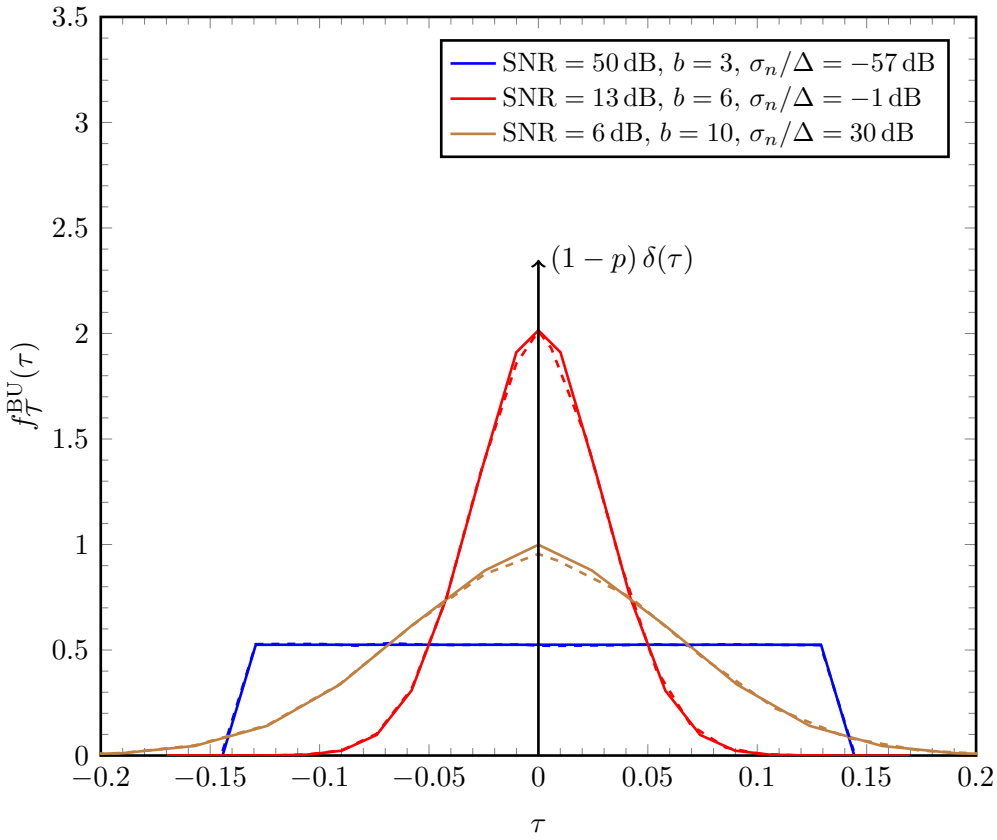

Figure 4.5: The PDF of the error for BU sources. Analytical (solid) and empirical (dashed), for various SNRs and bit depths b.

The PDF of the error due to both quantization and pre-quantization noise is shown in Fig. 4.5, for SNR $\in \{50, 13, 6\}$ dB and $b \in \{3, 6, 10\}$ bit/sample. Note that the PDF is a mixed distribution with a Dirac delta function at zero with weight $1-p$ representing a perfect recovery of the zero elements at the decoder. The empirical distributions are calculated from the normalized histogram corresponding to $p\, f_{\mathcal{T}|\mathcal{Z}}(\tau|1)$, while the relative frequency of zero elements tends to the theoretical probability $1-p$. As we can see, the theoretical PDF in (4.38) agrees with the normalized histogram obtained from simulation. On the other hand, the PDF of the non-zero entries is a combination of error due to quantization only (uniform distribution from $-\Delta/2$ to $\Delta/2$) and distortion from the pre-quantization noise (zero mean Gaussian distribution with variance σ_{n}^2). The resulting shape depends on $\sigma_{\mathrm{n}}/\Delta$, and $f_{\mathcal{T}}^{\mathrm{BU}}(\tau)$ tends more to a uniform distribution for small ratios.

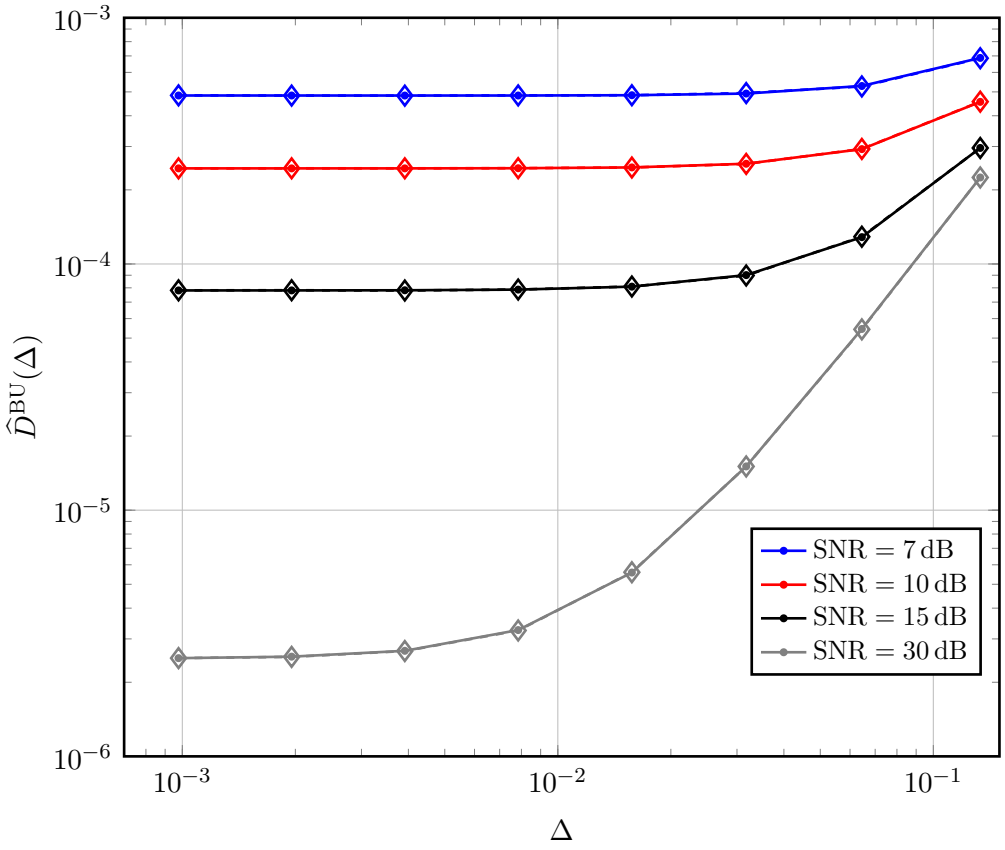

Figure 4.6: The distortion vs. step size, for noisy BU sources and various SNRs. The analytical performance (solid $*$) coincides with the simulation (dashed $\diamond$).

Fig. 4.6 shows the mean squared error distortion (B.2) (Appendix B) by varying the step size Δ of the uniform quantizer with $b \in \{4, 5, ..., 12\}$, for noisy BU sources and different SNRs. The distortion increases with both the step size and noise power. Moreover, the minimum distortion that one can achieve depends on the amount of pre-quantization noise, e.g, decreasing Δ from 10^{-2} to 10^{-3} has negligible effect on the distortion for SNR ≤ 15 dB.

Fig. 4.7 illustrates the ODR of RSSC, (4.43), and BCHSC, (4.39) and (4.44), for BU sources with $b \in \{4, 5, ..., 12\}$ and different SNRs. It is clear that $D_{\mathrm{BCH}}(R) \leq D_{\mathrm{RS}}(R)$, which is due to that $R_{\mathrm{BCH}} \leq R_{\mathrm{RS}}$ from (4.22) and (4.23). Also, the distortion tends approximately to $p\,\sigma_{\mathrm{n}}^2$ as $b \to \infty$, exhibiting a floor at high rates. Hence, increasing the rate from 2 to 3 bit/sample does not significantly decrease the distortion for low SNRs.

In Fig. 4.8, we compare the ODR of BCHSC and RSSC with that of the

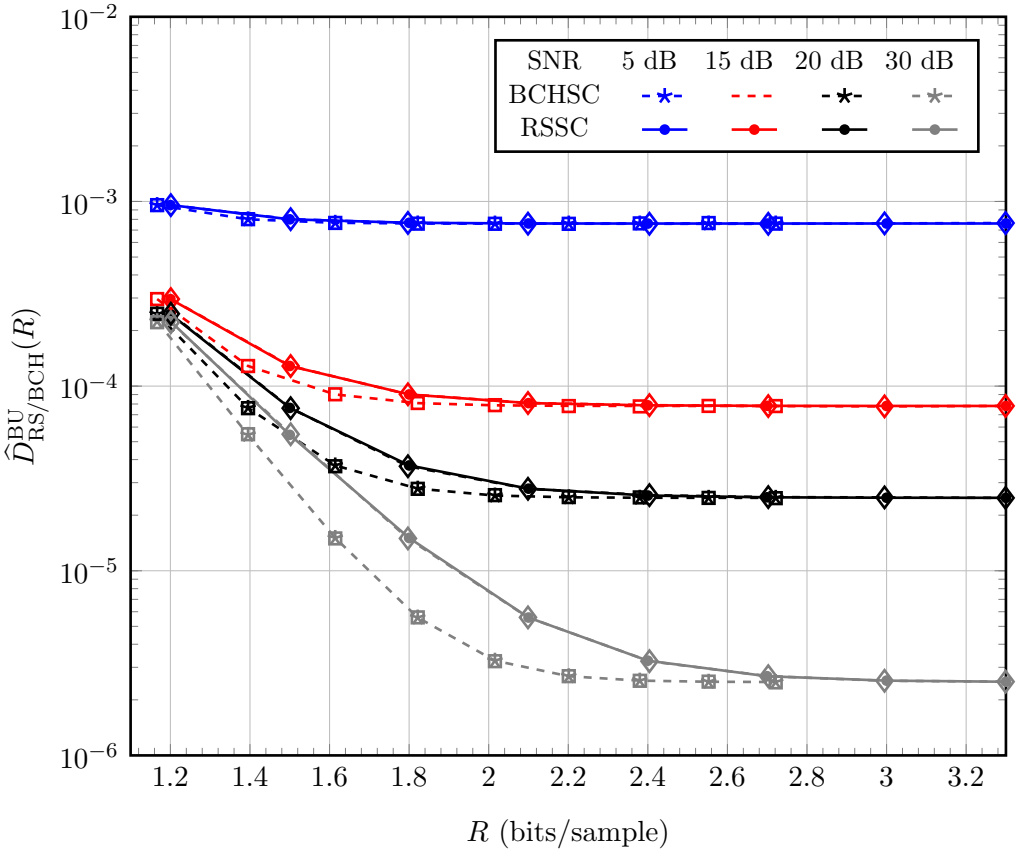

Figure 4.7: The ODR for the proposed BCHSC (solid) and RSSC (dashed) schemes, with $b \in \{4, 5, ..., 12\}$ and SNR $\in \{5, 15, 20, 30\}$ dB. The analytical performance for (RSSC $\bullet$) and (BCHSC $*$) coincides with simulation ($\diamond$, $\square$).

optimal uniform quantizer derived in Appendix D for BU and BG sources. We can see that the gap between the BCHSC and optimal $R(D)$ in (D.6) is small, especially in the low-rate region (high-distortion). Also, note that the upper bound (D.5) on the ODR of the optimal uniform quantizer for BG sources is tight.

The ODR of RSSC for BU, (4.55), with imperfect support recovery is depicted in Fig. 4.9. The location of the non-zero elements is estimated either by the excision filter described in Section 4.3.1 using the optimal threshold $\widehat{\eta}$, (4.56), and a threshold designed through the Neyman-Pearson criteria (4.13) for $\mathrm{P_{FA}} = 0.01$, or by the GIC estimator (4.7) with $\nu = 10$ for SNR $= 15$, and $\nu = 12$ for SNR $= 30$. The proposed optimal threshold achieves a better performance compared to that based on constant false alarm, especially for high SNR. For example, the optimal threshold achieves about 30% reduction

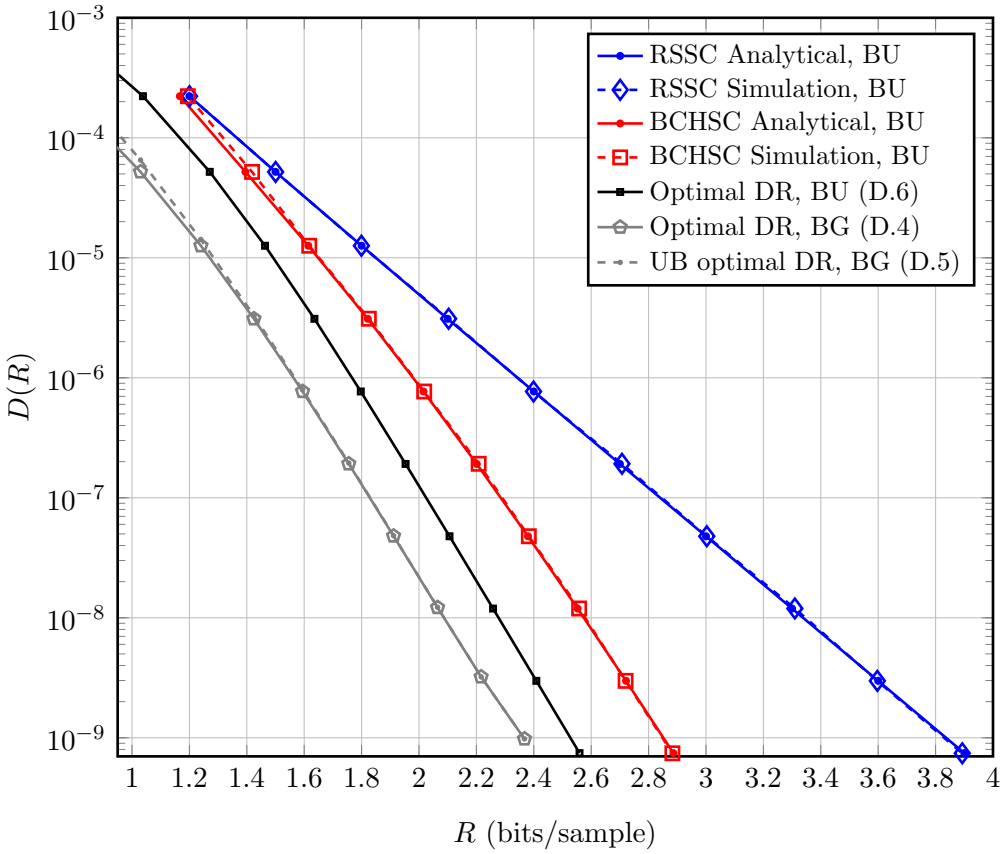

Figure 4.8: The ODR of BCHSC and RSSC along with upper bounds on the IDR, with $A = 1$, $\sigma_s = 1/5$, $b \in \{2, 3, ..., 13\}$, and SNR $= \infty$.

in the distortion, for $R = 1.8$ bit/sample and SNR $= 30$ dB. Moreover, the GIC performs well at high rate region.

4.8 Case Study: Internet of Things for Environmental Monitoring

In this section, we use the proposed syndrome encoders depicted in Fig. 4.1 to encode compressible signals acquired from a WSN. In particular, real data (temperature, humidity and rain level) collected by a WSN for landslides monitoring [150] are encoded. The measurements have been gathered for over a year with a rate of 1 sample per 15 min, thus the number of available samples from each sensor is around $40 \cdot 10^3$. The gathered readings from each sensor are grouped into vectors with length N, then separately compressed

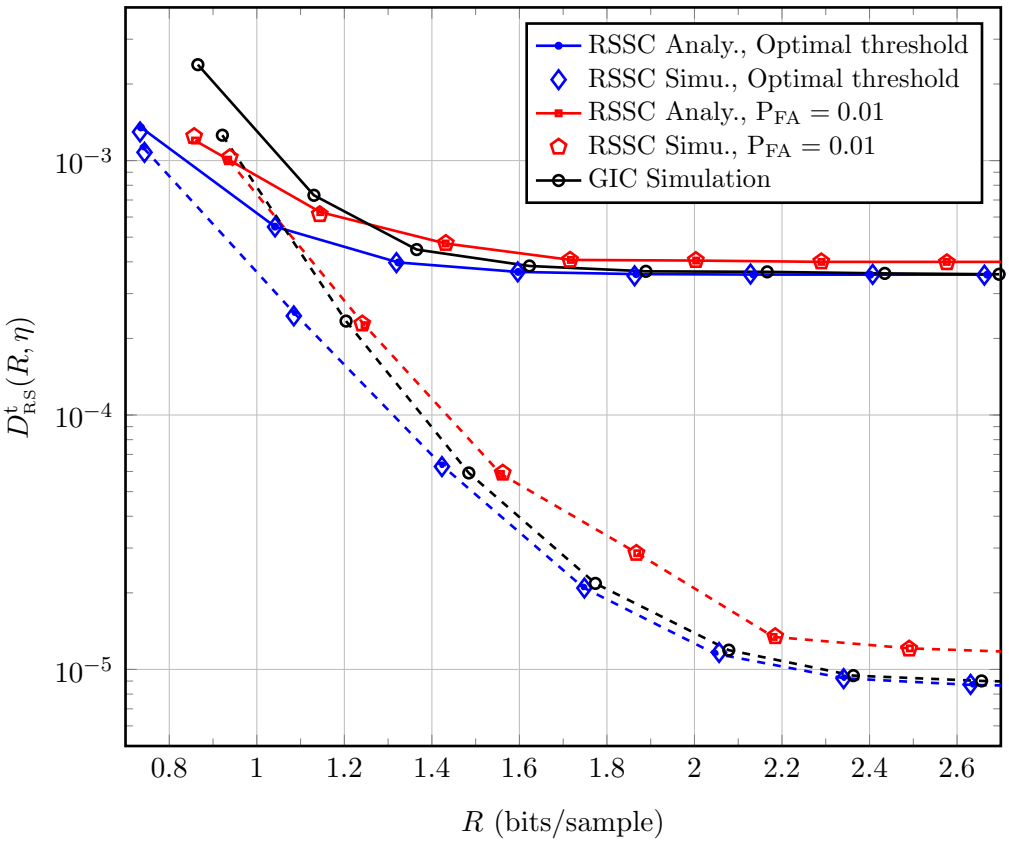

Figure 4.9: The ODR for noisy BU sources with excision filter using the optimal threshold (4.56) and Neyman-Pearson criteria (4.13), and with the GIC (4.8), for SNR = 15 dB (solid) and SNR = 30 dB (dashed).

using the proposed BCHSC and the CS encoder shown in Fig. 4.3 with rate identified by (4.23) and $r_{\mathrm{CS}} = M\,b/N$, respectively.

In this context, the output of the sparse source plus noise, $\mathbf{x}_{\mathrm{c}} \in \mathbb{R}^N$, represents a compressible signal in an appropriate transform domain, i.e., DCT. Then, the support of the significant samples is estimated using an excision filter with a threshold designed such that a predefined fraction, $\lambda \in [0, 1]$, of the total signal energy is preserved. We validate that these signals are compressible in the DCT domain. For example, letting $\hat{k}_0$ be the estimated number of significant coefficients, only $\hat{k}_0 = 17$ out of 127 are sufficient on average to guarantee that more than 99.9%, i.e., $\lambda = 0.999$, of the signal energy, $\|\mathbf{x}_{\mathrm{c}}\|^2$, is preserved for the temperature signal, while $\hat{k}_0 = 25$ and $\hat{k}_0 = 4$ for humidity and rain data, respectively.

Clearly, the distortion is due to the sparse approximation and the quan-

tization of the non-zero elements.[9] More precisely, the mean squared error distortion for the lossy encoding of the compressible source can be written as

$$D_{\text{comp}}(\Delta;\lambda) = \frac{1}{N}\,\mathbb{E}\left\{\left\|\mathbf{x}_{\text{c}} - \mathbf{F}^{-1}\,Q^{-1}\left(Q\left(\mathbf{M}\,\mathbf{F}\mathbf{x}_{\text{c}}\right)\right)\right\|^2\right\} \tag{4.64}$$

where $\mathbf{F} \in \mathbb{R}^{N\times N}$ is the DCT matrix and $\mathbf{M} = \text{diag}(\boldsymbol{\pi}) \in \mathbb{R}^{N\times N}$ is a selection matrix with $\boldsymbol{\pi} \in \{0,1\}^N$ indicating the locations of the $\hat{k}_0$ estimated significant elements.

In order to find the distortion, we notice that the significant and non-significant data entries follow uniform and Gaussian distributions, respectively (similar to noisy BU sources). The parameters of the distributions are estimated using moment matching method from the data set. Since the DCT is an orthonormal basis, and the quantization noise for large b is uniformly distributed with support $[-\Delta/2, \Delta/2]$, the distortion can be approximated as

$$D_{\text{comp}}(\Delta;\lambda) \simeq \widehat{p}(\lambda)\frac{\Delta^2}{12} + (1-\widehat{p}(\lambda))\;\widehat{\sigma}_n^2 \tag{4.65}$$

where $\widehat{p}(\lambda) \triangleq \hat{k}_0/N$ is the estimated average sparsity ratio and $\widehat{\sigma}_n^2$ is the estimated variance of the non-significant elements.

The ODR and ODE of the proposed encoder along with the CS scheme (Fig. 4.3) are examined in Fig. 4.10, for $b \in \{3,5,\ldots,13\}$. The energy consumption is calculated through the model presented in Section 4.6. In particular, we consider the power model of MICA 2 platform with Atmel Atmega 128L processor and CC1000 radio [148,149]. Each data packet consists of 1872 bits as a maximum payload and 168 additional bits as a header (p_{oh} = 9% payload), while the acknowledgment packet length is 160 bits (p_{ack} = 8.5% payload). This platform has $\epsilon_{\text{ack}} = 15.01$ mW, $T_{\text{ins}} = \frac{1}{7.5\times10^6}$ sec, $\epsilon_{\text{bck}} = 9.6$ mW, $\epsilon_{\text{add}} = 3.3$ pW, $\epsilon_{\text{mul}} = 9.9$ pW, $\epsilon_{\text{cmp}} = 3.3$ pW, $\epsilon_{\text{sh}} = 3.3$ pW, $\epsilon_{\text{rd}} = 0.26$ pW, and $\epsilon_{\text{wr}} = 4.3$ pW. We depict in Fig. 4.10 the convex hull (minimum) of the ODR and ODE, normalized by $\|\mathbf{x}_{\text{c}}\|^2$, varying $\lambda \in [0.5, 0.9999]$ for BCHSC and $M \in [3, N-1]$ for CS. It is evident that the rain sensor signals are more compressible than those representing the temperature and humidity. As can be seen, the proposed encoder indicates higher performance with respect to CS, in terms of the required rate and the consumed energy, e.g., about 60% reduction in the required rate and consumed energy, when the distortion is 10^{-2}.

[9] Unlike the sparse signal model in Section 4.2, the vector $\mathbf{w}$ is considered as a part of the signal.

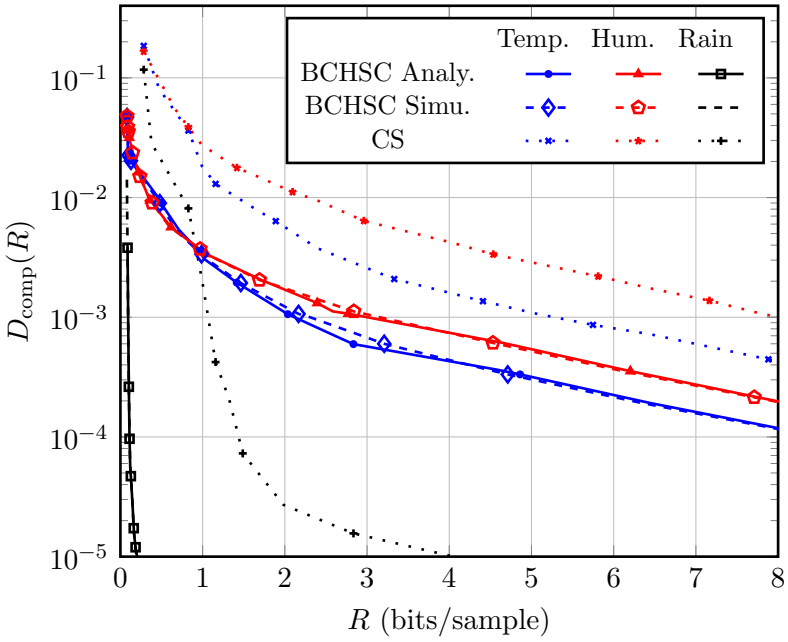

(a) Operational distortion-rate with $N = 127$.

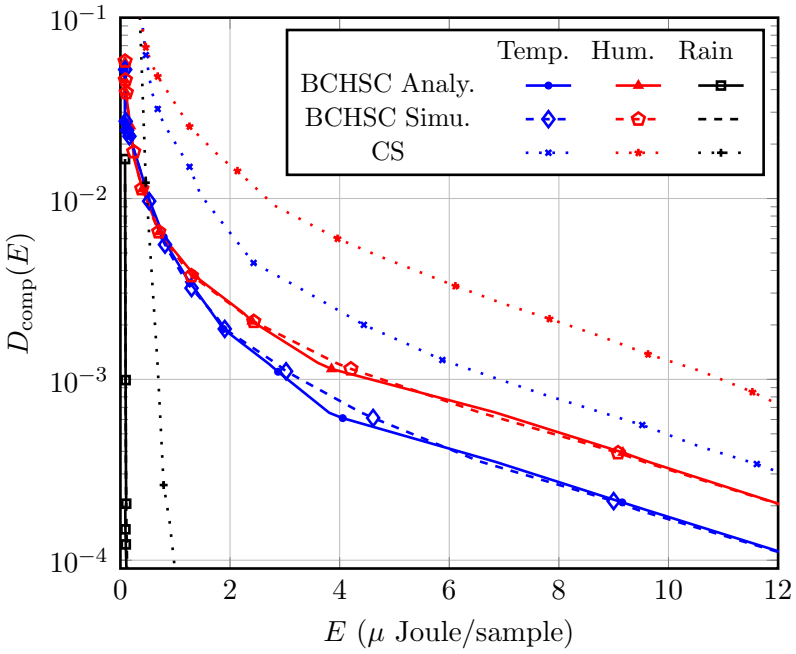

(b) Operational distortion-energy with $N = 255$.

Figure 4.10: The ODR and ODE of the proposed BCHSC (4.23) and CS for real data acquired from a WSN deployed in Torgiovannetto (Assisi, Italy).

4.9 Conclusion

This chapter provided two novel schemes for efficient encoding of noisy sparse sources, i.e., BU and BG. The proposed technique is based on the channel coding theory to build efficient source encoders. Also, two methods are suggested for the denoising of sparse signals; the first is a blind estimator based on model order selection, while the second is an excision filter requiring a prior knowledge of the signal model. The provided source encoders are particularly important for IoT scenarios involving the exchange of sparse signals, e.g, images and data from sensors, to reduce both the consumed power and bandwidth. The theoretical analysis of the proposed encoders has been provided in terms of the ODR and ODE. As illustrated by numerical results, the proposed schemes are superior to CS, run length and Huffman encoders, for low sparsity ratio. We found also that the ODR of BCHSC is upper bounded by that of RSSC. As illustrated by numerical results, the gap between the entropy based bounds and the proposed approaches is small. For a real scenario case study, we applied our techniques to compress real data gathered by a WSN deployed for monitoring landslides in the Apennines mountains. The presented approach is also superior to CS for the encoding of the collected real data.

Chapter 5

Frame Synchronization for M-ary Modulation with Phase Offsets

5.1 Introduction

Frame synchronization (FS) is a fundamental stage in most communication systems for achieving reliable radio links with low probability of error [151–168]. The FS mechanism considers finding the position of a known synchronization sequence, called here sync word (SW), which is inserted into a data stream composed of modulated symbols.

The optimal FS metric for binary transmission has been studied for binary symmetric channels (BSC) and additive white Gaussian noise (AWGN) channels in [151] and [152], respectively, where binary signalling with coherent demodulation and perfect carrier synchronization was assumed. The probability of correct frame synchronization for the metrics in [152] is analyzed in [162], where the concept of pairwise synchronization error probability (PSEP) is introduced. The derivation of the optimum metrics according to hypothesis testing theory and the acquisition time analysis is provided for variable (unknown) frame lengths in [159–161], where sequential FS is considered.

Nevertheless, in some systems FS is required to be performed prior to phase synchronization, referred throughout the chapter as "noncoherent" FS. For this "noncoherent" FS setting, it has been shown that, assuming a phase offset and negligible frequency offset, the common noncoherent correlation detector is not the optimum one [163]. In the presence of large frequency offsets the situation is even more difficult. For example, in code

division multiple access (CDMA) systems, suitable postdetection integration techniques, with combinations of successive partial noncoherent correlations, are employed to mitigate the effects of frequency offsets [169, 170]. Metrics for FS that are robust to frequency offsets have been provided for TDMA systems in [171, 172].

While the previous schemed are usually given for binary phase shift keying (BPSK), many modern systems use multilevel modulations. For example, in link adaptive schemes the number of levels in the modulation is chosen adaptively, depending on the channel characteristics and required throughput [173, 174]. Therefore, efficient FS is essential for such M-ary modulation based systems. Extensions of coherent FS of BPSK to multilevel modulation, frequency selective channels, and code-aided frame synchronization techniques are provided in several works [153–158].

On the other hand, less is known in the case of noncoherent FS for M-ary phase shift keying (M-PSK) modulated symbols, where the most common approach is to use a noncoherent correlator. The correlation is performed over a testing time equal to the duration of the SW if the phase offset is constant within that duration, while the performance significantly degrades when the phase varies considerably within the correlation time, due for example to the presence of frequency offset. Yet, optimal metrics for noncoherent FS of M-ary modulated symbols have not been fully addressed.

In this chapter, an optimal metric for noncoherent FS of M-PSK modulations with $M \geq 4$ is first derived, assuming a negligible frequency offset. We show that the optimal test requires numerical integration, which is not suitable for real-time implementations. Hence, suboptimal low-complexity metrics, i.e., accurate approximations of the optimal detector, are proposed for quadrature phase shift keying (QPSK) and 8-phase shift keying (8-PSK). Starting from the approach in [163], we also analyze for M-PSK a low-complexity metric consisting in the simple noncoherent correlator corrected by removing the ℓ_1-norm of the observed vector. The proposed metric shows a considerable performance improvement with respect to (w.r.t.) the (non-optimal) correlation based detector, also in the presence of small frequency offsets. Finally, we investigate the performance improvement of the new scheme when applied to M-ary quadrature amplitude modulation (M-QAM) systems.

5.2 Problem Statement

The frame structure is shown in Fig. 5.1 where a sync word composed of N_{SW} arbitrary symbols $(c_0, ..., c_{N_{\mathrm{SW}}-1})$ is periodically inserted, with period N_f, in

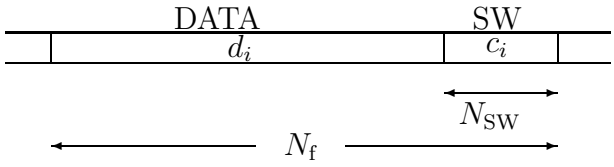

Figure 5.1: The frame structure.

a random M-PSK data stream. The SW symbols c_i are completely arbitrary. The data stream is assumed to be composed of M-PSK symbols d_i which are i.i.d. and uniformly distributed over the set $\left\{e^{j0}, e^{j2\pi/M}, \ldots, e^{j(M-1)2\pi/M}\right\}$.

We assume matched filter (MF) and perfect clock synchronization with sampling period T seconds. The observation window is composed of the N_{f} samples $r_0, r_1, \ldots, r_{N_{\mathrm{f}}-1}$. The SW is transmitted starting at position $m \in \{0, \cdots, N_{\mathrm{f}}-1\}$. The received baseband complex samples, $r_i = r_i^{\mathrm{I}} + j\, r_i^{\mathrm{Q}}$, are

$$\begin{aligned} r_{i \bmod N_{\mathrm{f}}} &= c_{i-m}\, e^{j\varphi} + n_{i \bmod N_{\mathrm{f}}}, && i = m, \ldots, N_{\mathrm{SW}}+m-1 \\ r_i &= d_i\, e^{j\varphi} + n_i, && \text{elsewhere} \end{aligned}$$

where φ is a r.v. uniformly distributed over $[-\pi, \pi)$ representing the carrier phase offset, assumed constant over the considered observation window, and n_i are the i.i.d. circularly symmetric complex Gaussian r.v.s, with zero mean and variance σ^2 per dimension, accounting for thermal noise. We normalize the constellation for the data so that the energy per symbol is unity, i.e., $E_s \triangleq \mathbb{E}\left\{|d_i|^2\right\} = 1$. Consequently, the SNR is $E_s/N_0 = 1/(2\sigma^2)$, where N_0 is the one-sided thermal noise power spectral density.

5.3 Testing Hypothesis for FS

In this section, we generalize the work in [163], which considered BPSK, to a broader class of multilevel modulation. More precisely, we derive optimal metrics for frame synchronization of M-PSK signals, $M \geq 4$. As described in [160, 162, 163], the metric for estimating if the SW position starts at position 0 (hypothesis $\mathcal{H}_1$) or not (hypothesis $\mathcal{H}_0$) is related to testing the following hypotheses:

$$\begin{aligned} \mathcal{H}_0 &: r_i = d_i\, e^{j\varphi} + n_i, && i = 0, \ldots, N_{\mathrm{SW}} - 1 \\ \mathcal{H}_1 &: r_i = c_i\, e^{j\varphi} + n_i, && i = 0, \ldots, N_{\mathrm{SW}} - 1\,. \end{aligned}$$

The common test used for synchronization is based on the so-called noncoherent correlation metric

$$\Lambda^{(\mathrm{corr})}(\mathbf{r}) = \left| \sum_{i=0}^{N_{\mathrm{SW}}-1} r_i^* \, c_i \right| \underset{\mathcal{D}_0}{\overset{\mathcal{D}_1}{\gtrless}} \lambda \tag{5.1}$$

where $\mathbf{r} = r_0, r_1 \ldots, r_{N_{\mathrm{SW}}-1}$ and $\mathcal{D}_0, \mathcal{D}_1$, are respectively decisions for $\mathcal{H}_0, \mathcal{H}_1$. Since this test is widely adopted, we will use it as a benchmark for the comparison with the new proposed tests. However, we remark that, although commonly used, the test based on noncoherent correlation metric (5.1) is by no way the optimal one, as shown in [163] for binary modulation formats.

In order to derive the optimal test for M-PSK, we start from the general form of the likelihood ratio test (LRT)

$$\Lambda(\mathbf{r}) = \frac{f_{\mathbf{R}|\mathcal{H}_1}(\mathbf{r}|\mathcal{H}_1)}{f_{\mathbf{R}|\mathcal{H}_0}(\mathbf{r}|\mathcal{H}_0)} \underset{\mathcal{D}_0}{\overset{\mathcal{D}_1}{\gtrless}} \lambda \tag{5.2}$$

where $f_{\mathbf{R}|\mathcal{H}_l}(\mathbf{r}|\mathcal{H}_l)$ is the PDF of the random vector $\mathbf{R} = (R_0, \ldots, R_{N_{\mathrm{SW}}-1})$ in the hypothesis $\mathcal{H}_l$ and R_i is the r.v. of the received sample r_i [175]. We have now to specialize the general expression (5.2) to our noncoherent frame synchronization problem.

5.3.1 Case $\mathcal{H}_0$

Assuming the $\mathcal{H}_0$ hypothesis, when the data vector $\mathbf{d} = (d_0, \ldots, d_{N_{\mathrm{SW}}-1})$ with phase offset φ is observed, we have the conditional PDF

$$f_{\mathbf{R}|\mathcal{H}_0,\varphi,\mathbf{d}}(\mathbf{r}|\mathcal{H}_0, \varphi, \mathbf{d}) = \prod_{i=0}^{N_{\mathrm{SW}}-1} \frac{1}{2\pi\sigma^2} \, e^{-\frac{\left| r_i - d_i \, e^{j\varphi} \right|^2}{2\sigma^2}}. \tag{5.3}$$

Taking the expectation with respect to the distribution of the M-PSK data symbols $\mathbf{d}$ and assuming M even, we have

$$f_{\mathbf{R}|\mathcal{H}_0,\varphi}(\mathbf{r}|\mathcal{H}_0, \varphi) = \left(\frac{2}{M} \right)^{N_{\mathrm{SW}}} K(\mathbf{r}) \prod_{i=0}^{N_{\mathrm{SW}}-1} \sum_{p=0}^{M/2-1} \cosh \Re \left\{ \tilde{r}_i e^{-jp2\pi/M} e^{-j\varphi} \right\} \tag{5.4}$$

where

$$K(\mathbf{r}) = (2\pi\sigma^2)^{-N_{\mathrm{SW}}} \prod_{i=0}^{N_{\mathrm{SW}}-1} e^{-\frac{|r_i|^2+1}{2\sigma^2}}.$$

To simplify the notation, we use the tilde to indicate normalization with respect to the noise variance, i.e., $\tilde{r}_i = r_i/\sigma^2$. Then, we evaluate $f_{\mathbf{R}|\mathcal{H}_0}(\mathbf{r}|\mathcal{H}_0)$ by averaging (5.4) with respect to φ, with different numerical approximation.

5.3.2 Case $\mathcal{H}_1$

For hypothesis $\mathcal{H}_1$, where we observe the known SW symbols c_i in additive Gaussian noise, we have the conditional PDF

$$f_{\mathbf{R}|\mathcal{H}_1,\varphi}(\mathbf{r}|\mathcal{H}_1,\varphi) = \prod_{i=0}^{N_{\mathrm{SW}}-1} \frac{1}{2\pi\sigma^2} e^{-\frac{\left|r_i - c_i\, e^{j\varphi}\right|^2}{2\sigma^2}}. \tag{5.5}$$

Averaging over φ, we obtain

$$f_{\mathbf{R}|\mathcal{H}_1}(\mathbf{r}|\mathcal{H}_1) = K(\mathbf{r})\, I_0\left(\left|\sum_{i=0}^{N_{\mathrm{SW}}-1} \tilde{r}_i^*\, c_i\right|\right) \tag{5.6}$$

where $I_0(x) = (2\pi)^{-1}\int_{-\pi}^{\pi} \exp(x\cos\theta)\, d\theta$ is the zeroth-order modified Bessel function of first kind [176, (8.406)]. In order to use (5.2), we need (5.6) and the expected value of (5.4) with respect to φ. In the following sections we discuss different methods to integrate (5.4) over φ for QPSK and 8-PSK.

5.4 Optimal and Suboptimal Tests for QPSK Modulation

In this section we provide the optimal likelihood ratio test for the QPSK modulated signal. Putting $M = 4$ in (5.4) we get

$$\begin{aligned} f_{\mathbf{R}|\mathcal{H}_0,\varphi}(\mathbf{r}|\mathcal{H}_0,\varphi) &= \left(\frac{1}{2}\right)^{N_{\mathrm{SW}}} K(\mathbf{r}) \prod_{i=0}^{N_{\mathrm{SW}}-1} \Big(\cosh \Re\left\{\tilde{r}_i e^{-j\varphi}\right\} + \cosh \Re\left\{\tilde{r}_i e^{-j\pi/2} e^{-j\varphi}\right\}\Big) \\ &= \left(\frac{1}{2}\right)^{N_{\mathrm{SW}}} K(\mathbf{r}) \prod_{i=0}^{N_{\mathrm{SW}}-1} \Big(\cosh\left(\tilde{r}_i^I \cos\varphi + \tilde{r}_i^Q \sin\varphi\right) + \cosh\left(\tilde{r}_i^I \sin\varphi - \tilde{r}_i^Q \cos\varphi\right)\Big) \end{aligned} \tag{5.7}$$

where $\tilde{r}_i = \tilde{r}_i^{\mathrm{I}} + j\,\tilde{r}_i^{\mathrm{Q}}$. Averaging with respect to φ we get, after some manipulation, the metric for the (optimum) LRT as

$$\Lambda(\mathbf{r}) \triangleq \frac{I_0\left(\left|\sum_{i=0}^{N_{\mathrm{SW}}-1} \tilde{r}_i^* c_i\right|\right)}{\Xi} \tag{5.8}$$

where

$$\Xi \triangleq \int_0^{\pi} \prod_{i=0}^{N_{\mathrm{SW}}-1} \cosh\left(\frac{(\tilde{r_i}^I - \tilde{r_i}^Q)\cos\varphi + (\tilde{r_i}^I + \tilde{r_i}^Q)\sin\varphi}{2}\right) \times \cosh\left(\frac{(\tilde{r_i}^I + \tilde{r_i}^Q)\cos\varphi + (\tilde{r_i}^Q - \tilde{r_i}^I)\sin\varphi}{2}\right) d\varphi.$$

Unfortunately, the LRT in the form (5.8) is not suitable for real time implementation as it requires numerical integration, thus we have to introduce some simplifications. At first, we approximate the denominator by applying both the quadrature rule with N_q points

$$\int_0^{\pi} f(\varphi)d\varphi \simeq \frac{\pi}{N_q} \sum_{l=0}^{N_q-1} f\left(l\frac{\pi}{N_q}\right) \tag{5.9}$$

and by considering that the hyperbolic cosine has exponential growth taking into account only the maximum contribution. Then, the corresponding approximate LLRT can be written as

$$\ln \Lambda^{(1)}(\mathbf{r}) \triangleq \ln I_0\left(\left|\sum_{i=0}^{N_{\mathrm{SW}}-1} \tilde{r}_i^* c_i\right|\right) - \max_l \left[\sum_{i=0}^{N_{\mathrm{SW}}-1} \ln\left(\cosh\left(\frac{(\tilde{r}_i^I - \tilde{r}_i^Q)\cos\varphi_l + (\tilde{r}_i^I + \tilde{r}_i^Q)\sin\varphi_l}{2}\right) \times \cosh\left(\frac{(\tilde{r}_i^I + \tilde{r}_i^Q)\cos\varphi_l + (\tilde{r}_i^Q - \tilde{r}_i^I)\sin\varphi_l}{2}\right)\right)\right] \tag{5.10}$$

where $\varphi_l = l\pi/N_q$.

Regarding the numerator of (5.8), $\ln \Lambda^{(1)}(\mathbf{r})$ can be approximated for high SNR as

$$\ln \Lambda^{(2)}(\mathbf{r}) \triangleq \left|\sum_{i=0}^{N_{\mathrm{SW}}-1} \tilde{r}_i^* c_i\right| - \max_l \left[\sum_{i=0}^{N_{\mathrm{SW}}-1} \left|\frac{(\tilde{r}_i^I - \tilde{r}_i^Q)\cos\varphi_l + (\tilde{r}_i^I + \tilde{r}_i^Q)\sin\varphi_l}{2}\right| + \sum_{i=0}^{N_{\mathrm{SW}}-1} \left|\frac{(\tilde{r}_i^I + \tilde{r}_i^Q)\cos\varphi_l + (\tilde{r}_i^Q - \tilde{r}_i^I)\sin\varphi_l}{2}\right|\right] \tag{5.11}$$

where we used the approximations

$$\ln I_0(x) \simeq |x| - \ln\sqrt{2\pi\,|x|} \simeq |x|$$
$$\ln\cosh(x) \simeq |x| - \ln 2$$

which are valid for $|x| \gg 1$.

In fact, (5.11) can be interpreted as a modification of the noncoherent correlator with an additive correction term. The approximation accuracy of the numerical integration in (5.10) increases with N_q. For $N_q = 2$ the metrics given in (5.10) and (5.11) specialize to:

$$\ln\Lambda^{(1)}(\mathbf{r}) \triangleq \ln I_0\left(\left|\sum_{i=0}^{N_{SW}-1} \tilde{r}_i^* c_i\right|\right) - \max\left[\sum_{i=0}^{N_{\mathrm{SW}}-1} \ln\left(\cosh\frac{\tilde{r}_i^I+\tilde{r}_i^Q}{2}\right), \sum_{i=0}^{N_{\mathrm{SW}}-1} \ln\left(\cosh\frac{\tilde{r}_i^I-\tilde{r}_i^Q}{2}\right)\right] \tag{5.12}$$

$$\ln\Lambda^{(2)}(\mathbf{r}) \triangleq \left|\sum_{i=0}^{N_{\mathrm{SW}}-1} r_i^* c_i\right| - \max\left[\sum_{i=0}^{N_{\mathrm{SW}}-1} \left|\frac{\tilde{r}_i^I+\tilde{r}_i^Q}{2}\right|, \sum_{i=0}^{N_{\mathrm{SW}}-1} \left|\frac{\tilde{r}_i^I-\tilde{r}_i^Q}{2}\right|\right]. \tag{5.13}$$

For $N_q = 4$ the metric for QPSK in (5.11) becomes

$$\ln\Lambda^{(2)}(\mathbf{r}) \triangleq -\max\left[\sum_{i=0}^{N_{\mathrm{SW}}-1} \left|\frac{\tilde{r}_i^I+\tilde{r}_i^Q}{2}\right|, \sum_{i=0}^{N_{\mathrm{SW}}-1} \left|\frac{\tilde{r}_i^I-\tilde{r}_i^Q}{2}\right|, \sum_{i=0}^{N_{\mathrm{SW}}-1} \left|\frac{\sqrt{2}|\tilde{r}_i^I|}{2}\right|, \sum_{i=0}^{N_{\mathrm{SW}}-1} \left|\frac{\sqrt{2}|\tilde{r}_i^Q|}{2}\right|\right] + \left|\sum_{i=0}^{N_{\mathrm{SW}}-1} r_i^* c_i\right|. \tag{5.14}$$

In Section 5.7 we numerically investigate the synchronization error probability as a function of the signal to noise ratio for the tests based on these metrics.

5.5 Optimal and Suboptimal Tests for 8-PSK Modulation

For 8-PSK signals the transmitted symbols are $d_i = \exp\{j\pi m/4\}$, $m \in \{0, 1, ..., 7\}$, and (5.4) becomes:

$$f_{\mathbf{R}|\mathcal{H}_0,\varphi}(\mathbf{r}|\mathcal{H}_0,\varphi) = \left(\frac{1}{2}\right)^{N_{\mathrm{SW}}} K(\mathbf{r}) \prod_{i=0}^{N_{\mathrm{SW}}-1} \Big(\cosh \Re\left\{\tilde{r}_i e^{-j\varphi}\right\} + \cosh \Re\left\{\tilde{r}_i e^{-j\pi/4} e^{-j\varphi}\right\} + \cosh \Re\left\{\tilde{r}_i e^{-j\pi/2} e^{-j\varphi}\right\} + \cosh \Re\left\{\tilde{r}_i e^{-j3\pi/4} e^{-j\varphi}\right\} \Big). \tag{5.15}$$

Taking into account that φ is uniformly distributed over the interval $[-\pi, \pi)$, we obtain from (5.15)

$$f_{\mathbf{R}|\mathcal{H}_0,\varphi}(\mathbf{r}|\mathcal{H}_0) = \frac{K(\mathbf{r})}{\pi} \int_0^{\pi} \prod_{i=0}^{N_{\mathrm{SW}}-1} \Bigg(\cosh\left(\tilde{r}_i^I \cos\varphi + \tilde{r}_i^Q \sin\varphi\right) + \cosh\left(\frac{(\tilde{r}_i^I + \tilde{r}_i^Q)\cos\varphi + (\tilde{r}_i^Q - \tilde{r}_i^I)\sin\varphi}{\sqrt{2}}\right) + \cosh\left(\frac{(\tilde{r}_i^I + \tilde{r}_i^Q)\cos\varphi + (\tilde{r}_i^I - \tilde{r}_i^Q)\sin\varphi}{\sqrt{2}}\right) + \cosh\left(\tilde{r}_i^Q \cos\varphi - \tilde{r}_i^I \sin\varphi\right) \Bigg) d\varphi\,. \tag{5.16}$$

The resulting exact metric (i.e., the LRT for 8-PSK modulation) is reported as

$$\Lambda(\mathbf{r}) \triangleq \frac{I_0\left(\left|\sum_{i=0}^{N_{\mathrm{SW}}-1} \tilde{r}_i^* c_i\right|\right)}{\Psi} \tag{5.17}$$

where

$$\Psi \triangleq \int_0^{\pi} \prod_{i=0}^{N_{\mathrm{SW}}-1} \Bigg(\cosh\left(\tilde{r}_{i,\varphi}^S\right) + \cosh\left(\tilde{r}_{i,\varphi}^D\right) + \cosh\left(\frac{\tilde{r}_{i,\varphi}^S + \tilde{r}_{i,\varphi}^D}{\sqrt{2}}\right) + \cosh\left(\frac{\tilde{r}_{i,\varphi}^{I+Q} + \tilde{r}_{i,\varphi}^{I-Q}}{\sqrt{2}}\right) \Bigg) d\varphi \tag{5.18}$$

and we put

$$\tilde{r}^S_{i,\varphi} = \tilde{r}^I_i \cos\varphi + \tilde{r}^Q_i \sin\varphi \qquad \tilde{r}^D_{i,\varphi} = \tilde{r}^Q_i \cos\varphi - \tilde{r}^I_i \sin\varphi$$
$$\tilde{r}^{I+Q}_{i,\varphi} = \left(\tilde{r}^I_i + \tilde{r}^Q_i\right)\cos\varphi \qquad \tilde{r}^{I-Q}_{i,\varphi} = \left(\tilde{r}^I_i - \tilde{r}^Q_i\right)\cos\varphi\,.$$

To simplify (5.17), we again use the rectangular quadrature rule and the approximations. More precisely, the LLRT can be approximated for large SNR as

$$\begin{aligned}\ln\Lambda^{(1)}(\mathbf{r}) \triangleq -\max_l \Bigg[\sum_{i=0}^{N_{\mathrm{SW}}-1} \ln\Bigg(&\cosh\left(\tilde{r}^I_i\cos\varphi_l + \tilde{r}^Q_i\sin\varphi_l\right) \\ &+ \cosh\left(\frac{(\tilde{r}^I_i + \tilde{r}^Q_i)\cos\varphi_l + (\tilde{r}^Q_i - \tilde{r}^I_i)\sin\varphi_l}{\sqrt{2}}\right) \\ &+ \cosh\left(\frac{(\tilde{r}^I_i + \tilde{r}^Q_i)\cos\varphi_l + (\tilde{r}^I_i - \tilde{r}^Q_i)\sin\varphi_l}{\sqrt{2}}\right) \\ &+ \cosh\left(\tilde{r}^Q_i\cos\varphi_l - \tilde{r}^I_i\sin\varphi_l\right)\Bigg)\Bigg] + \left|\sum_{i=0}^{N_{\mathrm{SW}}-1} \tilde{r}^*_i c_i\right|. \end{aligned} \tag{5.19}$$

For example, the formula based on the rectangular quadrature approximation with $N_q = 2$ is

$$\begin{aligned}\ln\Lambda^{(2)}(\mathbf{r}) \triangleq &\left|\sum_{i=0}^{N_{\mathrm{SW}}-1} \tilde{r}^*_i c_i\right| - \\ &\max\Bigg[\sum_{i=0}^{N_{\mathrm{SW}}-1} \ln\left(\cosh\tilde{r}^I_i + \cosh\tilde{r}^Q_i + 2\cosh\frac{\tilde{r}^I_i + \tilde{r}^Q_i}{\sqrt{2}}\right), \\ &\sum_{i=0}^{N_{\mathrm{SW}}-1} \ln\left(\cosh\tilde{r}^I_i + \cosh\tilde{r}^Q_i + 2\cosh\frac{\tilde{r}^I_i - \tilde{r}^Q_i}{\sqrt{2}}\right)\Bigg] \end{aligned} \tag{5.20}$$

and for $N_q = 4$ is

$$\begin{aligned}\ln\Lambda^{(2)}(\mathbf{r}) \triangleq &\left|\sum_{i=0}^{N_{\mathrm{SW}}-1} \tilde{r}^*_i c_i\right| \\ &-\max\Bigg[\sum_{i=0}^{N_{\mathrm{SW}}-1} \ln\left(\cosh\tilde{r}^I_i + \cosh\tilde{r}^Q_i + 2\cosh\frac{\tilde{r}^I_i + \tilde{r}^Q_i}{\sqrt{2}}\right), \\ &\sum_{i=0}^{N_{\mathrm{SW}}-1} \ln\left(\cosh\frac{\tilde{r}^I_i - \tilde{r}^Q_i}{\sqrt{2}} + \cosh\frac{\tilde{r}^I_i + \tilde{r}^Q_i}{\sqrt{2}} + \cosh\tilde{r}^I_i + \cosh\tilde{r}^Q_i\right), \\ &\sum_{i=0}^{N_{\mathrm{SW}}-1} \ln\left(\cosh\tilde{r}^I_i + \cosh\tilde{r}^Q_i + 2\cosh\frac{\tilde{r}^I_i - \tilde{r}^Q_i}{\sqrt{2}}\right)\Bigg]. \end{aligned} \tag{5.21}$$

5.6 Uniform Phase Approximation Based Metric

The previous tests are based on the LRT and specialized to particular data formats. Alternatively, in this section we propose a slightly different approach, where we approximate the phase distribution of the data symbols with a uniform random variable. More precisely, since we are dealing with $M \geq 4$, we approximate the data symbols as $d_i = e^{j\theta_i}$ where we treat $\theta_0, \theta_1, ..., \theta_{N_{\mathrm{SW}}-1}$ as i.i.d. continuous r.v.s uniformly distributed over $[-\pi, \pi)$. In this way, (5.4) becomes

$$\begin{aligned} f_{\mathbf{R}|\mathcal{H}_0,\varphi}(\mathbf{r}|\mathcal{H}_0,\varphi) &\simeq K(\mathbf{r}) \prod_{i=0}^{N_{\mathrm{SW}}-1} \frac{1}{2\pi} \int_{-\pi}^{\pi} e^{-|\tilde{r}_i|\cos(\arg c_i - \varphi - \theta_i)}\, d\theta_i \\ &= K(\mathbf{r}) \prod_{i=0}^{N_{\mathrm{SW}}-1} I_0(|\tilde{r}_i|). \end{aligned} \tag{5.22}$$

Note also that there is no more dependency on φ, so (5.22) is an approximation of $f_{\mathbf{R}|\mathcal{H}_0}(\mathbf{r}|\mathcal{H}_0)$. Now, substituting (5.22) and (5.6) into (5.2) we obtain the metric

$$\ln \Lambda^{(3)}(\mathbf{r}) \triangleq \ln I_0 \left(\left| \sum_{i=0}^{N_{\mathrm{SW}}-1} \tilde{r}_i^* c_i \right| \right) - \sum_{i=0}^{N_{\mathrm{SW}}-1} \ln I_0 \left(|\tilde{r}_i^*| \right). \tag{5.23}$$

Thus, for large SNR the metric becomes simply

$$\ln \Lambda^{(4)}(\mathbf{r}) \triangleq \left| \sum_{i=0}^{N_{\mathrm{SW}}-1} r_i^*\, c_i \right| - \sum_{i=0}^{N_{\mathrm{SW}}-1} |r_i| \tag{5.24}$$

which coincides with [163, (25)]. This metric is thus the noncoherent correlation corrected by removing the ℓ_1-norm of the observed sampled vector, which accounts for the non-gaussianity of the data symbols.

For M-PSK with $M \geq 4$, we found that (5.24) gives performance very close to the optimal metric obtained in the previous sections. In the next section we also show that the same test is better than noncoherent correlation for M-QAM modulations.

5.7 Numerical Results

In this section we investigate the performance of the proposed methods used for frame synchronization by adopting Monte Carlo simulations. All results

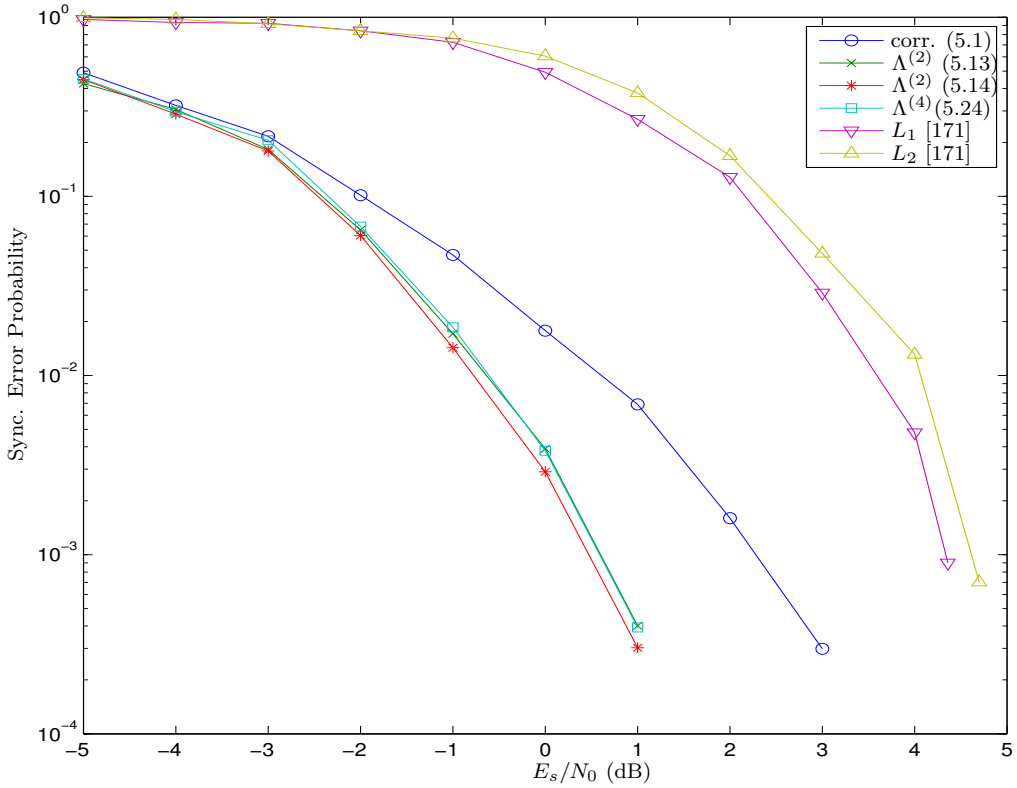

Figure 5.2: Frame synchronization error probability for peak detectors, QPSK over AWGN channels with phase offset. Comparison between the noncoherent correlation metric, the proposed metrics, and the tests from [171]. Frame composed of $N_{\mathrm{f}} = 240$ QPSK symbols, sync word of $N_{\mathrm{SW}} = 24$ QPSK symbols.

shown in the following have been obtained by counting at least 100 synchronization errors.

Regarding FS by peak detection for QPSK signals, we assume that the received samples are due to randomly generated QPSK symbols ($M = 4$) with a constant phase offset over the frame, in the presence of additive complex Gaussian noise. We consider the algorithms described in Section 5.4: for each observation window of N_{f} samples, the detector analyzes all N_{SW}-length sequences, estimating the SW position as that maximizing the metric. In particular, our metrics reported in (5.13) and (5.14) (high complexity), and (5.24) (low complexity) are compared with the common noncoherent correlation (5.1), and with the complex metrics L_1 and L_2 derived in [171].

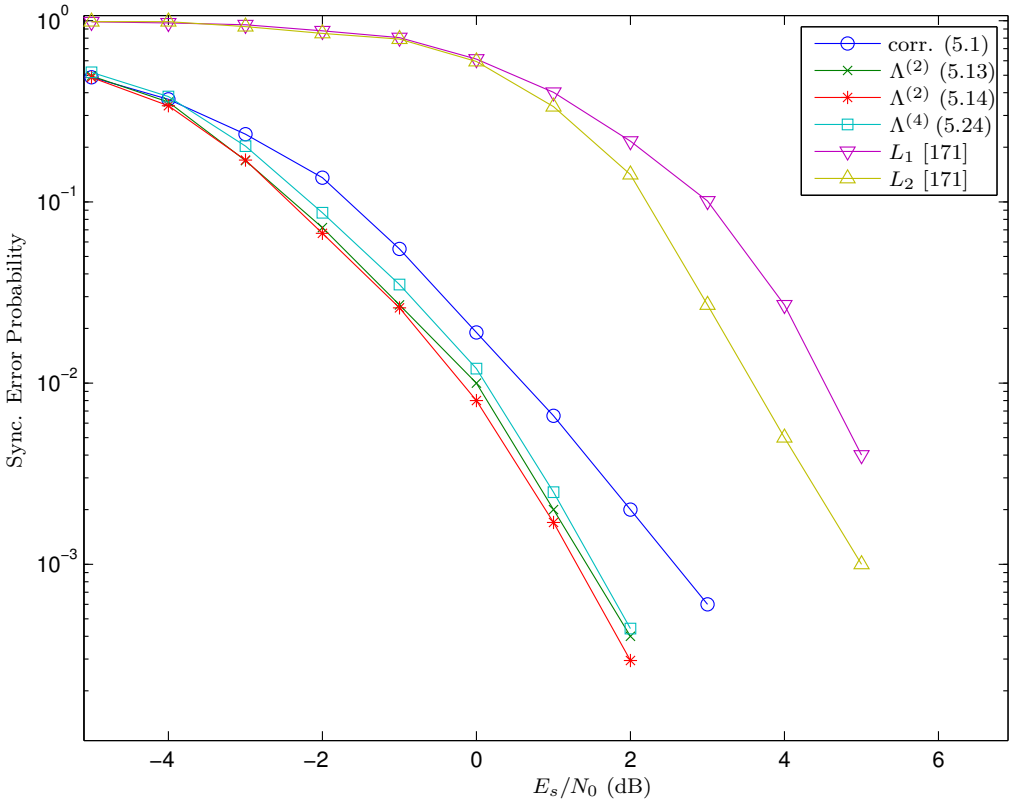

Figure 5.3: Frame synchronization error probability for peak detectors, QPSK over AWGN channels with phase and frequency offsets. Frame composed of $N_{\mathrm{f}} = 1000$ QPSK symbols, sync word of $N_{\mathrm{SW}} = 32$ QPSK symbols. For each simulation, the frequency offset is uniformly generated over the interval $[-\Delta f_{\max} T : \Delta f_{\max} T] = [-0.01; 0.01]$.

Fig. 5.2 shows the values of the synchronization error probability for the derived metrics, as a function of the SNR, obtained with $N_f = 240$ and $N_{SW} = 24$. The metrics L_1 and L_2 have poor performance in this case, as they are designed to be robust w.r.t. large frequency offsets. On the contrary, the proposed metrics, which are designed for phase offsets but negligible frequency offsets, show large improvements with respect to the noncoherent correlation metric. For example, for a target synchronization error probability of 10^{-3}, our tests require 2 dB less than the noncoherent correlation test. As shown, the performance for the metrics (5.13) and (5.14) are very close, and slightly outperforming that obtained by using (5.24). The metric (5.24)

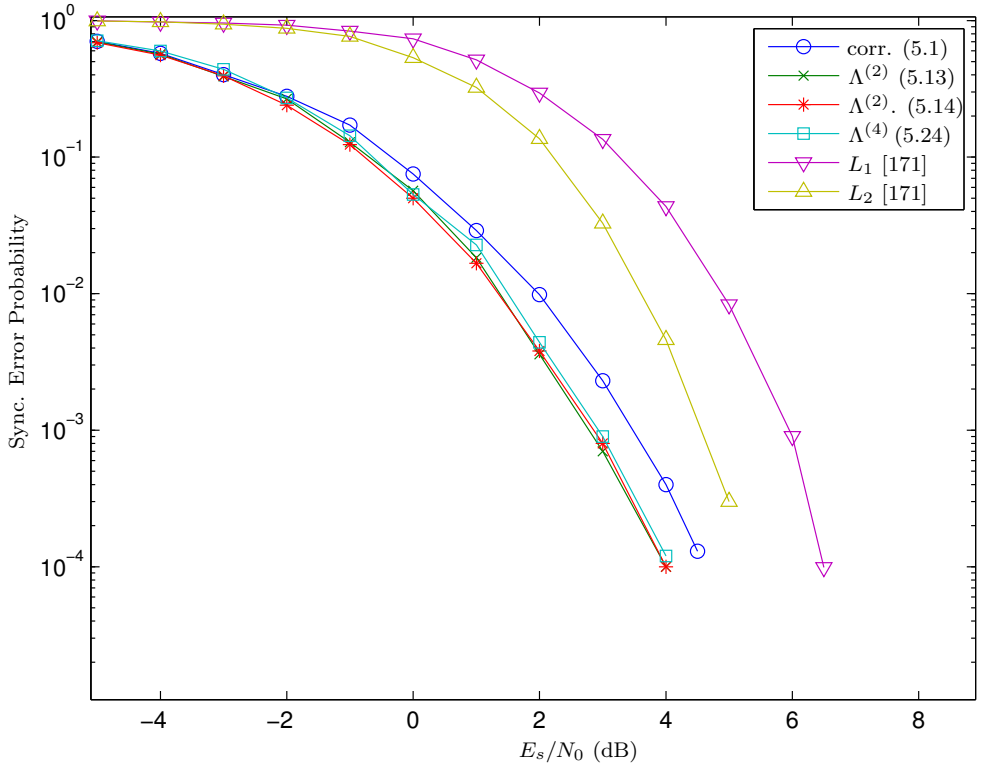

Figure 5.4: Frame synchronization error probability for peak detectors, QPSK over AWGN channels with phase and frequency offsets. Frame composed of $N_{\mathrm{f}} = 1000$ QPSK symbols, sync word of $N_{\mathrm{SW}} = 32$ QPSK symbols, frequency offset is $\Delta fT = 0.01$.

seems therefore the most appealing due to its simplicity.

The new metrics are also investigated in Fig. 5.3 and Fig. 5.4 in the presence of frequency offset. More precisely, we assume that the phase φ in Section 5.2 is replaced by $\varphi_0 + 2\pi\Delta fTi$, where the phase offset φ_0 is uniformly distributed over $[-\pi; \pi)$.

Fig. 5.3 refers to the case of uniformly distributed normalized frequency offset ΔfT over the interval $(-\Delta f_{\max}T; \Delta f_{\max}T]$. The maximum frequency offset here is $\Delta f_{\max}T = 0.01$, $N_f = 1000$, $N_{SW} = 32$. As it is shown, the proposed metrics give large improvements when compared to the noncoherent correlation and to the metrics from [171]. In fact, since the latter metrics are designed to work with a large frequency offset, they perform poorly when a small frequency offset is present. Since the difference between the proposed metrics is not significant, the metric (5.24) could be preferred due to its

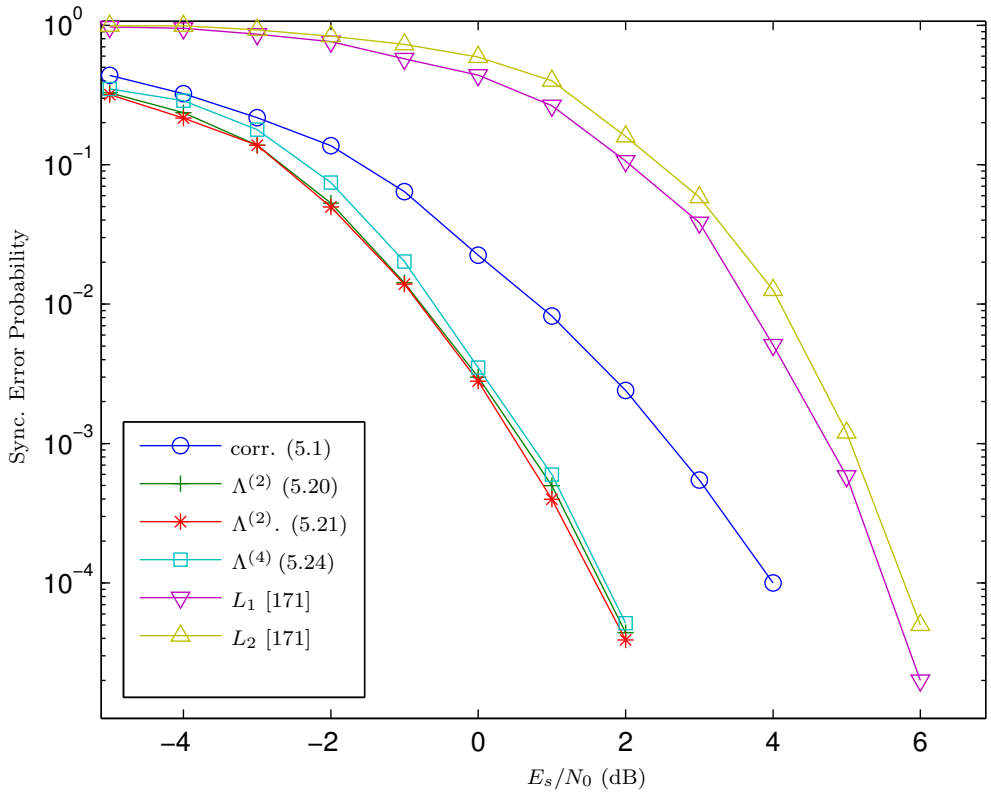

Figure 5.5: Frame synchronization error probability for peak detectors, 8-PSK over AWGN channels with phase offset. Frame composed of $N_{\mathrm{f}} = 240$ 8-PSK symbols, sync word of $N_{\mathrm{SW}} = 24$ 8-PSK symbols.

simplicity.

Fig. 5.4 shows the results for a fixed value of the frequency offset, taken at the interval edge of the previous figure, i.e., with $\Delta fT = 0.01$. In this case we can see the same behavior as in Fig. 5.3. The advantage of the proposed metrics (5.13), (5.14) and (5.24) is still large in comparison with (5.1), L_1 and L_2 from [171]. However, we observe that the gain with such large value of the frequency offset is reduced with respect to Fig. 5.3.

We now investigate the performance of the proposed synchronization metrics for 8-PSK modulation. We carried out several experiments with the common noncoherent correlation (5.1), the metrics L_1 and L_2 [171], and our proposed metrics from the Section 5.5. We use (5.20) and (5.21) as high complexity tests and (5.24) as the simplest one.[1]

[1]Note that the implementation of the tests (5.20), (5.21), L_1, and L_2 could be quite

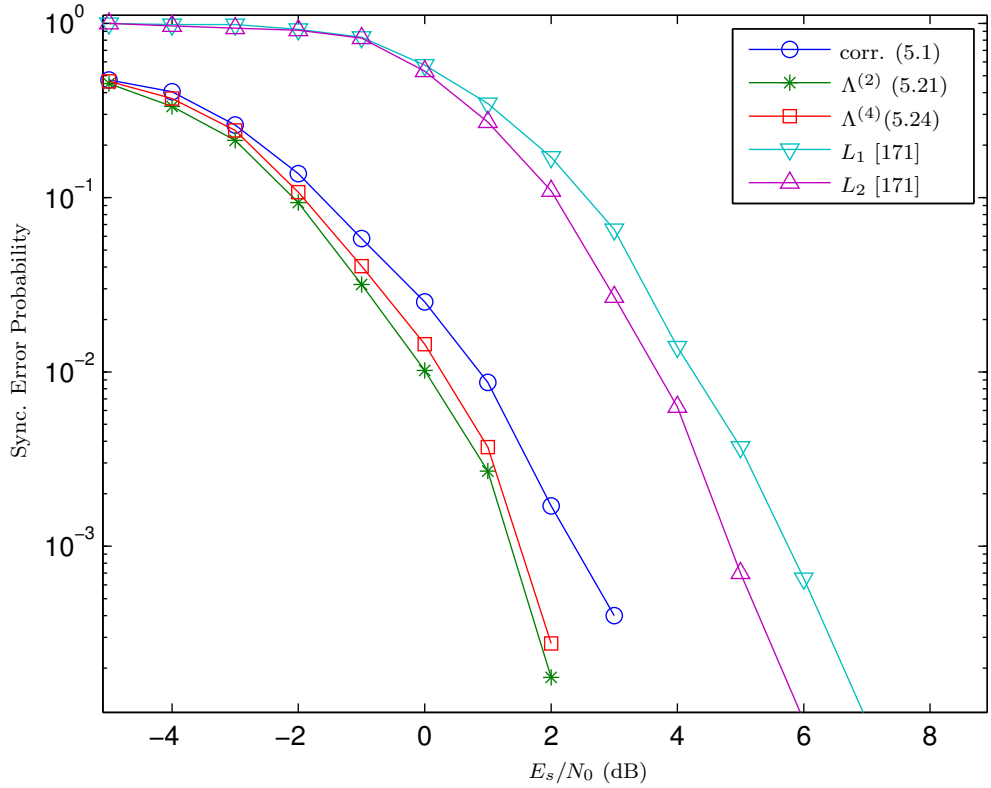

Figure 5.6: Frame synchronization error probability for peak detectors, 8-PSK over AWGN channels with phase and frequency offsets. Frame composed of $N_{\mathrm{f}} = 1000$ 8-PSK symbols, sync word of $N_{\mathrm{SW}} = 32$ 8-PSK symbols, frequency offset uniformly distributed over the interval $[-\Delta f_{\max}T : \Delta f_{\max}T] = [-0.01; 0.01]$.

Fig. 5.5 represents the values of the synchronization error probability for the derived metrics, as a function of the SNR, obtained for $N_f = 240$ and $N_{SW} = 24$. Again, the proposed metrics perform better than the others. For example, for a target synchronization error probability of 10^{-3}, our tests require at least 2 dB less than the noncoherent correlation test, and at least 4 dB less than the tests from [171].

Fig. 5.6 compares the synchronization error probability for different values of SNR, with the frequency offset ΔfT uniformly distributed over the interval $(-0.01; 0.01]$, $N_f = 1000$ and $N_{SW} = 32$. The proposed formulas are still preferable, however, the metrics from [171] are expected to be more robust

demanding.

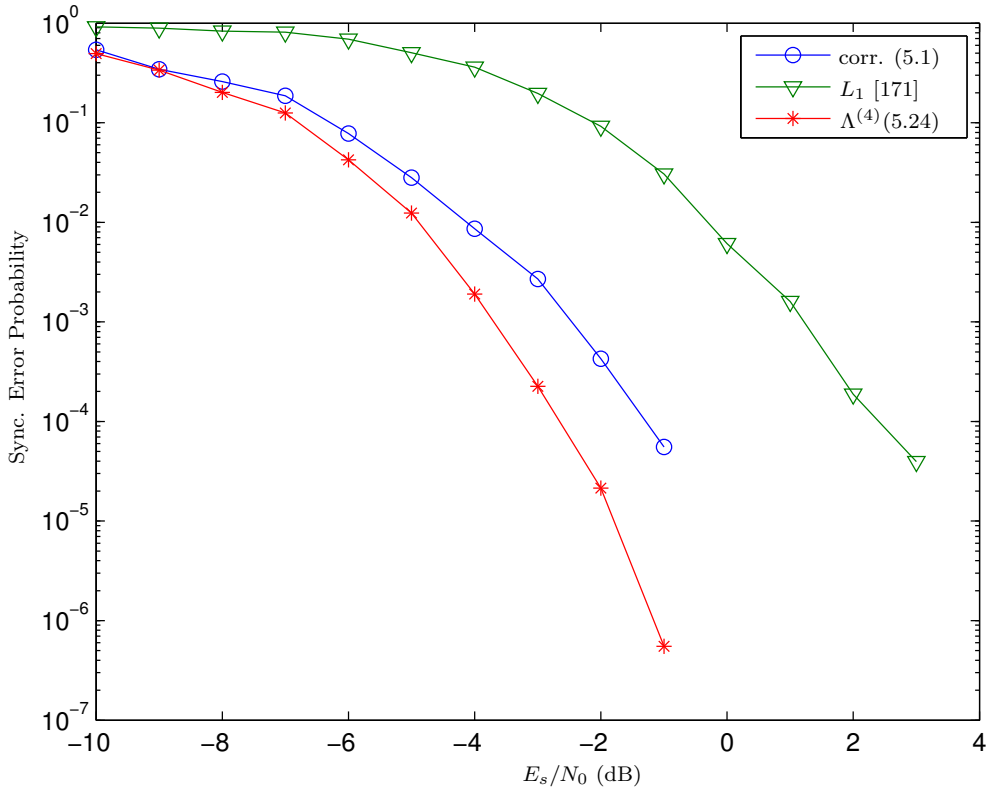

Figure 5.7: Frame synchronization error probability for peak detectors, 16-QAM over AWGN channels with phase offset. Frame composed of $N_{\mathrm{f}} = 240$ 16-QAM symbols, sync word of $N_{\mathrm{SW}} = 24$ 16-QAM symbols.

w.r.t. large frequency offsets.

Considering FS for M-QAM, the exact approach here used for M-PSK could be in theory extended to M-QAM data symbols. However, dealing with an alphabet of symbols with different phases and amplitudes would lead to complicated expressions of limited practical interest. Thus, it would be interesting to see if, e.g., the simple metric (5.24), which was derived assuming data symbols with constant amplitude and uniformly distributed phase, could give for M-QAM some improvements with respect to the noncoherent correlator.

In this regard, Fig. 5.7 shows simulation results assuming a 16−QAM constellation for the proposed test (5.24), the common noncoherent correlation rule (5.1), and L_2 from [171, eq. (11)], without frequency offsets. Again, we see that (5.24) outperforms the other approaches: for example, for a syn-

chronization error probability of 10^{-4} we save more than 1.5 dB in terms of SNR.

5.8 Conclusion

In the context of FS for IoT, the optimal synchronization rule and some suboptimal rules based on statistical inference theory are derived for M-PSK modulation in AWGN channels with phase offset. We verified numerically that our tests outperform the commonly used noncoherent correlation detector. Finally, we can conclude that the simple metric (5.24) (i.e., subtracting an ℓ_1-norm correction term from the noncoherent correlation) can be used in practice to replace the noncoherent correlation for a wide class of modulation formats, i.e., M-PSK, and M-QAM, in the presence of phase and small frequency offsets due to imperfect carrier recovery.

Conclusion

In this thesis, I proposed and analyzed several signal processing approaches for efficient acquisition and compression of sparse and compressible sources. The theory and the algorithms developed here fall under the frameworks of both transform coding and CS, motivated by the fact that signals originating from many sources, e.g., sensors, cameras, and IoT devices, exhibit various types of structures, i.e., sparsity and compressibility.

Chapter 2 provided a tool for the design of CS measurement matrices for real applications, involving always finite size problems with guaranteed recovery probability. In particular, upper bounds on the maximum recoverable sparsity order for sparse signals were derived, based on the RIC of finite Gaussian matrices. These limits guarantee perfect recovery with a predefined probability from a SMV via various sparse reconstruction algorithms, e.g., ℓ_1-minimization, IHT, and CoSaMP algorithms. We found that the proposed analysis, derived from the exact distribution of the extreme eigenvalues, provided tighter bounds compared to those based on the concentration of measure inequality. Also, the corresponding sparsity order limits for robust and stable recovery of compressible signals in noise were derived. The analysis illustrated that the more sparse is the signal, the more robust and stable is the reconstruction process.

Furthermore, it has been shown that a significant performance gain can be achieved by utilizing additional signal structure (i.e., joint sparsity). This model has gained increasing interest, as the data generated from dense IoT networks tend to be joint sparse. For this scenario, the worst-case analysis based on the RIC in Chapter 2 cannot justify the benefits of having MMV. On the contrary, sufficient conditions on the WRICs permit average-case analysis of the recovery. In this regard, Chapter 3 probabilistically investigated the WRICs of finite Gaussian matrices. Additionally, a unified framework was suggested for assessing signal reconstruction through different joint sparse recovery algorithms, e.g., $\ell_{2,1}$ minimization, SA-Music, and OSMP. This analysis provided tight bounds on the maximum joint sparsity order permitting recovery from MMV with a predefined probability. Also,

accurate closed-form approximations were provided, in terms of incomplete gamma functions. The numerical results illustrated that the proposed WRIC method, relying on the exact distribution of the extreme singular values, predicts higher probability of recovery compared to the bounds in [95, Proposition 6.1]. It is also demonstrated that the presented approximations are quite accurate.

Chapter 4 proposed two approaches for the compression and denoising of noisy sparse sources. The provided schemes are based on channel coding theory to provide adequate source compression. The operational distortion-rate and distortion-energy of the presented coders were derived for two classes of sparse sources, i.e., BU and BG, in the presence of pre-quantization noise. The numerical results showed that the gap in performance with respect to the information theoretic bounds is small, and the provided schemes are superior to CS, run length and Huffman encoders, for low sparsity ratio. Furthermore, the effectiveness of employing the syndrome encoding for the compression of signals from real WSNs has been illustrated.

Finally, Chapter 5 provided optimal and suboptimal metrics for FS of PSK modulated signals with phase offset. It has been verified numerically that the derived tests yielded lower probability of synchronization errors comparing to the well-known correlation detector and the metrics in [171], leading to better data extraction and lower power consumption in IoT networks.

Appendix A

Asymmetric Sparse Recovery Condition

In the following, we derive a new sufficient condition for perfect recovery using ℓ_1-minimization generalizing the result $\delta_s(\mathbf{A}) < \frac{1}{3}$ [54], to account for the asymmetric nature of the extreme eigenvalues distribution. In particular, we will prove that

$$\mu_{\mathrm{ECG}}(s, \mathbf{A}) \triangleq 2\,\underline{\delta}_s(\mathbf{A}) + \overline{\delta}_s(\mathbf{A}) < 1 \tag{A.1}$$

is a sufficient condition for recovery via ℓ_1-minimization.

Let us start considering that signal recovery using ℓ_1-minimization is guaranteed if and only if for all non-zero vectors $\mathbf{w}$ in the null space of $\mathbf{A}$, we have

$$\|\mathbf{w}_S\|_1 < \|\mathbf{w}_{\overline{S}}\|_1 \tag{A.2}$$

where $\mathbf{w}_S$ is a vector obtained from $\mathbf{w}$ by keeping its s largest absolute components then setting the remaining $n - s$ elements to zero, and $\mathbf{w}_{\overline{S}} = \mathbf{w} - \mathbf{w}_S$ [177]. Let us prove by contradiction that statement (A.2) is true: suppose that there exist a non-zero vector, $\mathbf{w}$, in the null space of $\mathbf{A}$ such that $\|\mathbf{w}_S\|_1 > \|\mathbf{w}_{\overline{S}}\|_1$. We can represent $\mathbf{w}$ as

$$\mathbf{w} = \sum_{i=1}^{n} a_i\,\mathbf{u}_i \tag{A.3}$$

where all the vectors $\mathbf{u}_i$ have different supports with only one non-zero component (1 or -1), and $a_1 > a_2 > \cdots > a_n \geq 0$. For even s, $\mathbf{w}$ can be

reformulated as a sum of the following vectors

$$\mathbf{w}_{11} = \sum_{i=1}^{s/2} a_i \mathbf{u}_i \qquad \mathbf{w}_{12} = \sum_{i=s/2+1}^{s} a_i \mathbf{u}_i \qquad \mathbf{w}_{21} = \sum_{i=s+1}^{3s/2} a_i \mathbf{u}_i$$

$$\mathbf{w}_{22} = \sum_{i=3s/2+1}^{2s} a_i \mathbf{u}_i \qquad \mathbf{w}_{31} = \sum_{i=2s+1}^{n} \mathbf{u}_i \left(\sum_{j=1}^{s/2} z_{ij} \right)$$

$$\mathbf{w}_{32} = \sum_{i=2s+1}^{n} \mathbf{u}_i \left(\sum_{j=s/2+1}^{s} z_{ij} \right)$$

where $\{z_{ij}\}_{1 \le i \le s\,, 2\,s+1 \le j \le m}$ are non-negative real numbers satisfying $\sum_{j=1}^{s} z_{ij} = a_i$. Then, recalling that $\mathbf{w}$ is in the null space of $\mathbf{A}$, we get

$$\mathbf{A}\left(\mathbf{w}_{11} + \mathbf{w}_{12} + \mathbf{w}_{21} + \mathbf{w}_{22} + \mathbf{w}_{31} + \mathbf{w}_{32}\right) = \mathbf{A}\,\mathbf{w} = \mathbf{0}$$

and from the parallelogram rule

$$\begin{aligned} &\|\mathbf{A}(-\mathbf{w}_{11} + \mathbf{w}_{22} + \mathbf{w}_{32})\|^2 + \|\mathbf{A}(-\mathbf{w}_{12} + \mathbf{w}_{21} + \mathbf{w}_{31})\|^2 \\ &= 2\|\mathbf{A}(\mathbf{w}_{11} + \mathbf{w}_{12})\|^2 + \|\mathbf{A}(\mathbf{w}_{11} + \mathbf{w}_{21} + \mathbf{w}_{31})\|^2 \\ &\qquad + \|\mathbf{A}(\mathbf{w}_{12} + \mathbf{w}_{22} + \mathbf{w}_{32})\|^2 . \end{aligned} \tag{A.4}$$

Then, from Definition 2 of the ARICs, [54, Lemma 5.2], and (A.4) we get

$$\begin{aligned} 0 \ge\; & 2\left(1 - \underline{\delta}_s(\mathbf{A})\right) \sum_{i=1}^{s} a_i^2 \\ & + \left(1 - \underline{\delta}_s(\mathbf{A})\right) \left[\sum_{i=1}^{s} a_i^2 + \sum_{i=s+1}^{2s} \left(a_i + \sum_{j=2s+1}^{n} k_{ij} \right)^2 \right] \\ & - \left(1 + \overline{\delta}_s(\mathbf{A})\right) \left[\sum_{i=1}^{s} a_i^2 + \sum_{i=s+1}^{2s} \left(a_i + \sum_{j=2s+1}^{n} k_{ij} \right)^2 \right] \\ =\; & \left(-3\,\underline{\delta}_s(\mathbf{A}) - \overline{\delta}_s(\mathbf{A}) + 2\right) \sum_{i=1}^{s} a_i^2 \\ & - \left(\underline{\delta}_s(\mathbf{A}) + \overline{\delta}_s(\mathbf{A})\right) \left[\sum_{i=s+1}^{2s} \left(a_i + \sum_{j=2s+1}^{n} k_{ij} \right)^2 \right] \end{aligned} \tag{A.5}$$

and from [54, Lemma 3.1], we have

$$\left(a_{s+i} + \sum_{j=2s+1}^{n} k_{ij} \right) \le \frac{1}{s} \sum_{i=1}^{s} a_i \,. \tag{A.6}$$

Finally, combining (A.5) with (A.6), we get

$$\left(2\,\underline{\delta}_s(\mathbf{A}) + \overline{\delta}_s(\mathbf{A}) - 1\right) \sum_{i=1}^{s} a_i^2 \geq 0\,. \tag{A.7}$$

Since $\mathbf{w} \neq \mathbf{0}$ and $2\,\underline{\delta}_s(\mathbf{A}) + \overline{\delta}_s(\mathbf{A}) < 1$, then (A.7) does not hold, contradicting our assumption. Hence, we conclude that (A.2) is valid and perfect recovery is guaranteed.

Appendix B

Quantizer Distortion for Noisy BU Sources

The PDF in (4.38) can be approximated, considering that $\lfloor x \rfloor \simeq x - 1/2$, as

$$f_{\mathcal{T}}^{\mathrm{BU}}(\tau) \simeq \tilde{f}_{\mathcal{T}}^{\mathrm{BU}}(\tau) \triangleq (1-p)\delta(\tau) + \frac{p}{2A} \times \begin{cases} 1 + \Phi(\tau)\left(\frac{2A}{\Delta} - 1\right), & |\tau| < \frac{\Delta}{2} \\ \Phi(\tau)\left(\frac{2A}{\Delta} - \frac{|\tau|}{\Delta}\right) + \phi(|\tau|), & \frac{\Delta}{2} \le |\tau| \le 2A - \frac{\Delta}{2} \\ 0, & \text{otherwise.} \end{cases} \quad \text{(B.1)}$$

Consequently, the distortion $D^{\mathrm{BU}}(\Delta)$ can be approximated as

$$\begin{aligned} D^{\mathrm{BU}}(\Delta) \simeq \widehat{D}^{\mathrm{BU}}(\Delta) \triangleq \int_{-\infty}^{\infty} \tau^2 \, \tilde{f}_{\mathcal{T}}^{\mathrm{BU}}(\tau)\, d\tau = \frac{p}{48\sqrt{2\pi}\, A\, \Delta} \\ \times \Bigg(2\sigma_{\mathrm{n}} e^{-\frac{2A^2}{\sigma_{\mathrm{n}}^2}} \Big(16A^3 - 32A^2\Delta + 18A\Delta^2 - 4\sigma_{\mathrm{n}}^2(A - 2\Delta) - 3\Delta^3 \Big) - 12\Delta \\ \times e^{-\frac{\Delta^2}{2\sigma_{\mathrm{n}}^2}} \sigma_{\mathrm{n}}^3 + 4\sigma_{\mathrm{n}} e^{-\frac{(\Delta - 2A)^2}{2\sigma_{\mathrm{n}}^2}} \Big(-8A^3 - 4A^2\Delta + A\left(\Delta^2 + 2\sigma_{\mathrm{n}}^2\right) + 3\Delta\sigma_{\mathrm{n}}^2 \Big) \\ + \sqrt{2\pi}\, \mathrm{erf}\left(\frac{\sqrt{2}A}{\sigma_{\mathrm{n}}} \right) \Big(32A^4 + 3\Delta\sigma_{\mathrm{n}}^2(8A - \Delta) + 18\sigma_{\mathrm{n}}^4 \Big) + 4\sqrt{2\pi} A\Delta^3 \\ + 2\sqrt{2\pi} A\Delta\, \mathrm{erfc}\left(\frac{\sqrt{2}A}{\sigma_{\mathrm{n}}} \right) \Big(32A^2 - 18A\Delta + 3\Delta^2 \Big) - \sqrt{2\pi}\, \mathrm{erf}\left(\frac{2A - \Delta}{\sqrt{2}\sigma_{\mathrm{n}}} \right) \\ \times \Big(32A^4 + 3\Delta\sigma_{\mathrm{n}}^2(3\Delta - 8A) + 18\sigma_{\mathrm{n}}^4 \Big) + 2\sqrt{2\pi} A\Delta^2 \Big(\Delta - 6A \Big) \mathrm{erfc}\left(\frac{2A - \Delta}{\sqrt{2}\sigma_{\mathrm{n}}} \right) \\ + 2\Delta\sigma_{\mathrm{n}} \left(3\Delta^2 - 8\sigma_{\mathrm{n}}^2 \right) - 9\sqrt{2\pi}\sigma_{\mathrm{n}}^2 \left(\Delta^2 + 2\sigma_{\mathrm{n}}^2 \right) \mathrm{erf}\left(\frac{\Delta}{\sqrt{2}\sigma_{\mathrm{n}}} \right) \Bigg). \end{aligned} \quad \text{(B.2)}$$

In order to obtain a more compact formula, $\widehat{D}^{\mathrm{BU}}(\Delta)$ can be further approximated for $A \gg \sigma_{\mathrm{n}}$, as in (4.40). Also, the exact distortion, $D^{\mathrm{BU}}(\Delta)$, can be upper and lower bounded by noting that the floor function in (4.38) is

$$-\frac{1}{2} - \frac{|\tau|}{\Delta} < \left\lfloor \frac{1}{2} - \frac{|\tau|}{\Delta} \right\rfloor \leq \frac{1}{2} - \frac{|\tau|}{\Delta}\,.$$

Appendix C

Entropy of Quantized BG and BU Sources

The entropy of the quantized sources is essential to understand the fundamental limits on the minimum number of bits required to encode these signals [108]. In this regards, the entropy of $\widetilde{\mathcal{S}} \triangleq Q^{-1}\left(Q\left(\mathcal{S}\right)\right)$ at the output of the uniform quantizer is given from (4.28) as

$$\mathcal{H}\left(\widetilde{\mathcal{S}}\right) = \sum_{i=i_{\min}}^{i_{\max}} -\mathbb{P}\left\{\widetilde{\mathcal{S}} = i\,\Delta\right\} \log_2 \mathbb{P}\left\{\mathcal{S} = i\,\Delta\right\} \tag{C.1}$$

where the quantizer has finite number of levels.

In particular, the entropy of the quantized BU sources can be derived from (4.3), (4.14), (4.28), and (C.1) as

$$\mathcal{H}^{\mathrm{BU}}(p,b) = -\left(1-p+\frac{p}{2^b-1}\right)\log_2\left(1-p+\frac{p}{2^b-1}\right) - p\,\frac{2^b-2}{2^b-1}\log_2\frac{p}{2^b-1} \tag{C.2}$$

where the PMF of $\widetilde{\mathcal{S}}$ is given by

$$\mathbb{P}\left\{\widetilde{\mathcal{S}} = i\,\Delta\right\} = \begin{cases} 1-p+\dfrac{p}{2^b-1}, & i=0 \\ \dfrac{p}{2^b-1}, & 0<|i|\leq i_{\max} \\ 0, & \text{otherwise.} \end{cases}$$

The corresponding result for BG distributions, taking into account the

saturation effect of the quantizer, is derived from (4.14), (4.28), and (C.1) as

$$\begin{aligned}\mathcal{H}^{\mathrm{BG}}(p,b,\widetilde{A}) = &-\left(p\,\mathrm{erf}\left(\frac{\widetilde{A}}{2^b-1}\right)-p+1\right)\log_2\left(p\,\mathrm{erf}\left(\frac{\widetilde{A}}{2^b-1}\right)-p+1\right)\\ &-p\left(1-\mathrm{erf}\left(\widetilde{A}-\frac{2\widetilde{A}}{2^b-1}\right)\right)\log_2\left(p\left(1-\mathrm{erf}\left(\widetilde{A}-\frac{2\widetilde{A}}{2^b-1}\right)\right)\right)\\ &-\mathbf{1}_{b\geq 3}\cdot\left(\sum_{i=1}^{2^{b-1}-2}p\left(\mathrm{erf}\left(\frac{\widetilde{A}(2i+1)}{2^b-1}\right)-\mathrm{erf}\left(\frac{\widetilde{A}(2i-1)}{2^b-1}\right)\right)\right.\\ &\left.\times\log_2\left(p\left(\mathrm{erf}\left(\frac{\widetilde{A}(2i+1)}{2^b-1}\right)-\mathrm{erf}\left(\frac{\widetilde{A}(2i-1)}{2^b-1}\right)\right)\right)\right)\end{aligned}\tag{C.3}$$

where $\widetilde{A}=A/(\sqrt{2}\sigma_{\mathrm{s}})$.

Appendix D

Optimal ODR of Uniform Quantizers for BU and BG Sources

The mean squared error distortion for quantized BG noiseless sources, considering the saturation effect, can be calculated as

$$\begin{aligned} D^{\mathrm{BG}}(\Delta) = 2\,p\Bigg(& \int_0^{\Delta/2} x^2 f(x;\sigma_{\mathrm{s}}^2)\,dx + \int_{A-\Delta}^{\infty} (x-A+\Delta/2)^2 f(x;\sigma_{\mathrm{s}}^2)\,dx \\ & + \mathbf{1}_{\{A/\Delta \geq 7/2\}} \underbrace{\sum_{i=1}^{\frac{A}{\Delta}-\frac{3}{2}} \int_{(i-1/2)\Delta}^{(i+1/2)\Delta} |x-i\Delta|^2 f(x;\sigma_{\mathrm{s}}^2)\,dx}_{\Xi} \Bigg) \\ = 2p\Bigg(& -\frac{\Delta\sigma_{\mathrm{s}} e^{-\frac{\Delta^2}{8\sigma_{\mathrm{s}}^2}}}{2\sqrt{2\pi}} + \frac{1}{8}\left((\Delta-2A)^2+4\sigma_{\mathrm{s}}^2\right)\mathrm{erfc}\left(\frac{A-\Delta}{\sqrt{2}\sigma_{\mathrm{s}}}\right) \\ & + \frac{1}{2}\sigma_{\mathrm{s}}^2 \mathrm{erf}\left(\frac{\Delta}{2\sqrt{2}\sigma_{\mathrm{s}}}\right) - \frac{A\sigma_{\mathrm{s}} e^{-\frac{(A-\Delta)^2}{2\sigma_{\mathrm{s}}^2}}}{\sqrt{2\pi}} + \mathbf{1}_{\{A/\Delta\geq 7/2\}}\,\Xi \Bigg). \end{aligned} \tag{D.1}$$

The term Ξ can be bounded, considering that $f(x;\sigma_{\mathrm{s}}^2)$ is a decreasing function for $x > 0$ [123] and that

$$\int_{(i-3/2)\Delta}^{(i-1/2)\Delta} f\left(x;\sigma_{\mathrm{s}}^2\right) dx > \Delta\, f\left((i-1/2)\Delta;\sigma_{\mathrm{s}}^2\right) \qquad \forall i \geq 2$$

as

$$\begin{aligned}\Xi &< \sum_{i=1}^{\frac{A}{\Delta}-\frac{3}{2}} f\left((i-1/2)\Delta;\sigma_{\rm s}^2\right)\int_{(i-1/2)\Delta}^{(i+1/2)\Delta}|x-i\Delta|^2\,dx\\ &= \frac{\Delta^3}{12}\sum_{i=1}^{\frac{A}{\Delta}-\frac{3}{2}} f\left((i-1/2)\Delta;\sigma_{\rm s}^2\right)\\ &< \frac{\Delta^3}{12}\left[f\left(\Delta/2;\sigma_{\rm s}^2\right)+\frac{1}{2\,\Delta}\left(\mathrm{erf}\left(\frac{A-2\,\Delta}{\sqrt{2}\sigma_{\rm s}}\right)+\mathrm{erf}\left(\frac{\Delta}{2\sqrt{2}\sigma_{\rm s}}\right)\right)\right]. \qquad \text{(D.2)}\end{aligned}$$

Substituting (D.2) into (D.1) yields

$$\begin{aligned}&D^{\rm BG}(\Delta) < \widetilde{D}^{\rm BG}(\Delta) \triangleq \frac{p}{12}\Bigg(\sigma_{\rm s}\sqrt{\frac{2}{\pi}}\left(-12Ae^{-\frac{(A-\Delta)^2}{2\sigma_{\rm s}^2}}-6\Delta e^{-\frac{\Delta^2}{8\sigma_{\rm s}^2}}\right)\\ &+12\,\sigma_{\rm s}^2\,\mathrm{erf}\left(\frac{\Delta}{2\sqrt{2}\sigma_{\rm s}}\right)+3\left((\Delta-2A)^2+4\sigma_{\rm s}^2\right)\mathrm{erfc}\left(\frac{A-\Delta}{\sqrt{2}\sigma_{\rm s}}\right)+\\ &\mathbf{1}_{\{A/\Delta\geq 7/2\}}\cdot\left(\sqrt{\frac{2}{\pi}}\frac{\Delta^3}{\sigma_{\rm s}}e^{-\frac{\Delta^2}{8\sigma_{\rm s}^2}}+\Delta^2\left(\mathrm{erf}\left(\frac{A-2\Delta}{\sqrt{2}\sigma_{\rm s}}\right)-\mathrm{erf}\left(\frac{\Delta}{2\sqrt{2}\sigma_{\rm s}}\right)\right)\right)\Bigg). \qquad \text{(D.3)}\end{aligned}$$

Consequently, the optimal rate-distortion of the considered uniform quantizer can be found from (C.3), (D.1), and (D.3) as

$$\begin{aligned}R^{\rm BG}(p,D,A) &= \inf_{\{b\geq 2\,|\,D^{\rm BG}\left(2A/(2^b-1)\right)\leq D\}}\mathcal{H}^{\rm BG}(p,b,\widetilde{A})\\ &= \mathcal{H}^{\rm BG}\left(p,\log_2\left(1+\frac{2A}{\Delta(D)}\right),\widetilde{A}\right) \qquad \text{(D.4)}\\ &< \mathcal{H}^{\rm BG}\left(p,\log_2\left(1+\frac{2A}{\widetilde{\Delta}(D)}\right),\widetilde{A}\right) \qquad \text{(D.5)}\end{aligned}$$

where $\Delta(D)$ and $\widetilde{\Delta}(D)$ are the inverse of $D^{\rm BG}(\Delta)$, (D.1), and $\widetilde{D}^{\rm BG}(\Delta)$, (D.3), respectively.[1]

Similarly, for BU sources the rate-distortion is given by

$$R^{\rm BU}(p,D)=\mathcal{H}^{\rm BU}\left(p,\log_2\left(1+A\sqrt{\frac{p}{3\,D}}\right)\right) \qquad \text{(D.6)}$$

where for noiseless BU sources the distortion is simply $D^{\rm BU}(\Delta)=p\,\Delta^2/12$.

[1]Note that for $A\gg\sigma_{\rm s}$ and $\Delta\ll\sigma_{\rm s}$, the asymptotic distortion in high resolution regime, $p\Delta^2/12$, is approached.

Dissemination of Results

- A. Elzanaty, A. Giorgetti, and M. Chiani, "Weak RIC analysis of finite Gaussian matrices for joint sparse recovery," *IEEE Signal Processing Letters*, vol. 24, no. 10, pp. 1473-1477, Oct. 2017.

- A. Elzanaty, A. Giorgetti, and M. Chiani, "Syndrome-based encoding of compressible sources for M2M communication," in Proc. *IEEE Global Communication Conference (GLOBECOM)*, Singapore, Dec. 2017.

- A. Elzanaty, K. Koroleva, S. Gritsutenko, and M. Chiani, "Frame synchronization for M-ary modulation with phase offsets," in Proc. *IEEE International Conference on Ubiquitous Wireless Broadband (ICUWB)*, Salamanca, Spain, Sept. 2017, **Best Paper Award**.

- A. Elzanaty, A. Giorgetti, and M. Chiani, "Efficient compression of noisy sparse sources based on syndrome encoding", in Proc. *IEEE Global Communication Conference (GLOBECOM)*, Washington DC, USA, Dec. 2016.

- A. Elzanaty, A. Giorgetti, and M. Chiani, "On sparse recovery using finite Gaussian matrices: RIP-based analysis", in Proc. *IEEE Statistical Signal Processing Workshop (SSP)*, Palma de Mallorca, Spain, June 2016, pp. 1-5.

- M. Chiani, A. Elzanaty and A. Giorgetti, "Analysis of the restricted isometry property for Gaussian random matrices," in Proc. *IEEE Global Communications Conference (GLOBECOM)*, San Diego, CA, Dec. 2015, pp. 1-6.

- A. Elzanaty, A. Giorgetti, M. Chiani, "Limits on sparse data acquisition: RIC analysis of finite Gaussian matrices," *arXiv preprint arXiv: 1802.03195*, 2018 (Submitted to *IEEE Transactions on Information Theory*).

- A. Elzanaty, A. Giorgetti, M. Chiani, "Lossy compression of noisy sparse sources based on syndrome encoding," Submitted to *IEEE Transactions on Communications*.

Acknowledgment

I would like to take this opportunity to express my grateful for all people that helped me during pursuing my PhD, without their support this work would not have been possible.

In particular, I want to express my sincere gratitude to my supervisor Prof. Marco Chiani for welcoming me into his research group and for his guidance, support, and help to participate in seasonal schools, conferences and to publication in proceedings and journals. His great passion and capability for fundamental theoretical research and in simplifying complicated concepts have been a great inspiration to me.

I would like also to thank my co-supervisor Prof. Andrea Giorgetti for his encouragement, insightful comments, and dedicated time, which have been invaluable to me. He has been very helpful throughout my PhD both academically and socially.

Friends, PhD colleagues, professors and other staff at our lab in Cesena deserve much gratitude for the conducive environment and hospitality during my studies. My special thanks go to Prof. Davide Dardari, Prof. Enrico Paolini, and Prof. Franco Callegati. I cant forget my colleagues and dear friends for the amazing and long time that we have spent together: Andrea Mariani, Anna Guerra, Ashraf Alhalabi, Danilo Pianini, Francesco Guidi, Nicol Decarli, and Simone Moretti.

My most gratitude and appreciation goes to my wife Rana for the all the unfailing support, love, care, sacrifice, encouragement, understanding, patience, and perseverance over the past years, which enabled me to finish my work. I would like also to thank my mother and father in law for their encouragement. I would like to express my gratitude to my mother, sister, and brothers for their endless love and prayers. Finally, I want to dedicate this work to the soul of my father, who always supported and believed in me.

Finally, many thanks to the EU-METALIC II project, within the framework of Erasmus Mundus Action2, that funded my Ph.D. scholarship for 34 months and to the EuroCPS project for supporting my research for further 12 months.

Bibliography

[1] D. Reinsel, J. Gantz, and J. Rydning, "Data age 2025: The evolution of data to life-critical," International Data Corporation (IDC), White Paper, Tech. Rep., 2010.

[2] D. Donoho, M. Vetterli, R. DeVore, and I. Daubechies, "Data compression and harmonic analysis," *IEEE Trans. Inf. Theory*, vol. 44, no. 6, pp. 2435–2476, Oct 1998.

[3] S. Mallat, *A wavelet tour of signal processing: the sparse way*. Academic press, 2008.

[4] D. Donoho, "Compressed sensing," *IEEE Trans. Inf. Theory*, vol. 52, no. 4, pp. 1289 –1306, April 2006.

[5] E. Candes and T. Tao, "Decoding by linear programming," *IEEE Trans. Inf. Theory*, vol. 51, no. 12, pp. 4203–4215, Dec. 2005.

[6] S. Foucart and H. Rauhut, *A mathematical introduction to compressive sensing*. Springer, 2013.

[7] M. Trocan, T. Maugey, J. Fowler, and B. Pesquet-Popescu, "Disparity-compensated compressed-sensing reconstruction for multiview images," in *Proc. IEEE International Conference on Multimedia and Expo*, July 2010, pp. 1225–1229.

[8] F. Chen, A. Chandrakasan, and V. Stojanovic, "Design and analysis of a hardware-efficient compressed sensing architecture for data compression in wireless sensors," *IEEE J. Solid-State Circuits*, vol. 47, no. 3, pp. 744–756, March 2012.

[9] G. Coluccia, A. Roumy, and E. Magli, "Operational rate-distortion performance of single-source and distributed compressed sensing," *IEEE Trans. Commun.*, vol. 62, no. 6, pp. 2022–2033, June 2014.

[10] D. Valsesia, G. Coluccia, and E. Magli, "Graded quantization for multiple description coding of compressive measurements," *IEEE Trans. Commun.*, vol. 63, no. 5, pp. 1648–1660, May 2015.

[11] H. Schepker, C. Bockelmann, and A. Dekorsy, "Efficient detectors for joint compressed sensing detection and channel decoding," *IEEE Trans. Commun.*, vol. 63, no. 6, pp. 2249–2260, June 2015.

[12] A. Kipnis, G. Reeves, Y. Eldar, and A. Goldsmith, "Fundamental limits of compressed sensing under optimal quantization," in *Proc. IEEE Inter. Sympos. on Information Theory (ISIT)*, June 2017.

[13] O. Musa and N. Goertz, "Quantization of compressed sensing measurements using analysis-by-synthesis with bayesian-optimal approximate message passing," in *Proc. IEEE 16th Inter. Workshop on Sig. Process. Advances in Wireless Comm. (SPAWC)*, June 2015, pp. 510–514.

[14] J. Mota, N. Deligiannis, and M. Rodrigues, "Compressed sensing with prior information: Strategies, geometry, and bounds," *IEEE Trans. Inf. Theory*, vol. 63, no. 7, pp. 4472–4496, July 2017.

[15] C. Colbourn, D. Horsley, and C. McLean, "Compressive sensing matrices and hash families," *IEEE Trans. Commun.*, vol. 59, no. 7, pp. 1840–1845, July 2011.

[16] F. Fazel, M. Fazel, and M. Stojanovic, "Random access compressed sensing for energy-efficient underwater sensor networks," *IEEE J. Sel. Areas Commun.*, vol. 29, no. 8, pp. 1660–1670, Sep. 2011.

[17] W. Chen, M. Rodrigues, and I. Wassell, "A frechet mean approach for compressive sensing date acquisition and reconstruction in wireless sensor networks," *IEEE Trans. Wireless Commun.*, vol. 11, no. 10, pp. 3598–3606, October 2012.

[18] G. Yang, V. Tan, C. Ho, S. Ting, and Y. Guan, "Wireless compressive sensing for energy harvesting sensor nodes," *IEEE Trans. Signal Process.*, vol. 61, no. 18, pp. 4491–4505, Sept. 2013.

[19] M. Mayer and N. Goertz, "RFID tag acquisition via compressed sensing: Fixed vs. random signature assignment," *IEEE Trans. Wireless Commun.*, vol. 15, no. 3, pp. 2118–2129, March 2016.

[20] L. Potter, E. Ertin, J. Parker, and M. Cetin, "Sparsity and compressed sensing in radar imaging," *Proc. of the IEEE*, vol. 98, no. 6, pp. 1006–1020, June 2010.

[21] M. Rossi, A. Haimovich, and Y. Eldar, "Spatial compressive sensing for MIMO radar," *IEEE Trans. Signal Process.*, vol. 62, no. 2, pp. 419–430, Jan. 2014.

[22] M. Mishali and Y. Eldar, "From theory to practice: Sub-Nyquist sampling of sparse wideband analog signals," *IEEE J. Sel. Topics Signal Process.*, vol. 4, no. 2, pp. 375–391, April 2010.

[23] A. Elzanaty, M. Abdelkader, and K. Seddik, "A collaborative approach for compressive spectrum sensing," in *Handb. of Res. on Softw. Defined and Cogn. Radio Technol. for Dyn. Spect. Manag.* IGI Global, Oct. 2014, pp. 153–178.

[24] Z. Qin, Y. Liu, Y. Gao, M. Elkashlan, and A. Nallanathan, "Wireless powered cognitive radio networks with compressive sensing and matrix completion," *IEEE Trans. Commun.*, vol. 65, no. 4, pp. 1464–1476, April 2017.

[25] M. Eltayeb, T. Al-Naffouri, and H. Bahrami, "Compressive sensing for feedback reduction in MIMO broadcast channels," *IEEE Trans. Commun.*, vol. 62, no. 9, pp. 3209–3222, Sept. 2014.

[26] N. Rajamohan and A. P. Kannu, "Downlink synchronization techniques for heterogeneous cellular networks," *IEEE Trans. Commun.*, vol. 63, no. 11, pp. 4448–4460, Nov. 2015.

[27] M. Firooz and S. Roy, "Link delay estimation via expander graphs," *IEEE Trans. Commun.*, vol. 62, no. 1, pp. 170–181, Jan. 2014.

[28] E. Candes and M. B. Wakin, "An introduction to compressive sampling," *IEEE Signal Process. Mag.*, vol. 25, no. 2, pp. 21–30, March 2008.

[29] S. Kirolos, J. Laska, M. Wakin, M. Duarte, D. Baron, T. Ragheb, Y. Massoud, and R. Baraniuk, "Analog-to-Information conversion via random demodulation," in *Proc IEEE Dallas/CAS Workshop on Design, App., Integ. and Softw.*, Oct 2006, pp. 71–74.

[30] F. Chen, F. Lim, O. Abari, A. Chandrakasan, and V. Stojanovic, "Energy-aware design of compressed sensing systems for wireless sensors under performance and reliability constraints," *IEEE Trans. Circuits Syst.*, vol. 60, no. 3, pp. 650–661, March 2013.

[31] E. Candes and Y. Plan, "A probabilistic and RIPless theory of compressed sensing," *IEEE Trans. Inf. Theory*, vol. 57, no. 11, pp. 7235–7254, Nov. 2011.

[32] M. Trakimas, R. D'Angelo, S. Aeron, T. Hancock, and S. Sonkusale, "A compressed sensing analog-to-information converter with edge-triggered SAR ADC core," *IEEE Trans. Circuits Syst. I*, vol. 60, no. 5, pp. 1135–1148, May 2013.

[33] O. Leneman and J. Lewis, "Random sampling of random processes: Mean-square comparison of various interpolators," *IEEE Trans. Autom. Control*, vol. 11, no. 3, pp. 396–403, Jul 1966.

[34] H. Landau, "Necessary density conditions for sampling and interpolation of certain entire functions," *Acta Mathematica*, vol. 117, no. 1, pp. 37–52, 1967.

[35] D. Dardari, A. Conti, C. Buratti, and R. Verdone, "Mathematical evaluation of environmental monitoring estimation error through energy-efficient wireless sensor networks," *IEEE Trans. Mobile Comput.*, vol. 6, no. 7, pp. 790–802, July 2007.

[36] F. Zabini, A. Calisti, D. Dardari, and A. Conti, "Random sampling via sensor networks: estimation accuracy vs. energy consumption," in *Proc. 24th European Sig. Process. Conf. (EUSIPCO)*, Aug 2016, pp. 130–134.

[37] F. Zabini and A. Conti, "Inhomogeneous Poisson sampling of finite-energy signals with uncertainties in $\mathbb{R}^d$," *IEEE Trans. Signal Process.*, vol. 64, no. 18, pp. 4679–4694, Sept 2016.

[38] A. Sandryhaila and J. Moura, "Big data analysis with signal processing on graphs: representation and processing of massive data sets with irregular structure," *IEEE Signal Process. Mag.*, vol. 31, no. 5, pp. 80–90, Sept 2014.

[39] V. Goyal, A. Fletcher, and S. Rangan, "Compressive sampling and lossy compression," *IEEE Signal Process. Mag.*, vol. 25, no. 2, pp. 48–56, March 2008.

[40] D. Donoho, "For most large underdetermined systems of linear equations the minimal ℓ_1-norm solution is also the sparsest solution," *Comm. on Pure and Applied Math.*, vol. 59, no. 6, pp. 797–829, 2006.

[41] E. Candes and T. Tao, "Near-optimal signal recovery from random projections: Universal encoding strategies?" *IEEE Trans. Inf. Theory*, vol. 52, no. 12, pp. 5406 –5425, Dec. 2006.

[42] Y. Eldar and G. Kutyniok, *Compressed sensing: theory and applications*. Cambridge University Press, 2012.

[43] T. Y. Al-Naffouri, A. A. Quadeer, and G. Caire, "Impulse noise estimation and removal for OFDM systems," *IEEE Trans. Commun.*, vol. 62, no. 3, pp. 976–989, March 2014.

[44] D. Donoho and J. Tanner, "Precise undersampling theorems," *Proc. IEEE*, vol. 98, no. 6, pp. 913–924, May 2010.

[45] M. Rudelson and R. Vershynin, "On sparse reconstruction from Fourier and Gaussian measurements," *Comm. on Pure and Applied Math.*, vol. 61, no. 8, pp. 1025–1045, 2008.

[46] M. Bayati, M. Lelarge, and A. Montanari, "Universality in polytope phase transitions and message passing algorithms," *The Annals of Applied Probability*, vol. 25, no. 2, pp. 753–822, March 2015.

[47] D.Donoho and J. Tanner, "Exponential bounds implying construction of compressed sensing matrices, error-correcting codes, and neighborly polytopes by random sampling," *IEEE Trans. Inf. Theory*, vol. 56, no. 4, pp. 2002–2016, April 2010.

[48] V. Chandrasekaran, B. Recht, P. A. Parrilo, and A. Willsky, "The convex geometry of linear inverse problems," *Found. of Computational Math.*, vol. 12, no. 6, pp. 805–849, 2012.

[49] E. J. Candès, "The restricted isometry property and its implications for compressed sensing," *Comptes Rendus Mathematique*, vol. 346, no. 9, pp. 589–592, May 2008.

[50] S. Foucart and M.-J. Lai, "Sparsest solutions of underdetermined linear systems via ℓ_q-minimization for $0 < q \leq 1$," *Appl. Comput. Harmon. Anal.*, vol. 26, no. 3, pp. 395 – 407, 2009.

[51] S. Foucart, "A note on guaranteed sparse recovery via ℓ_1-minimization," *Appl. Comput. Harmon. Anal.*, vol. 29, no. 1, pp. 97–103, 2010.

[52] T. Cai, L. Wang, and G. Xu, "New bounds for restricted isometry constants," *IEEE Trans. Inf. Theory*, vol. 56, no. 9, pp. 4388–4394, Sept. 2010.

[53] Q. Mo and S. Li, "New bounds on the restricted isometry constant δ_{2k}," *Appl. Comput. Harmon. Anal.*, vol. 31, no. 3, pp. 460–468, Nov. 2011.

[54] T. Cai and A. Zhang, "Sharp RIP bound for sparse signal and low-rank matrix recovery," *Appl. Comput. Harmon. Anal.*, vol. 35, no. 1, pp. 74–93, 2013.

[55] T. Blumensath and M. Davies, "Iterative thresholding for sparse approximations," *J. Fourier Anal. Appl.*, vol. 14, no. 5-6, pp. 629–654, Sep. 2008.

[56] S. Foucart, "Sparse recovery algorithms: Sufficient conditions in terms of restricted isometry constants," *Approximation Theory XIII, San Antonio 2010*, vol. 13, pp. 65–77, 2012.

[57] J. Tropp, D. Needell, and R. Vershynin, "Iterative signal recovery from incomplete and inaccurate measurements," San Diego, USA, Jan. 2008.

[58] W. Dai and O. Milenkovic, "Subspace pursuit for compressive sensing signal reconstruction," *IEEE Trans. Inf. Theory*, vol. 55, no. 5, pp. 2230–2249, May 2009.

[59] D. Needell and R. Vershynin, "Signal recovery from incomplete and inaccurate measurements via regularized orthogonal matching pursuit," *IEEE J. Sel. Topics Signal Process.*, vol. 4, no. 2, pp. 310–316, April 2010.

[60] T. Zhang, "Sparse recovery with orthogonal matching pursuit under RIP," *IEEE Trans. Inf. Theory*, vol. 57, no. 9, pp. 6215–6221, Sept 2011.

[61] W. Wang, M. Wainwright, and K. Ramchandran, "Information-theoretic limits on sparse signal recovery: Dense versus sparse measurement matrices," *IEEE Trans. Inf. Theory*, vol. 56, no. 6, pp. 2967–2979, June 2010.

[62] J. Blanchard, C. Cartis, and J. Tanner, "Compressed sensing: How sharp is the restricted isometry property," *SIAM review*, vol. 53, no. 1, pp. 105–125, 2011.

[63] B. Bah and J. Tanner, "Improved bounds on restricted isometry constants for Gaussian matrices," *SIAM J. Matrix Anal. Appl.*, vol. 31, no. 5, pp. 2882–2898, 2010.

[64] ——, "Bounds of restricted isometry constants in extreme asymptotics: formulae for Gaussian matrices," *Linear Algebra and Its Applications*, vol. 441, no. Complete, pp. 88–109, Jan. 2014.

[65] A. Edelman, "Eigenvalues and condition numbers of random matrices," *SIAM J. Matrix Anal. Appl.*, vol. 9, no. 4, pp. 543–560, 1988.

[66] M. Chiani, "On the probability that all eigenvalues of Gaussian, Wishart, and double Wishart random matrices lie within an interval," *IEEE Trans. Inf. Theory*, vol. 63, no. 07, pp. 4521–4531, July 2017.

[67] J. Blanchard and A. Thompson, "On support sizes of restricted isometry constants," *Appl. Comput. Harmon. Anal.*, vol. 29, no. 3, pp. 382–390, 2010.

[68] S. Foucart, "Hard thresholding pursuit: An algorithm for compressive sensing," *SIAM J. Numer. Anal.*, vol. 49, no. 6, pp. 2543–2563, 2011.

[69] J. Blanchard, C. Cartis, J. Tanner, and A. Thompson, "Phase transitions for greedy sparse approximation algorithms," *Appl. Comput. Harmon. Anal.*, vol. 30, no. 2, pp. 188–203, 2011.

[70] R. Tibshirani, "Regression shrinkage and selection via the LASSO," *J. R. Stat. Soc.. Series B (Methodological)*, pp. 267–288, 1996.

[71] E. Candes and T. Tao, "The Dantzig selector: Statistical estimation when p is much larger than n," *The Annals of Statistics*, vol. 35, no. 6, pp. 2313–2351, Dec. 2007.

[72] S. Chen and D. Donoho, "Basis pursuit," in *Proc. of the Twenty-Eighth Asilomar Conf. on Signals, Systems and Computers*, vol. 1, Pacific Grove, CA, USA, Oct. 1994, pp. 41–44.

[73] Z. Xue, J. Ma, and X. Yuan, "D-OAMP: A denoising-based signal recovery algorithm for compressed sensing," in *Proc. IEEE Global Conf. on Signal and Inf. Process. (GlobalSIP)*, Dec. 2016, pp. 267–271.

[74] R. Saab, R. Chartrand, and O. Yilmaz, "Stable sparse approximations via nonconvex optimization," in *Proc. IEEE Int. Conf. Acoust. Speech Signal Process. (ICASSP)*, Las Vegas, USA, 2008, pp. 3885–3888.

[75] L. Jacques, D. K. Hammond, and J. Fadili, "Weighted ℓ_p constraints in noisy compressed sensing," in *Proc. Signal Process. with Adaptive Sparse Structured Represent. Work., Edinburgh, Scotland, UK*, June 2011, p. 49.

[76] W. Zeng, H. So, and X. Jiang, "Outlier-robust greedy pursuit algorithms in ℓ_p-space for sparse approximation," *IEEE Trans. Signal Process.*, vol. 64, no. 1, pp. 60–75, Jan 2016.

[77] C. Tracy and H. Widom, "Level-spacing distributions and the Airy kernel," *Comm. Math. Phys.*, vol. 159, no. 1, pp. 151–174, Dec. 1994.

[78] K. Johansson, "Shape fluctuations and random matrices," *Comm, in Math. Physics*, vol. 209, no. 2, pp. 437–476, 2000. [Online]. Available: http://dx.doi.org/10.1007/s002200050027

[79] M. Johnstone, "On the distribution of the largest eigenvalue in principal components analysis," *The Annals of Statistics*, vol. 29, no. 2, pp. 295–327, 2001.

[80] C. Tracy and H. Widom, "The distributions of random matrix theory and their applications," *New Trends in Mathematical Physics, V. Sidoravicius (ed.)*, pp. 753–765, 2009.

[81] F. Bornemann, "On the numerical evaluation of distributions in random matrix theory: a review," *J. Markov Process. Related Fields*, vol. 16, p. 803866, 2010.

[82] Z. Ma, "Accuracy of the TracyWidom limits for the extreme eigenvalues in white Wishart matrices," *Bernoulli*, vol. 18, no. 1, pp. 322–359, 02 2012.

[83] E. Basor, Y. Chen, and L. Zhang, "PDEs satisfied by extreme eigenvalues distributions of GUE and LUE," *Random Matrices: Theory and Applications*, vol. 01, no. 01, p. 1150003, 2012.

[84] M. Ledoux and B. Rider, "Small deviations for beta ensembles," *Electron. J. Prob.*, vol. 15, pp. 1319–1343, 2010.

[85] G. Aubrun, "A sharp small deviation inequality for the largest eigenvalue of a random matrix," in *Séminaire de Probabilités XXXVIII*. Springer, 2005, pp. 320–337.

[86] L. Dumaz and B. Virág, "The right tail exponent of the Tracy-Widom distribution," *Ann. l'institut Henri Poincare Prob. Stat.*, vol. 49, no. 4, pp. 915–923, 2011.

[87] O. Feldheim and S. Sodin, "A universality result for the smallest eigenvalues of certain sample covariance matrices," *Geometric and Functional Analysis*, vol. 20, no. 1, pp. 88–123, 2010.

[88] S. Péché, "Universality results for the largest eigenvalues of some sample covariance matrix ensembles," *Probability Theory and Related Fields*, vol. 143, no. 3, pp. 481–516, 2009.

[89] C. Dossal, G. Peyr, and J. Fadili, "A numerical exploration of compressed sampling recovery," *Linear Algebra Appl.*, vol. 432, no. 7, pp. 1663 – 1679, 2010.

[90] M. Duarte, S. Sarvotham, D. Baron, M. Wakin, and R. Baraniuk, "Distributed compressed sensing of jointly sparse signals," in *Proc. Thirty-Ninth Asilomar Conf. on Signals, Systems and Comp.*, Oct. 2005, pp. 1537–1541.

[91] R. Baraniuk, V. Cevher, M. Duarte, and C. Hegde, "Model-based compressive sensing," *IEEE Trans. Inf. Theory*, vol. 56, no. 4, pp. 1982–2001, April 2010.

[92] J. Tropp, "Algorithms for simultaneous sparse approximation. Part II: Convex relaxation," *Signal Processing*, vol. 86, no. 3, pp. 589–602, March 2006.

[93] J. Chen and X. Huo, "Theoretical results on sparse representations of multiple-measurement vectors," *IEEE Trans. Signal Process.*, vol. 54, no. 12, pp. 4634–4643, Dec. 2006.

[94] Y. Eldar and H. Rauhut, "Average case analysis of multichannel sparse recovery using convex relaxation," *IEEE Trans. Inf. Theory*, vol. 56, no. 1, pp. 505–519, Jan. 2010.

[95] K. Lee, Y. Bresler, and M. Junge, "Subspace methods for joint sparse recovery," *IEEE Trans. Inf. Theory*, vol. 58, no. 6, pp. 3613–3641, June 2012.

[96] K. S. Kim and S.-Y. Chung, "Greedy subspace pursuit for joint sparse recovery," *arXiv preprint arXiv:1601.07087*, Jan 2016.

[97] S. Cotter, B. Rao, K. Engan, and K. Kreutz-Delgado, "Sparse solutions to linear inverse problems with multiple measurement vectors," *IEEE Trans. Signal Process.*, vol. 53, no. 7, pp. 2477–2488, July 2005.

[98] R. Gribonval, H. Rauhut, K. Schnass, and P. Vandergheynst, "Atoms of all channels, unite! average case analysis of multi-channel sparse recovery using greedy algorithms," *J. Fourier Anal. Appl.*, vol. 14, no. 5, pp. 655–687, 'Oct. 2008.

[99] J. A. Tropp, A. C. Gilbert, and M. J. Strauss, "Algorithms for simultaneous sparse approximation. Part I: Greedy pursuit," *Signal Processing*, vol. 86, no. 3, pp. 572–588, March 2006.

[100] J. Blanchard, M. Cermak, D. Hanle, and Y. Jing, "Greedy algorithms for joint sparse recovery," *IEEE Trans. Signal Process.*, vol. 62, no. 7, pp. 1694–1704, Apr. 2014.

[101] J. Blanchard, J. Tanner, and K. Wei, "Conjugate gradient iterative hard thresholding: Observed noise stability for compressed sensing," *IEEE Trans. Signal Process.*, vol. 63, no. 2, pp. 528–537, Jan 2015.

[102] M. Davies and Y. Eldar, "Rank awareness in joint sparse recovery," *IEEE Trans. Inf. Theory*, vol. 58, no. 2, pp. 1135–1146, Feb. 2012.

[103] S. Gogineni and A. Nehorai, "Target estimation using sparse modeling for distributed MIMO radar," *IEEE Trans. Signal Process.*, vol. 59, no. 11, pp. 5315–5325, Nov. 2011.

[104] D. Ge, X. Jiang, and Y. Ye, "A note on the complexity of ℓ_p minimization," *Math. Program.*, vol. 129, no. 2, pp. 285–299, Oct. 2011.

[105] R. Schmidt, "Multiple emitter location and signal parameter estimation," *IEEE Trans. Antennas Propag.*, vol. 34, no. 3, pp. 276–280, Mar. 1986.

[106] P. Feng and Y. Bresler, "Spectrum-blind minimum-rate sampling and reconstruction of multiband signals," in *Proc. IEEE Int. Conf. Acoust. Speech Signal Process. (ICASSP)*, vol. 3, May 1996, pp. 1688–1691.

[107] G. Borot and C. Nadal, "Right tail asymptotic expansion of Tracy-Widom beta laws," *Random Matrices: Theory and Applications*, vol. 1, no. 3, pp. 1–23, Jul. 2012.

[108] C. Shannon, "A mathematical theory of communication," *The Bell System Technical Journal*, vol. 27, no. 3, pp. 379–423, July 1948.

[109] S. Lin and D. Costello, *Error control coding, Fundamentals and applications*. Prentice Hall, Inc. Englewood Cliffs, New Jersey, 1983.

[110] M. Vetterli, "Wavelets, approximation, and compression," *IEEE Signal Process. Mag.*, vol. 18, no. 5, pp. 59–73, Sep. 2001.

[111] W. Ryan and S. Lin, *Channel codes: classical and modern*. Cambridge University Press, 2009.

[112] C. Weidmann and M. Vetterli, "Rate distortion behavior of sparse sources," *IEEE Trans. Inf. Theory*, vol. 58, no. 8, pp. 4969–4992, Aug 2012.

[113] J. Fowler and B. Pesquet-Popescu, "An overview on wavelets in source coding, communications, and networks," *EURASIP Journal on Image and Video Processing*, vol. 2007, no. 1, pp. 1–27, June 2007.

[114] P. Westerink, J. Biemond, and D. Boekee, "An optimal bit allocation algorithm for sub-band coding," in *Proc. IEEE Int. Conf. Acoust. Speech Signal Process. (ICASSP)*, vol. 2, Apr. 1988, pp. 757–760.

[115] A. Ortega and K. Ramn, "Rate-distortion methods for image and video compression," *IEEE Signal Process. Mag.*, vol. 15, no. 6, pp. 23–50, Nov. 1998.

[116] M. Kaaniche, A. Fraysse, B. Pesquet-Popescu, and J. Pesquet, "A bit allocation method for sparse source coding," *IEEE Trans. Image Process.*, vol. 23, no. 1, pp. 137–152, Jan. 2014.

[117] H. Gao, L. Dai, S. Han, Z. Wang, L. Hanzo *et al.*, "Compressive sensing techniques for next-generation wireless communications," *arXiv preprint arXiv:1709.01757*, 2017.

[118] G. Myers, "Quantization of a signal plus random noise," *IEEE Trans. Instrum.**, vol. PGI-5, pp. 181–186, June 1956.

[119] A. Gyorgy and T. Linder, "Optimal entropy-constrained scalar quantization of a uniform source," *IEEE Trans. Inf. Theory*, vol. 46, no. 7, pp. 2704–2711, Nov. 2000.

[120] A. Fraysse, B. Pesquet-Popescu, and J. Pesquet, "Rate-distortion results for Generalized Gaussian distributions," in *Proc. IEEE Int. Conf. Acoust. Speech Signal Process. (ICASSP)*, Las Vegas, USA, March 2008, pp. 3753–3756.

[121] G. Sullivan, "Efficient scalar quantization of exponential and Laplacian random variables," *IEEE Trans. Inf. Theory*, vol. 42, no. 5, pp. 1365–1374, Sep. 1996.

[122] D. Leporini, J. Pesquet, and H. Krim, *Best Basis Representations with Prior Statistical Models*. New York, NY: Springer New York, 1999, pp. 155–172.

[123] A. Fraysse, B. Pesquet-Popescu, and J. Pesquet, "On the uniform quantization of a class of sparse sources," *IEEE Trans. Inf. Theory*, vol. 55, no. 7, pp. 3243–3263, July 2009.

[124] H. Rosenthal and J. Binia, "On the epsilon entropy of mixed random variables," *IEEE Trans. Inf. Theory*, vol. 34, no. 5, pp. 1110–1114, Sep. 1988.

[125] A. Gyorgy, T. Linder, and K. Zeger, "On the rate-distortion function of random vectors and stationary sources with mixed distributions," *IEEE Trans. Inf. Theory*, vol. 45, no. 6, pp. 2110–2115, Sep. 1999.

[126] M. Kaaniche, A. Fraysse, B. Pesquet-Popescu, and J. Pesquet, "Accurate rate-distortion approximation for sparse Bernoulli-Generalized Gaussian models," in *Proc. IEEE Int. Conf. Acoust. Speech Signal Process. (ICASSP)*, Florence, Italy, May 2014, pp. 2020–2024.

[127] A. Wyner, "Recent results in the Shannon theory," *IEEE Trans. Inf. Theory*, vol. 20, no. 1, pp. 2–10, Jan 1974.

[128] A. Wyner and J. Ziv, "The rate-distortion function for source coding with side information at the decoder," *IEEE Trans. Inf. Theory*, vol. 22, no. 1, pp. 1–10, Jan 1976.

[129] S. Pradhan and K. Ramchandran, "Distributed source coding using syndromes (DISCUS): design and construction," *IEEE Trans. Inf. Theory*, vol. 49, no. 3, pp. 626–643, March 2003.

[130] E. Magli, M. Barni, A. Abrardo, and M. Grangetto, "Distributed source coding techniques for lossless compression of hyperspectral images," *EURASIP J. Appl. Signal Process.*, vol. 2007, no. 1, pp. 24–24, Jan. 2007.

[131] A. Gabay, M. Kieffer, and P. Duhamel, "Joint source-channel coding using real BCH codes for robust image transmission," *IEEE Trans. Image Process.*, vol. 16, no. 6, pp. 1568–1583, June 2007.

[132] C. Yaacoub, J. Farah, and B. Pesquet-Popescu, "Joint source-channel Wyner-Ziv coding in wireless video sensor networks," in *Proc. IEEE Inter. Symp. on Sig. Process. and Inform. Technology*, Dec. 2007, pp. 225–228.

[133] F. Bassi, M. Kieffer, and C. Weidmann, "Source coding with intermittent and degraded side information at the decoder," in *Proc. IEEE Int. Conf. Acoust. Speech Signal Process. (ICASSP)*, March 2008, pp. 2941–2944.

[134] F. Bassi, M. Kieffer, and C. Dikici, "Multiterminal source coding of Bernoulli-Gaussian correlated sources," in *Proc. IEEE Int. Conf. Acoust. Speech Signal Process. (ICASSP)*, April 2009, pp. 2501–2504.

[135] T. Cover and J. Thomas, *Elements of information theory*. John Wiley & Sons, 2012.

[136] M. Vaezi and F. Labeau, "Distributed source-channel coding based on real-field BCH codes," *IEEE Trans. Signal Process.*, vol. 62, no. 5, pp. 1171–1184, March 2014.

[137] S. B. Korada and R. L. Urbanke, "Polar codes are optimal for lossy source coding," *IEEE Trans. Inf. Theory*, vol. 56, no. 4, pp. 1751–1768, April 2010.

[138] F. Abramovich, T. Sapatinas, and B. Silverman, "Wavelet thresholding via a Bayesian approach," *Journal of the Royal Statistical Society: Series B (Statistical Methodology)*, vol. 60, no. 4, pp. 725–749, 1998.

[139] A. Mariani, A. Giorgetti, and M. Chiani, "Model order selection based on information theoretic criteria: Design of the penalty," *IEEE Trans. Signal Process.*, vol. 63, no. 11, pp. 2779–2789, June 2015.

[140] P. Stoica and Y. Selen, "Model-order selection: a review of information criterion rules," *IEEE Signal Process. Mag.*, vol. 21, no. 4, pp. 36–47, July 2004.

[141] M. Chiani and M. Win, "Estimating the number of signals observed by multiple sensors," in *Proc. IEEE IAPR Workshop on Cognitive Inform. Process. (CIP)*, Elba Island, Italy, Jun. 2010, pp. 156–161.

[142] A. Mariani, A. Giorgetti, and M. Chiani, "Wideband spectrum sensing by model order selection," *IEEE Trans. Wireless Commun.*, vol. 14, no. 12, pp. 6710–6721, Dec. 2015.

[143] A. Giorgetti and M. Chiani, "Time-of-arrival estimation based on information theoretic criteria," *IEEE Trans. Signal Process.*, vol. 61, no. 8, pp. 1869–1879, April 2013.

[144] Y. You, *Audio Coding: Theory and Applications*. Springer Science & Business Media, 2010.

[145] I. Reed and G. Solomon, "Polynomial codes over certain finite fields," *SIAM. J. Appl. Math.*, vol. 8, no. 2, pp. 300–304, 1960.

[146] E. Berlekamp, *Algebraic coding theory*. McGraw-Hill, 1968.

[147] B. Widrow, I. Kollar, and M.-C. Liu, "Statistical theory of quantization," *IEEE Trans. Instrum. Meas.*, vol. 45, no. 2, pp. 353–361, Apr. 1996.

[148] J. Vales-Alonso, E. Egea-López, A. Martínez-Sala, P. Pavón-Mariño, M. Bueno-Delgado, and J. García-Haro, "Performance evaluation of MAC transmission power control in wireless sensor networks," *Computer Networks*, vol. 51, no. 6, pp. 1483–1498, April 2007.

[149] C. Karakus, A. Gurbuz, and B. Tavli, "Analysis of energy efficiency of compressive sensing in wireless sensor networks," *IEEE Sensors J.*, vol. 13, no. 5, pp. 1999–2008, May 2013.

[150] A. Giorgetti, M. Lucchi, E. Tavelli, M. Barla, G. Gigli, N. Casagli, M. Chiani, and D. Dardari, "A robust wireless sensor network for landslide risk analysis: System design, deployment, and field testing," *IEEE Sensors J.*, vol. 16, no. 16, pp. 6374–6386, Aug 2016.

[151] R. Barker, "Group synchronization of binary digital systems," in *Communication Theory*. London: W. Jackson, 1953.

[152] J. Massey, "Optimum frame synchronization," *IEEE Trans. on Commun.*, vol. 20, no. 2, pp. 115–119, Apr 1972.

[153] P. Nielsen, "Some optimum and suboptimum frame synchronizers for binary data in Gaussian noise," *IEEE Trans. on Commun.*, vol. 21, no. 6, pp. 770–772, Jun 1973.

[154] G. Lui and H. Tan, "Frame synchronization for Gaussian channels," *IEEE Trans. on Commun.*, vol. 35, no. 8, pp. 818–829, Aug 1987.

[155] P. Robertson, "Improving frame synchronization when using convolutional codes," *Proc. Global Telecommunications Conference, Houston. GLOBECOM, IEEE*, pp. 1606–1611 vol.3, Nov-2 Dec 1993.

[156] M. Howlader and B. Woerner, "Decoder-assisted frame synchronization for packet transmission," *IEEE J. on Select. Areas in Commun.*, vol. 19, no. 12, pp. 2331–2345, December 2001.

[157] Y. Wang, K. Shi, and E. Serpedin, "Continuous-mode frame synchronization for frequency-selective channels," *IEEE Trans. on Veh. Technol.*, vol. 53, no. 3, pp. 865–871, May 2004.

[158] T. Cassaro and C. Georghiades, "Frame synchronization for coded systems over AWGN channels," *IEEE Trans. on Commun.*, vol. 52, no. 3, pp. 484–489, March 2004.

[159] M. Chiani and M. Martini, "Practical frame synchronization for data with unknown distribution on AWGN channels," *IEEE Commun. Lett.*, vol. 9, no. 5, pp. 456–458, May 2005.

[160] ——, "On sequential frame synchronization in AWGN channels," *IEEE Trans. Commun.*, vol. 54, no. 2, pp. 339–348, Feb. 2006.

[161] W. Suwansantisuk, M. Chiani, and M. Z. Win, "Frame synchronization for variable-length packets," *IEEE J. Select. Areas Commun.*, vol. 26, no. 1, pp. 52–69, Jan. 2008, special Issue on Cognitive Radio.

[162] M. Chiani and M. Martini, "Analysis of optimum frame synchronization based on periodically embedded sync words," *IEEE Trans. Commun.*, vol. 55, no. 11, pp. 2056–2060, Nov. 2007.

[163] M. Chiani, "Noncoherent frame synchronization," *IEEE Trans. Commun.*, vol. 58, no. 5, pp. 1536 –1545, May 2010.

[164] C. Georghiades and E. Serpedin, *Communication handbook*. CRC Press, 2002, ch. 18.

[165] Y. Liang, D. Rajan, and O. E. Eliezer, "Sequential frame synchronization based on hypothesis testing with unknown channel state information," *IEEE Trans. on Commun.*, vol. 63, no. 8, pp. 2972–2984, Aug 2015.

[166] V. Chandar, A. Tchamkerten, and G. Wornell, "Optimal sequential frame synchronization," *IEEE Trans. on Inform. Theory*, vol. 54, no. 8, pp. 3725–3728, Aug. 2008.

[167] L. Sanguinetti, M. Morelli, and V. Poor, "Frame detection and timing acquisition for OFDM transmissions with unknown interference," *IEEE Trans. on Wireless Commun.*, vol. 9, no. 3, 2010.

[168] E. Bastaki, H. Tan, Y. Shi, and K. Letaief, "Frame synchronization based on multiple frame observations," *IEEE Trans. on Wireless Commun.*, vol. 9, no. 3, 2010.

[169] M. Simon, J. Omura, R. Scholtz, and B. Levitt, *Spread Spectrum Communications Handbook*, electronic ed. New York, NY, 10020: McGraw-Hill, Inc., 2001.

[170] A. Viterbi, *CDMA: Principles of Spread Spectrum Communication*, 1st ed. Reading, Massachusetts 01867: Addison-Wesley, 1995.

[171] Z. Choi and Y. Lee, "Frame synchronization in the presence of frequency offset," *IEEE Trans. Commun.*, vol. 50, no. 7, pp. 1062–1065, July 2002.

[172] R. Pedone, M. Villanti, A. Vanelli-Coralli, G. Corazza, and P. Mathiopoulos, "Frame synchronization in frequency uncertainty," *IEEE Trans. on Commun.*, vol. 58, no. 4, pp. 1235–1246, 2010.

[173] T. Rappaport, *Wireless communications: principles and practice*. Prentice Hall PTR New Jersey, 1996, vol. 2.

[174] A. Conti, M. Win, and M. Chiani, "Slow adaptive M-QAM with diversity in fast fading and shadowing," *IEEE Trans. Commun.*, vol. 55, no. 5, pp. 895–905, May 2007.

[175] H. Van Trees, *Detection, Estimation, and Modulation Theory*, 1st ed. New York, NY 10158-0012: John Wiley & Sons, Inc., 1968.

[176] I. Gradshteyn and I. Ryzhik, *Tables of Integrals, Series, and Products*, 6th ed. San Diego, CA: Academic Press, Inc., 1994.

[177] M. Stojnic, W. Xu, and B. Hassibi, "Compressed sensing- probabilistic analysis of a null-space characterization," in *Proc. IEEE Int. Conf. Acoust. Speech Signal Process. (ICASSP)*, Las Vegas, USA, March 2008, pp. 3377–3380.